

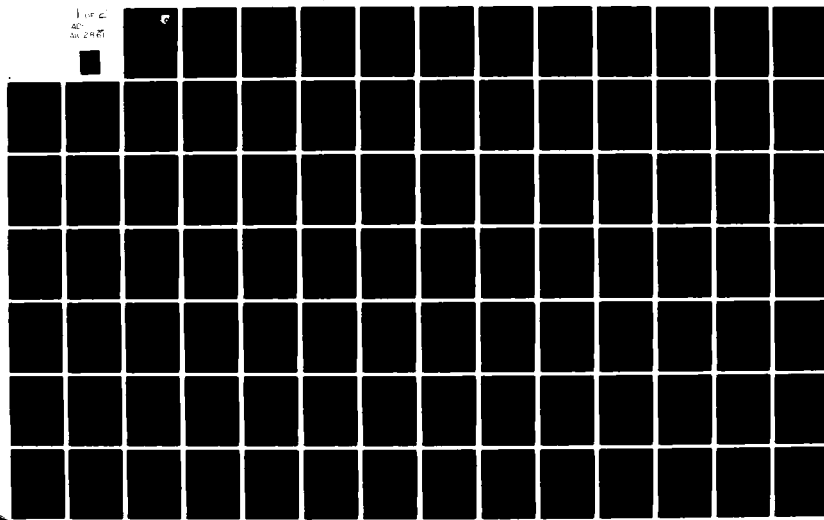
AD-A102 861

AIR FORCE WRIGHT AERONAUTICAL LABS WRIGHT-PATTERSON AFB OH F/G 20/3  
THERMIONIC EMISSION AND SPACE-CHARGE THEORY. (U)

UNCLASSIFIED  
MAY 81 J B SCOTT  
AFWAL-TR-81-1019

NL

1 of 2  
40-  
00 2487



FILE NUMBER  
ADA102861

AFWAL-TR-81-1019

LEVEL  
12



## THERMIONIC EMISSION AND SPACE-CHARGE THEORY

Microwave Technology Branch  
Electronic Technology Division  
Avionics Laboratory

May 1981

DATE  
AUG 14 1981

A

Final Report for the Period October 1976 - December 1980

Approved for public release; distribution unlimited.

AVIONICS LABORATORY  
AIR FORCE WRIGHT AERONAUTICAL LABORATORIES  
AIR FORCE SYSTEMS COMMAND  
WRIGHT-PATTERSON AIR FORCE BASE, OHIO 45433

NOTICE

When Government drawings, specifications, or other data are used for any purpose other than in connection with a definitely related Government procurement operation, the United States Government thereby incurs no responsibility nor any obligation whatsoever; and the fact that the Government may have formulated, furnished, or in any way supplied the said drawings, specifications, or other data, is not to be regarded by implication or otherwise as in any manner licensing the holder or any other person or corporation, or conveying any rights or permission to manufacture, use, or sell any patented invention that may in any way be related thereto.

This report has been reviewed by the Office of Public Affairs (ASD/PA) releasable to the National Technical Information Service (NTIS). At NTIS, it will be available to the general public, including foreign nations.

This technical report has been reviewed and is approved for publication.

Jess B. Scott

JESS B. SCOTT, Capt, USA<sup>W</sup>  
Project Engineer  
Microwave Device Group

Gary L. McCoy

GARY L. MCCOY, Chief  
Microwave Device Group  
Microwave Tech Branch

FOR THE COMMANDER:

Donald S. Rees

DONALD S. REES, Chief  
Microwave Technology Branch  
Electronic Technology Division  
Avionics Laboratory

If your address has changed, if you wish to be removed from our mailing list, or if the addressee is no longer employed by your organization please notify AFWAL/AADM-1, W-P AFB, OH 45433 to help us maintain a current mailing list.

Copies of this report should not be returned unless return is required by security considerations, contractual obligations, or notice on a specific document.

REPORT DOCUMENTATION PAGE		READ INSTRUCTIONS BEFORE COMPLETING FORM
1. REPORT NUMBER AFWAL-TR-81-1019	2. GOVT ACCESSION NO. AD A102 861	3. RECIPIENT'S CATALOG NUMBER
4. TITLE (and Subtitle) THERMIONIC EMISSION AND SPACE-CHARGE THEORY	5. TYPE OF REPORT & PERIOD COVERED Final Report 1 Oct 76 — 30 Dec 80	
7. AUTHOR(s) Jess B. Scott, Capt, USAF	6. PERFORMING ORG. REPORT NUMBER	
9. PERFORMING ORGANIZATION NAME AND ADDRESS Avionics Laboratory (AADM-1) Air Force Wright Aeronautical Laboratories (AFSC) Wright-Patterson Air Force Base, Ohio 45433	10. PROGRAM ELEMENT, PROJECT, TASK AREA & WORK UNIT NUMBERS 2002/02 44 62204F	
11. CONTROLLING OFFICE NAME AND ADDRESS Avionics Laboratory (AAD) Air Force Wright Aeronautical Laboratories (AFSC) Wright-Patterson Air Force Base, Ohio 45433	12. REPORT DATE May 1981	
14. MONITORING AGENCY NAME & ADDRESS (if different from Controlling Office)	13. NUMBER OF PAGES 100	
	15. SECURITY CLASS. (of this report) Unclassified	
	16. DECLASSIFICATION DOWNGRADING SCHEDULE	
16. DISTRIBUTION STATEMENT (of this Report) Approved for public release; distribution unlimited.		
17. DISTRIBUTION STATEMENT (of the abstract entered in Block 20, if different from Report)		
18. SUPPLEMENTARY NOTES		
19. KEY WORDS (Continue on reverse side if necessary and identify by block number) Thermionic emission space charge cathodes electron tubes		
20. ABSTRACT (Continue on reverse side if necessary and identify by block number) The work presented in this report extends the space-charge theory of parallel-plane diodes in several ways. Space-charge effects are included in the accelerating field range to remove the incompatibility between Langmuir theory and Schottky theory. A method is developed to use a measurement of the current density at the exponential point to calculate the zero field current density of the cathode. This is done without the necessity of matching data to a family of curves. A number of properties of Langmuir space-charge theory		

is described in much greater detail than has previously been done through the use of functional notation to express the current density as a function of the applied voltage. Some of these details are brought out in a discussion of the fields and charge in the interelectrode space. As a side light, a method is developed to handle the edge effects in a class of parallel-plane diode testers.

FOREWORD

This report describes an in-house effort conducted by personnel of the Microwave Technology Branch (AADM), Electronic Technology Division (AAD), Avionics Laboratory (AA), Air Force Wright Aeronautical Laboratories, Wright-Patterson Air Force Base, Ohio, under Project 2002, "Microwave Technology," Task 200202, "Thermionics," Work Unit 20020244, "Physics of Matrix Cathodes."

The work reported herein was performed during the period 1 October 1976 to 30 December 1980, under the direction of the author, Capt Jess B. Scott (AFWAL/AADM-1), project engineer. The report was submitted by the author in January 1981.

The author is indebted to Dr. G. K. Medicus for helpful discussions and guidance during the course of the theoretical work, to Lt D. L. Allen for assistance in maintaining the computing equipment, and to Lt J. Targove for assistance in some of the programming.

## TABLE OF CONTENTS

SECTION	PAGE
I      INTRODUCTION	1
1. Background	2
2. Overview	3
3. Thermionic Emission	6
II     SPACE-CHARGE THEORY	10
1. Derivation of Langmuir's Differential Equation	10
2. Series Solutions for the $n$ , $\xi$ Functions	14
3. Numerical Solutions for the $n$ , $\xi$ Functions	20
4. The Current-Voltage Relationship for $J \leq J_0$	25
5. Behavior of $J(V)$ for Space-Charge-Limited Conditions	27
a. Transition to $J = J_0$	29
b. The Inflection Point	29
c. Transition from Retarding-Field to Space-Charge Limited Conditions	31
d. Experimental Use of the Exponential Point	33
6. Comparison of $J(V)$ with Child's Law	37
III    SCHOTTKY THEORY	39
1. Derivation of the Schottky Equation	39
2. Edge Effects and Schottky Theory	41
IV    EXTENDING SPACE-CHARGE THEORY INTO THE ACCELERATING FIELD RANGE	49
1. Background	49
2. Generation of $J(V)$ in the Accelerating Field Range	51
3. Behavior of $J(V)$ Near $J$ Equal to and Greater than $J_0$	52
4. Fields and Charge in the Interelectrode Space	55
5. Effects of Diode Spacing on $J(V)$	61
V     CONCLUSIONS	63
REFERENCES	91

## LIST OF ILLUSTRATIONS

FIGURE	PAGE
1 Schematic of the Space-Charge Region Outside an Emitting Surface	64
2 Schematic of the Potential Distribution Between the Anode and Cathode Under Retarding Field Conditions	65
3 Schematic of the J-V Curve Under Retarding Field Conditions	65
4 The Function $\eta(\xi)$ and its First and Second Derivatives	66
5 Series Solution to Langmuir's Differential Equation for the $\eta$ , $\varepsilon$ function for $\eta_0 = 0.5$	67
6 BASIC Language Program Using Mixed Runge-Kutta-Taylor Method to Solve for $\eta(\xi)$	68
7 Sample Output from the Program of Figure 5	69
8 Schematic of the Potential Distribution Between the Anode and Cathode under Space-Charge Limited Conditions	70
9 The Current Density and its First and Second Derivatives as a Function of the Applied Voltage for an Example Cathode	71
10 Detail of the First Derivative of $J(V)$ for the Example in Figure 8	72
11 The Zero Field Current $J_0$ as a Function of $J_e$ the Current at the Transition from Retarding Field to Space-Charge-Limited Operation for $D = 1$ mm, $T = 900^\circ$ and for $D = 0.2$ mm, $T = 700^\circ$ C	73
12 BASIC Program to Solve Equation 113 and Generate $J_e$ and $V_e$ as Functions of $J_0$	74
13 The Zero Field Current $J_0$ and the Transition Current $J_e$ Plotted as Functions of the Transition Voltage $V_e$ for $D = 0.2$ mm, $T = 700^\circ$ C	75
14 Graphs of $J_e$ and $J_0$ as Functions of $V_e$	76
15 Comparison of the Derivative $d\eta_a/d\xi$ from Langmuir's Theory with the Approximate form of the Derivative Which Leads to Child's Law	77

## LIST OF ILLUSTRATIONS (CONCLUDED)

FIGURE	PAGE
16 Potential as a Function of Distance from a Metal Surface	78
17 The Electric Potential as a Function of Distance from a Metal Surface Shown as the Sum of a Surface Field and an Applied External Field	79
18 Schematic of a Close-Spaced Diode Tester Showing the Cross Section of a Cylindrical Cathode and Anode	80
19 A Plane Edge above a Conducting Plane	80
20 Schematic Showing Details of the Mapping from the $Z'$ Plane to the $Z$ Plane	81
21 Current Density and Electric Field at the Cathode Surface as a Function of Distance from the Cathode Edge - All in Normalized Units	82
22 Theoretical Schottky Plots	83
23 Electric Potential as a Function of Distance from the Cathode Surface for (a) The Image Field and for (b) The Space-Charge Field of an Example Cathode	84
24 Current-Voltage Plot for $J$ Ranging from Small Values up through $J > J_0$	85
25 Current-Voltage Plot Showing a Break in the Slope of $J$ as a Function of $V$ at $J = J_0$	86
26 The Electric Potential as a Function of Distance from the Cathode Surface for Various Values of Cathode Loading $J/J_0$	87
27 The Negative of the Electric Field	88
28 The Number Density of Electrons as a Function of Distance from the Cathode Surface for Various Values of Cathode Loading $J/J_0$	89
29 Current Density as a Function of Applied Voltage for Two Values of Diode Spacing, 0.3 mm and 0.9 mm, for a Cathode Temperature of 900°C and $J_0$ of 5 A/cm <sup>2</sup>	90

SECTION I  
INTRODUCTION

One purpose of thermionic-emission theory and space-charge theory is to relate in a sensible way the current drawn from a cathode to the voltage applied to the anode. Tests are made on cathodes in geometries kept as simple as possible to make it easier to relate measured current density  $J$  as a function of voltage  $V$  back to the basic characteristics of the cathode. The usual cathode property of interest is the cathode work function  $\phi$  or the zero-field current density  $J_0$  which is an exponential function of  $\phi$  and the temperature. Once the basic properties of the cathode are known the performance of the cathode can be predicted for the desired application.

Different techniques are available for relating the zero-field current density  $J_0$  of the cathode to the  $J\{V\}$  measurements depending on the magnitude of  $J_0$  and the range of voltage used in the test. The development of theory covering three modes of operation - two which neglect the effect of space charge and one which includes space-charge effects - is reviewed below. (1) If the voltage is sufficiently large to overcome space-charge effects in the interelectrode space, the current becomes an exponential function of the square root of the voltage. This relationship between the current and voltage is known as the Schottky effect. (2) If  $J_0$  is sufficiently small, space charge effects can be neglected for values of  $J$  up to  $J_0$ . For this experimental condition the data do not show the increase of current due to the Schottky effect until the voltage is increased far beyond the value needed to obtain  $J_0$ . In this case the current is an exponential function of the voltage up to  $J_0$  and then a very sharp saturation for  $J$  greater than  $J_0$ . (3) If space-charge effects are significant at  $J_0$ , the current departs from the exponential behavior at low voltages and rises to  $J_0$  according to the space-charge theory. Following a review of the historical development of theory for these three modes of operation is an overview of the new additions to this theory. The new additions to the theory are then developed in detail in the body of the report.

## 1. BACKGROUND

The exponential nature of the current as a function of voltage in the retarding field range is discussed by Davisson (Reference 1). If space-charge effects are small, the current density saturates abruptly and remains steady at  $J = J_0$ . Shelton (Reference 2) gives experimental data which fit this theory very precisely and shows how to evaluate the basic cathode properties in terms of the experimental data for his particular example. Medicus (Reference 3) generalizes the work of Shelton and Davisson to develop a systematic method for analyzing retarding field data.

Schottky (Reference 4) explains the exponential rise in current with the square root of the voltage for large voltages (accelerating field at the cathode). In the absence of space-charge effects the applied potential interacts with the surface fields near the cathode to lower the work function. The fact that the surface field is accurately represented by the image of the electron in the conducting surface has been established by the agreement of Schottky theory with experimental data (Reference 5, p 109). Hutchison (Reference 6, p 305) gives a review of Schottky theory.

Langmuir (References 7 and 8) summarizes and extends previous work to give a theoretical treatment of the effects of space charge in the interelectrode space. Langmuir develops functions  $n$  and  $\xi$  representing the voltage and distance in the space between a parallel-plane cathode and anode and outlines a series of steps to calculate the current as a function of voltage for this type of diode. Van der Ziel (Reference 9) shows that Langmuir's  $n$ ,  $\xi$  functions can be extended to cover retarding-field and accelerating-field conditions as well as space-charge conditions, however, he neglects the effect of the electron image field. Van der Ziel mentions the transition point from retarding field to space charge conditions and names it the "exponential point". Although Van der Ziel gives a method of computing  $n$  and  $\xi$  for accelerating field conditions, his theory still predicts that the current density is identically  $J_0$  for accelerating field conditions since he neglects the Schottky effect. Kleynen (Reference 10) gives several useful formulas for calculating  $n$  and  $\xi$  and extends the tables of  $n$ ,  $\xi$  values given by Langmuir.

Ferris (Reference 11) takes the space-charge theory developed to this point and presents it as a family of normalized  $J(V)$  curves which can be used to analyze experimental data. The experimental data are presented in normalized form and superimposed on the family of  $J(V)$  curves allowing  $J_0$  to be determined. The normalizing constant introduced by Ferris is  $I_e$ , which represents the maximum current density which can be drawn to the anode under retarding-field conditions for the condition that  $I_0$  tends to infinity. Crowell (Reference 12) presents a slightly amended normalization technique which simplifies the family of curves presented by Ferris. Nottingham (Reference 13, p 65) uses  $I_e$ , the current at the "exponential point", as a normalizing constant to give a family of  $J(V)$  curves only slightly different from those of Ferris. Nottingham presents experimental data showing that the second derivative of  $J(V)$  has a sharp peak at the exponential point. However, Nottingham uses the second derivative only in conjunction with his family of  $J(V)$  curves to evaluate  $J_0$ . Finally Rittner (Reference 14) presents Langmuir's  $n$ ,  $r$  tables as interpolation formulas suitable for use on a digital computer and shows that Langmuir's theory accurately matches experimental  $J(V)$  data.

Aside from this main development of the space-charge theory Crowell (Reference 15) discusses a method using the second derivative of  $J(V)$  in an approximate determination of  $J_0$ . Crowell uses a numerical study covering a wide range of  $J_0$  values to show that Langmuir's theory predicts an inflection point in the  $J(V)$  function. This gives theoretical justification to the standard practice of associating the inflection point of experimental  $J(V)$  data with  $J_0$  (IRE standard definition of inflection point current (Reference 16). Crowell gives formulas for calculating  $dJ/dV$  and  $d^2J/dV^2$  implying a functional relationship for  $J(V)$ . However Crowell does not exhibit  $J(V)$  in functional notation. He continues to rely on a series of descriptive steps for calculating  $J(V)$ .

## 2. OVERVIEW

The work presented in this report extends the space-charge theory of parallel-plane diodes in several ways. Space-charge effects are included in the accelerating field range to remove the incompatibility between Langmuir theory and Schottky theory. A method is developed to use

a measurement of  $J_e$  at the exponential point to calculate  $J_0$  without resorting to matching a family of curves. A number of properties of Langmuir space-charge theory is described in much greater detail than has previously been done through the use of functional notation to express  $J(V)$ . These details are brought out in a discussion of the fields and charge in the interelectrode space. As a side light, a method is developed to handle the edge effects in a class of parallel-plane diode testers.

The effects of space-charge in the accelerating-field range are accounted for through the interaction of the space-charge field with the electron image field. The theory calculates a  $J(V)$  curve which rises from  $J = J_0$  with the Child's law slope and then approaches the  $J(V)$  curve generated from Schottky theory. Since Langmuir space-charge theory predicts that  $J(V)$  approaches  $J = J_0$  with zero slope, this theory predicts a discontinuity in the slope of  $J(V)$  at  $J = J_0$ . This discontinuity is pronounced in the  $J(V)$  plots for low values of  $J_0$  while it occurs over such a narrow range of  $J$  values for large  $J_0$  that it is not visible in the  $J(V)$  plots. However, the theoretical discontinuity shows up as a sharp minimum in experimental second derivative plots (Reference 13, p 135) and is expected to be apparent even for large  $J_0$ . Observation of this discontinuity should aid in the evaluation of cathodes even in the presence of multiple work-function patches. An application of this extended theory is given to show how a common "cathode evaluation technique" lacks theoretical justification. The theory shows how this "evaluation technique" leads to erroneous values of  $J_0$  which are dependent on the diode spacing. (Reference 17 gives experimental data demonstrating this problem.) A close examination of the transition point from the retarding-field range into the accelerating field range (the "exponential point") results in a method for determining  $J_0$  from a measurement of the current density  $J_e$  at this transition point. This evaluation of  $J_0$  is accomplished with a single graph of  $J_0$  as a function of  $J_e$  without the matching of experimental  $J(V)$  data to a family of  $J(V)$  curves as was previously necessary. The theory calculates a discontinuity in the second derivative which shows up as a sharp peak in second derivative data measured by

Nottingham (Reference 13, p 135). This evaluation technique is valid for high-work-function cathodes and can be applied to low-work-function cathodes at reduced temperature.

Previously, Langmuir space-charge theory has been used to calculate values of  $V$  for given values of  $J$  through a series of steps (or flow chart) without the use of a mathematical expression for  $V$  as a function of  $J$ . By exhibiting  $V(J)$  as a mathematical expression, trends can be observed and limits and derivatives can be calculated. As an example of the importance of functional notation the braces  $\{ \}$  are reserved in this report for designating "function of" (for example  $\{F\}$ ,  $J(V)$ ,  $\ln(x)$ ).

The use of functional notation for the  $V(J)$  relationship has led to the description of a number of properties of Langmuir space-charge theory in much greater detail, than has previously been done. The theory shows mathematically that there is always an inflection point for  $J(V)$  in the space-charge range and this inflection point coincides with a discontinuity in the second derivative  $d^2J/dV^2$  when  $J_0$  is very small. The theory shows that  $J$  always approaches  $J_0$  with a slope  $dJ/dV$  equal to zero. The limiting values of several other derivatives of current, fields and charge density functions are evaluated at the exponential point, at the transition point from space-charge to accelerating field conditions, and at the cathode surface.

As a side light the report gives an extension of Schottky theory (without space-charge) to include the effects of edges in a class of parallel-plane diodes. The field solution of a plane edge above an infinite plane is used to estimate the departure from parallel-plane fields near the cathode edge. For a typical example the edge effects introduce a  $66^\circ\text{C}$  error in temperature calculations based on Schottky theory while introducing no significant error in the determination of the zero field current  $J_0$ .

## 3. THERMIONIC EMISSION

The behavior of a free-electron gas in a three-dimensional potential well is sufficient to explain the basic properties of thermionic emission from metallic cathodes. The number density of electrons in the free-electron gas with momentum values lying in the interval  $dp_x dp_y dp_z$  is given by Reference 6.

$$N\{p\} dp_x dp_y dp_z = \frac{2}{h^3} \frac{dp_x dp_y dp_z}{\exp\{[(p_x^2 + p_y^2 + p_z^2)/2m - E_F]/kT\} + 1} \quad (1)$$

where

$m = 9.109 \times 10^{-31}$  [kg] = mass of an electron

$k = 1.380 \times 10^{-28}$  [J/°K] = Boltzmann's constant

$h = 6.625 \times 10^{-34}$  [J.sec] = Planck's constant

$T$  = temperature [°K]

$E_F$  = energy of the Fermi level [J]

Equation 1 is the product of the number of states existing in the potential well within that range of momentum, times the probability that the states are occupied at temperature  $T$ . The wave nature of the electron is used to obtain the number of energy states available. The statistical theory of particles, in which only two particles are allowed in an energy state at one time, is used to determine which of the possible energy states are occupied at a given, nonzero temperature. The Fermi level  $E_F$  is the highest energy state which is filled when all lower energy states are filled (at 0°K). The reference level for zero energy is the bottom of the conduction band for this derivation.

If the potential well has a finite depth, with wall height  $\phi$  electron volts above  $E_F$ , Equation 1 shows that some electrons will have sufficient energy to escape. For these escaping electrons, the exponential term in Equation 1 will be  $\exp\{e\phi/kT\}$  or larger where  $e$  ( $= 1.602 \times 10^{-19}$  [C]) is the charge of an electron. For thermionic emitters  $\phi$  is of the order of a

few electron volts so the exponential term is of the order of  $1 \times 10^5$ . So, for the escaping electrons, the 1 in Equation 1 can be neglected compared to the exponential term. Equation 1 then becomes

$$N(p) dp_x dp_y dp_z = (2/\hbar^3) \exp\{[E_F - (p_x^2 + p_y^2 + p_z^2)/2m]/kT\} dp_x dp_y dp_z \quad (2)$$

For convenience let the normal to the surface lie in the x direction. Since the integral

$$\int_{-\infty}^{\infty} \exp\{-p_u^2/2mkT\} dp_u = \sqrt{2\pi mkT} \quad (3)$$

for  $u = x$  or  $y$ , the number density of electrons with momentum in the interval  $dp_x$  is given by

$$N(p_x) dp_x = (4\pi mkT/\hbar^3) \exp\{E_F/kT\} \exp\{-p_x^2/2mkT\} dp_x \quad (4)$$

If there are no fields external to the potential well, electrons with momentum  $p_{x_0}$  can escape where

$$p_{x_0}/2m = E_F + e\phi \quad (5)$$

Then the total current escaping from the potential well is the charge of the electron  $e$  times the number density of the electrons  $N(p_x)$  times the velocity of the electrons  $p_x/m$  summed over those values of momentum from  $p_{x_0}$  to infinity:

$$J_0 = \int_{p_{x_0}}^{\infty} (e/m) p_x N(p_x) dp_x \quad (6)$$

The subscript "0" denotes the absence of external fields, and  $J_0$  is referred to as the zero-field current density. After integration, Equation 6 becomes

$$J_0 = (4\pi mek^2T^2/\hbar^3) \exp\{-e\phi/kT\} [A/m^2] \quad (7)$$

which is the Richardson-Dushman equation (Reference 6).

Equation 7 is more commonly expressed as

$$J_0 = AT^2 \exp(-e\phi/kT) \quad (8)$$

where

$$A = 4\pi mek^2/h^3 \quad (9)$$

and A has a numerical value of approximately 120 [ $A/(cm^2 \cdot 0K^2)$ ].

If the electrons experience an external retarding potential of height  $V_s$  above  $\phi$  as shown in Figure 1, fewer electrons will escape so the current  $J$  escaping from the cathode will be less than  $J_0$ . The derivation of Equation 7 applies with the use of  $\phi + V_s$  instead of  $\phi$ . Then Equation 7 becomes

$$J = (4\pi mek^2 T^2/h^3) \exp\{-e(\phi + V_s)/kT\} \quad (10)$$

where the zero field subscript is omitted. Equation 10 can also be written

$$J = J_0 \exp\{-eV_s/kT\} \quad (11)$$

where  $J_0$  is given by Equation 7.

Since the Fermi level  $E_F$  is measured relative to the bottom of the conduction band, current will flow in an external circuit connected between the cathode and an anode unless the Fermi levels are at the same potential. So, the applied voltage  $V_{app}$  (or measured voltage) of the anode with respect to the cathode is just the difference in potential between the Fermi levels of the anode and cathode. Figure 2 shows for the case where the potential minimum occurs at a collecting body (or anode) that the applied voltage is

$$V_{app} = -V_s - (\phi_c - \phi_a) \quad (12)$$

The derivation through Equation 11 applies to particles of charge  $+e$ , although electrons are conventionally assigned a negative charge. This conflict causes no trouble if the direction of increasing potential is

taken downward in Figures 1 and 2 for the development through Equation 11. However when measurements are involved such as  $V_{app}$  which assume the negative charge for the electron, the direction of increasing potential must be taken upward. For this reason  $V_s$  appears with a negative sign in Equation 12.

For the condition that the potential minimum occurs at the anode, combination of Equations 11 and 12 gives

$$J = J_0 \exp \{e(V_{app} + \phi_c - \phi_a)/kT\} \quad (13)$$

which shows that the current is an exponential function of the applied voltage. This is known as the "retarding-field" or "exponential" range of the J-V curve. A plot of  $\ln\{J\}$  as a function of  $V_{app}$  gives a straight line with slope  $e/kT$ . The current  $J$  equals  $J_0$  when

$$V_{app} = \phi_a - \phi_c \quad (14)$$

Figure 3 shows a schematic of the I-V Curve under these conditions. Note that Equation 13 is actually independent of  $\phi_c$ , as long as  $J$  is less than  $J_0$ , since  $\phi_c$  is cancelled by the  $J_0$  term. This is shown through the combination of Equations 8 and 13 which yields

$$J = AT^2 \exp \{e(V_{app} - \phi_a)/kT\} \quad (15)$$

## SECTION II

### SPACE-CHARGE THEORY

Figure 1 shows a schematic of the space-charge region outside an emitting surface. The position and magnitude of the potential minimum determines the amount of current which is collected at an anode spaced some distance away from the cathode. If the potential minimum occurs at the anode, the potential decreases at each point from the cathode to the anode. If the potential minimum occurs at the cathode, the potential increases at each point from the cathode to the anode. For the intermediate case of a potential minimum somewhere between the cathode and anode, retarding-field conditions occur near the cathode and accelerating-field conditions apply near the anode. For this intermediate case the electric field  $-dV/dx$  at the minimum is, of course, zero. Since, for the intermediate condition, the current is greatly influenced by the mutual repulsion of the electrons, this is known as the space-charge region of the  $J(V)$  curve.

#### 1. DERIVATION OF LANGMUIR'S DIFFERENTIAL EQUATION

The following discussion derives the basic equations which describe the effect of space-charge on  $J(V)$ . Electrons with energy less than  $E_F + e\phi$  are turned back right at the metal-vacuum interface. Electrons with energy greater than  $E_F + e\phi$  enter the space outside the cathode and are acted on by the external potential. At a position  $x$  outside the cathode surface, electrons of a given energy from the momentum distribution of Equation 4 have lost momentum due to the barrier at the surface and due to the potential field outside the surface. As indicated in Figure 1, which shows a schematic of the space charge region outside an emitting surface, the net loss of energy is  $E_F + e\phi + eV_s - eV(x)$  at position  $x$ . Note that  $V(x)$  is measured relative to the potential minimum. If Equation 4 is adjusted for this lost energy, it gives the number density of electrons as a function of momentum at position  $x$  as written in Equation 16

$$N(p_x)dp_x = (4\pi m k T / h^3) \exp\{E_F/kT\} \exp\{-(p_x^2/2m + E_F + e\phi + eV_s - eV(x))/kT\} dp_x \quad (16)$$

To the anode side of the potential minimum, the lowest energy electrons at position  $x$  will have energy  $+ eV(x)$  due to electric field acceleration. To the cathode side of the minimum, electrons will be present with momentum from zero to infinity toward the anode. In addition, electrons will be present with energy from 0 to  $eV(x)$  returning toward the cathode from the direction of the potential minimum. Then to find the total number density of electrons at  $x$  the limits of integration will be  $\pm (2meV(x))^{1/2}$  with the + sign taken in the anode space (to the anode side of the potential minimum) and the - sign taken in the cathode space. This integration of Equation 16 then gives

$$N\{V(x)\} = [(2\pi m k T)^{3/2} / h^3] \exp \{-e(V_s + \phi)/kT\} \exp\{eV(x)/kT\} \cdot [1 \mp P\{(eV(x)/kT)^{1/2}\}] \quad (17)$$

where  $P(u) = (2/\sqrt{\pi}) \int_0^u e^{-t^2} dt = \text{error function integral}$  (18)

In Equation 17 the - sign applies in the anode space and the + sign applies in the cathode space.

The electric potential outside the metal is governed by Poisson's equation

$$d^2V(x)/dx^2 = eN/\epsilon_0 \quad (19)$$

where

$$\epsilon_0 = 1/(36\pi \times 10^9) [C/Vm] = \text{permittivity of vacuum}$$

and  $x$  is measured from the position of the potential minimum. The combination of Equations 17 and 19 and the introduction of the normalized variables

$$\eta = eV(x)/kT \quad (20)$$

and

$$\xi = x/x_1 \quad (21)$$

where

$$x_1^2 = \epsilon_0 k T h^3 \exp \{e(V_s + \phi)/kT\} / 2e^2 (2\pi m kT)^{3/2} \quad (22)$$

yields the equation

$$d^2 n / d\xi^2 = 1/2 \exp \{n\} [1 \mp P\{\sqrt{n}\}] \quad (23)$$

This equation represents the potential distribution as a function of distance from the potential minimum. The normalizing constant  $x_1$  as more conveniently written

$$x_1^2 = \epsilon_0 (kT)^{3/2} / Je (2\pi m)^{1/2} \quad (24)$$

where  $J$  is given by Equation 10.

Multiplication of Equation 23 by  $dn/d\xi$  and integration with respect to  $\xi$  gives

$$(dn/d\xi)^2 - \dot{n}_0^2 = [1 \mp P\{\sqrt{n}\}] \exp \{n\} - [1 \mp 2(n/\pi)^{1/2}] \quad (25)$$

where  $\dot{n}_0$  is defined as

$$\dot{n}_0 \equiv dn/d\xi|_{\xi=0} \quad (26)$$

As before, the - sign of the  $\mp$  applies in the anode space and the + sign applies in the cathode space. In order to maintain a positive direction for  $\xi$  from cathode to anode, the square root of Equation 25 must be taken with a negative sign in the cathode space and positive sign in the anode space, giving

$$\text{anode space } dn_a/d\xi = (\dot{n}_0^2 + [1 - P\{\sqrt{n_a}\}] \exp \{n_a\} - [1 - 2(n_a/\pi)^{1/2}])^{1/2} \quad (27)$$

$$\text{cathode space } d\xi/dn_c = -(\dot{n}_0^2 + [1 + P\{\sqrt{n_c}\}] \exp \{n_c\} - [1 + 2(n_c/\pi)^{1/2}])^{-1/2} \quad (28)$$

The subscripts on  $\eta_a$  and  $\eta_c$  are added to distinguish the anode space and cathode space respectively. The reciprocal expression  $d\xi/d\eta_c$  is used in the cathode space since the following development of the J-V curve requires  $\eta_a$  as a function of  $\xi$  and requires  $\xi$  as a function of  $\eta_c$ . Rittner (Reference 14) has compiled a collection of accurate approximation formulas for the solutions to Equations 27 and 28 for  $\eta_0 = 0$ . Rittner claims a maximum of .01% relative error within the cited range for the following formulas:

$$0 \leq \eta_c \leq 0.20; \quad \xi_c = -2\eta_c^{1/2} + .376126\eta_c + .0251956\eta_c^{3/2} + .00069163\eta_c^2 - .0009409\eta_c^{5/2} \quad (29)$$

$$0.20 \leq \eta_c \leq 3.0; \quad \xi_c = \frac{-6.156143\eta_c - 65.9123\eta_c^2 - 59.4892\eta_c^3 + 4.103353\eta_c^4}{-0.2629089 - 14.62018\eta_c - 49.59515\eta_c^2 - 16.06387\eta_c^3 + \eta_c^4} \quad (30)$$

$$3.0 \leq \eta_c; \quad \xi_c = -2.55389 + \sqrt{2} \exp \{-\eta_c/2\} - 0.0123 \exp \{-\eta_c\} + (1/3\sqrt{2})[(\eta_c/\pi)^{1/2} + 1] \exp \{-3\eta_c/2\} \quad (31)$$

$$0 \leq \eta_a \leq 0.05; \quad \eta_a = 0.25 \xi_a^2 - 0.047016 \xi_a^3 + 0.012627 \xi_a^4 - 0.003820 \xi_a^5 \quad (32)$$

$$0.05 \leq \eta_a \leq 11.0; \quad \eta_a = 0.0003053192 - 0.0010857509 \xi_a + .2509922 \xi_a^2 - 0.04648354 \xi_a^3 + 0.01094699 \xi_a^4 - 0.002286296 \xi_a^5 + 0.0003642352 \xi_a^6 - 0.00004062638 \xi_a^7 + 0.000002943653 \xi_a^8 - 0.000000123597 \xi_a^9 + 0.0000000022744 \xi_a^{10} \quad (33)$$

$$11.0 \leq n_a : n_a = [(\xi_a + 0.5088)/1.2552]^{4/3} - 1.5232(\xi_a + 0.5088)^{2/3} + 1.347 - 0.495 (\xi_a + 0.5088)^{-2/3} - 0.140(\xi_a + 0.5088)^{-4/3} \quad (34)$$

Equation 31 comes from Langmuir (Reference 7), and Equation 34 is the inverse of a series given by Langmuir. Equations 29 and 32 are series solutions to the differential equations, Equations 28 and 27 respectively, taken from Kleynen (Reference 10). Rittner developed Equations 30 and 33 by applying standard curve fitting techniques to tables of  $n$  and  $\xi$  values given by Langmuir. Langmuir generated the  $n$ ,  $\xi$  values by numerical integration of the differential equations. (Rittner gives a different coefficient for  $\xi_a^5$  than the value shown here from Kleynen. The discussions in subsection 2 show how to verify that Kleynen's value is the correct one.)

For space-charge conditions, as discussed above, the potential minimum occurs between the cathode and anode and  $dV/dx$  is zero at the minimum. For this reason one has

$$dn/d\xi|_{\xi=0} = \dot{n}_0 = 0 \quad (35)$$

for space charge conditions. A plot of  $n(\xi)$  is shown in Figure 4 along with the first and second derivatives. These derivatives will be useful below in discussions of the behavior of  $J(V)$ . Figure 4 was generated through the use of Equations 29 through 34 and Equations 23, 27, and 28. Notice that  $\xi$  approaches the limiting value of -2.55389 as shown by Equation 31 when  $n_c$  tends to  $\infty$ .

## 2. SERIES SOLUTIONS FOR THE $n$ , $\xi$ FUNCTIONS

Although Kleynen (Reference 10) does not discuss how he derived the series solutions for the  $n$ ,  $\xi$  functions given in Equations 29 and 32, the following discussion gives one way of deriving the terms which Kleynen gives and of deriving additional terms:

Let  $\dot{n}_0 = 0$  and let

$$u = \sqrt[n]{n_a} \quad (36)$$

then Equation 27 becomes

$$du/d\xi = ([1 - P(u)] \exp \{u^2\} - [1-2u/\sqrt{\pi}])^{1/2}/2u \quad (37)$$

From Equation 18 the derivative of  $P(u)$  is

$$dP/du = (2/\sqrt{\pi}) \exp \{-u^2\} \quad (38)$$

so the derivative of Equation 37 becomes

$$d^2u/d\xi^2 = ((u^2-1)[1 - P(u)] \exp \{u^2\} + [1-2u/\sqrt{\pi}])/4u^3 \quad (39)$$

Successive derivatives give

$$\begin{aligned} d^3u/d\xi^3 &= ([2u^4-3u^2+3][1-P(u)]\exp\{u^2\}-[3-6u/\sqrt{\pi}+2u^3/\sqrt{\pi}]) \\ &\quad \cdot (du/d\xi)/4u^4 \end{aligned} \quad (40)$$

and

$$\begin{aligned} d^4u/d\xi^4 &= (d^3u/d\xi^3)(d^2u/d\xi^2)/(du/d\xi) \\ &\quad + ([4u^6-6u^4+12u^2-12][1-P(u)]\exp\{u^2\}-[4u^5+8u^3-24u]/\sqrt{\pi}+12) \\ &\quad \cdot (du/d\xi)^2/4u^5 \end{aligned} \quad (41)$$

Application of L'Hospital's rule (Reference 18) to  $(du/d\xi)^2$ ,  $d^2u/d\xi^2$  and the zero/zero terms in  $d^3u/d\xi^3$  and  $d^4u/d\xi^4$  gives the following values for these derivatives at  $\xi = 0$ :

$$\begin{aligned} du/d\xi &= 1/2; \quad d^2u/d\xi^2 = -1/6\sqrt{\pi}; \quad d^3u/d\xi^3 = 1/16 \\ d^4u/d\xi^4 &= -29/240 \sqrt{\pi} \end{aligned} \quad (42)$$

The Taylor series (Reference 18) about  $\xi = 0$  then gives

$$u(\xi) = a_1 \xi + a_2 \xi^2 + a_3 \xi^3 + a_4 \xi^4 \quad (43)$$

where

$$a_1 = 1/2; a_2 = -1/12\sqrt{\pi}; a_3 = 1/96; a_4 = -29/5760\sqrt{\pi} \quad (44)$$

The coefficient  $a_0 = u(\xi = 0)$  is zero since the reference voltage and hence  $u$  is chosen to be zero at  $\xi = 0$ .

To obtain an equation of the form of Equation 32 requires  $n_a = u^2$ , that is:

$$n_a = b_2 \xi^2 + b_3 \xi^3 + b_4 \xi^4 + b_5 \xi^5 \quad (45)$$

The coefficients  $b_n$  are found from a product of Equation 43 with itself.

$$b_2 = a_1^2; b_3 = 2a_1a_2; b_4 = 2a_1a_3 + a_2^2; b_5 = 2a_1a_4 + 2a_2a_3 \quad (46)$$

Here  $b_0$  and  $b_1$  are zero since  $a_0$  is zero. Combination of Equations 44 and 46 gives:

$$b_2 = 1/4; b_3 = -1/12\sqrt{\pi}; b_4 = (1/2 + 1/3\pi)/48 \quad (47)$$

$$b_5 = -39/5760\sqrt{\pi}$$

Equation 32 results from a substitution of the numerical values from Equation 47 into Equation 45.

In order to establish Equation 29, let

$$v = \sqrt{n_c} \quad \text{and} \quad \xi = -z \quad (48)$$

Then the derivatives of  $v$  with respect to  $z$  are very similar to those shown in Equations 37 through 41. In fact, the numerical values at  $z = 0$  of  $d^n v/d z^n$  are the same as the values of  $d^n u/d \xi^n$  with the variations appearing only in the sign. The values of the derivatives at  $z = 0$  are shown in Equation 49:

$$\begin{aligned} dv/dz &= 1/2; \quad d^2 v/dz^2 = 1/6\sqrt{\pi}; \quad d^3 v/dz^3 = 1/16; \\ d^4 v/dz^4 &= 29/240\sqrt{\pi}; \quad d^5 v/dz^5 = 1/10\pi + 9/128 \end{aligned} \quad (49)$$

The Taylor series about  $z = 0$  then gives

$$v(z) = c_1 z + c_2 z^2 + c_3 z^3 + c_4 z^4 + c_5 z^5 \quad (50)$$

where

$$c_n = (1/n!)(d^n v/dz^n) \quad (51)$$

The function  $v(z)$  is then obtained by substituting  $\xi = -z$  back in Equation 50:

$$v(\xi) = g_1 \xi + g_2 \xi^2 + g_3 \xi^3 + g_4 \xi^4 + g_5 \xi^5 \quad (52)$$

where

$$g_1 = -1/2; g_2 = 1/12\sqrt{\pi}; g_3 = -1/96; g_4 = 29/5760\sqrt{\pi} \quad (53)$$

$$g_5 = -(1/10\pi + 9/128)/120$$

A comparison of Equations 52 and 53 with Equations 43 and 44 show that

$$u(\xi) = -v(\xi) \quad (54)$$

where the equality is taken in the sense of the Taylor series representation. Consequently the square of Equation 54 shows that the Taylor series representation for  $n_a(\xi)$  is exactly the same as the Taylor series representation of  $n_c(\xi)$  at  $\xi = 0$ . This shows that the function  $n_a$  taken as an extension of the function  $n_c$  is continuous at  $\xi = 0$  and has continuous derivatives.

To obtain an equation of the form of Equation 29 requires  $z(v)$  rather than  $v(z)$ , that is

$$z = d_1 v + d_2 v^2 + d_3 v^3 + d_4 v^4 + d_5 v^5 \quad (55)$$

The derivatives of the inverse function  $z(v)$  can be found from formulas relating the derivatives of the inverse function to the derivatives of

the original function, some of which are given by Pierce (Reference 19, p 100). The formulas necessary in this case are

$$\frac{dz}{dv} = 1/\dot{v} \quad (56)$$

$$\frac{d^2z}{dv^2} = -\dot{v}/(\dot{v})^3 \quad (57)$$

$$\frac{d^3z}{dv^3} = [3(\ddot{v})^2 - \dot{v}\ddot{v}]/(\dot{v})^5 \quad (58)$$

$$\frac{d^4z}{dv^4} = [10\dot{v}\ddot{v}\ddot{v} - 15(\ddot{v})^3 - (\dot{v})^2v^{iv}]/(\dot{v})^7 \quad (59)$$

$$\begin{aligned} \frac{d^5z}{dv^5} = 10[(\ddot{v})^2(\dot{v})^2 + 15\dot{v}v^{iv}(\dot{v})^2 - 105(\ddot{v})^2\dot{v}\dot{v} \\ + 105(\dot{v})^4 - v^v(\dot{v})^3]/(\dot{v})^9 \end{aligned} \quad (60)$$

where, for example,  $d^3v/dz^3$  has been shortened to  $\ddot{v}$ , and  $d^4v/dz^4$  has been shortened to  $v^{iv}$ . Using the formula

$$d_n = (1/n!)(d^n z/dv^n) \quad (61)$$

with Equations 49 and 56 through 60 gives:

$$\begin{aligned} d_1 &= 2; \quad d_2 = -2/3\sqrt{\pi}; \quad d_3 = -(1 - 8/3\pi)/6; \\ d_4 &= -2(5/3\pi - 21/40)/9\sqrt{\pi}; \quad d_5 = (1/2 - 72/5\pi + 1120/27\pi^2)/120 \end{aligned} \quad (62)$$

Substitution of Equation 48 into Equation 55 gives

$$\xi = -d_1 \frac{1}{c}^{1/2} - d_2 \frac{1}{c}^{3/2} - d_3 \frac{1}{c}^{5/2} - d_4 \frac{1}{c}^2 - d_5 \frac{1}{c}^{5/2} \quad (63)$$

Finally, the use of Equation 62 in Equation 63 gives the series shown in Equation 29.

For the case where  $\dot{\eta}_0 = 0$ , Taylor series do not exist for  $\eta_a(\xi)$  or  $\dot{\eta}_a(\xi)$ . This is seen on examination of the third derivative of Equation 27

$$\begin{aligned} d^3\eta_a/d\xi^3 &= (1/2)[(1 - P(\sqrt{\eta_a})) \exp(\eta_a) - 1/\sqrt{\pi\eta_a}] \\ &\cdot [\eta_0^2 + (1 - P(\sqrt{\eta_a})) \exp(\eta_a) - (1 - 2\sqrt{\eta_a}/\pi)]^{1/2} \end{aligned} \quad (64)$$

The term  $1/\sqrt{\eta_a}$  increases without bound as  $\eta_a$  approaches zero, showing that the third derivative of  $\eta_a(\xi)$  is unbounded at  $\xi = 0$ . Equations 23 and 27 show that at  $\xi = 0$

$$\frac{d\eta_a}{d\xi} = \dot{\eta}_0 \quad \text{and} \quad \frac{d^2\eta_a}{d\xi^2} = 1/2 \quad (65)$$

This information along with Equations 58 and 64 shows that  $d^3\xi/dn_a^3$  is also unbounded at  $\xi = 0$ .

Further evaluation of the derivatives shows that the derivatives  $d^n n_a/d\xi^n$  has a term involving  $1/n_a^{(n-5/2)}$ . If  $n_0 = 0$ , this term is multiplied by a term

$$[(1 - P\{\sqrt{n_a}\}) \exp\{n_a\} - (1 - 2\sqrt{n_a/\pi})]^{(n-2)/2}$$

which tends to zero at  $n_a = 0$ . This gives a zero/zero form which has a limit and allows the series of Equation 32 to be developed. If  $n_0 \neq 0$  all these derivatives are unbounded at  $n_a = 0$ .

However, it may be possible to find functions  $u\{n_a\}$  so that the series

$$u = u_0 + u_1\xi + u_2\xi^2 + u_3\xi^3 + \dots \quad (66)$$

or

$$\xi = v_0 + v_1u + v_2u^2 + v_3u^3 + \dots \quad (67)$$

exists at  $n_a = \xi = 0$ . In fact, if  $u\{n_a\}$  is chosen as

$$u = \sqrt{n_a} \quad (68)$$

the derivatives  $d^n\xi/du^n$  follow from Equation 27 and are well behaved at  $u = \xi = 0$ . For example the fourth derivative is

$$\begin{aligned} \frac{d^4\xi}{du^4} &= \frac{-(8u^4 + 24u^2 + 6)(1 - P\{u\}) \exp\{u^2\} + 2(4u^3 + 10u)/\sqrt{\pi}}{(\dot{n}_0^2 + [1 - P\{u\}] \exp\{u^2\} - [1 - 2u/\sqrt{\pi}])^{3/2}} \\ &+ \frac{36(u^4 + u^2)[1 - P\{u\}]^2 \exp\{2u^2\} - (36u^3/\sqrt{\pi})[1 - P\{u\}]\exp\{u^2\}}{(\dot{n}_0^2 + [1 - P\{u\}] \exp\{u^2\} - [1 - 2u/\sqrt{\pi}])^{5/2}} \\ &- \frac{30u^4[1 - P\{u\}]^3 \exp\{3u^2\}}{(\dot{n}_0^2 + [1 - P\{u\}] \exp\{u^2\} - [1 - 2u/\sqrt{\pi}])^{7/2}} \end{aligned} \quad (69)$$

Since Equation 67 is a Taylor series, the terms  $v_n$  are given by

$$v_n = (1/n!) \left. \frac{d^n\xi}{du^n} \right|_{u=0} \quad (70)$$

The calculation of the derivatives as in Equation 69 and their evaluation at  $u = \xi = 0$  gives

$$v_0 = v_1 = 0; \quad v_2 = 1/\dot{n}_0; \quad v_3 = 0; \quad v_4 = -1/4\dot{n}_0^3; \quad (71)$$

$$v_5 = 4/15\sqrt{\pi}\dot{n}_0^3; \quad v_6 = -(2/\dot{n}_0^3 - 3/\dot{n}_0^5)/24; \quad v_7 = 2(4/\dot{n}_0^3 - 15/\dot{n}_0^5)/105\sqrt{\pi}$$

The combination of Equations 67 and 68 and omission of the zero terms gives

$$\xi = v_2 n_a + v_4 n_a^2 + v_5 n_a^{5/2} + v_6 n_a^3 + v_7 n_a^{7/2} \quad (72)$$

Figure 5 shows a plot of  $n_a$  versus  $\xi$  generated from Equation 72 with  $\dot{n}_0 = 0.5$ . The series solution with up to the seventh power of  $u$  from Equation 72 is shown along with the series solution truncated at the sixth power of  $u$ . The full series solution is useful up to  $\xi$  equal to about 0.6. Since the coefficients involve reciprocal powers of  $\dot{n}_0$  in Equation 71, one might expect the series to behave better at larger values of  $\dot{n}_0$ . Although the series is able to handle larger values of  $n_a$  as  $\dot{n}_0$  becomes large, the range of accuracy for  $\xi$  is still  $\xi < 1$ . Note that  $n_a$  is a steeply rising function of  $\xi$  for large values of  $\dot{n}_0$ . The function  $n_a(\xi)$  calculated by numerical integration is shown in Figure 5 for comparison with the series solution. The numerical-integration solution procedure will be discussed in the next section.

### 3. NUMERICAL SOLUTIONS FOR THE $n$ , $\xi$ FUNCTIONS

If  $\dot{n}_0 = 0$ , integration of Equation 28 for  $n_c$  cannot be started at  $n_c = \xi = 0$  since  $dn_c/dn_c$  is unbounded at this point. Most numerical solution techniques for differential equations, such as the Runge-Kutta methods, can be used, however, if Equation 29 is used to start the solution procedure. The function  $n_a(\xi)$  also has starting problems with Runge-Kutta techniques.

The problem with  $n_a(\xi)$  is that  $dn_a/d\xi$  is a specified function of  $n_a$  starting at  $n_a = 0$ . Any solution technique such as the Runge-Kutta types which extrapolate values of  $n_a$  based on  $dn_a/d\xi$  will always give  $n_a(\xi) = 0$  for all  $\xi$  if it begins with  $n_a(0) = 0$ . This problem is solved through the

use of a Taylor method of second order or higher. A method which has been very useful is the mixed Runge-Kutta-Taylor method (Reference 20, p. 275). This method yields convergence of order  $h^3$ , where  $h$  is the step size, and uses the first and second derivatives of  $\eta_a$  from Equations 23 and 27. This solution method is especially convenient since the second derivative from Equation 23 has a simple form. The mixed Runge-Kutta-Taylor method for  $\eta_a$  generates a sequence of numbers  $\eta_n$ , for a fixed value of  $h$ , by the recurrence relation

$$\eta_0 = 0 \quad (73)$$

$$\eta_{n+1} = \eta_n + hG_3\{\eta_n; h\}$$

with

$$G_3\{\eta_a; h\} = f\{\eta_a\} + (h/2) f\{\eta_a + hf\{\eta_a\}/3\} \quad (74)$$

where

$$f = d\eta_a/d\xi \quad (75)$$

and  $f$  and  $f' = df/d\xi$  are given by Equations 23 and 27.

The accuracy of the Runge-Kutta-Taylor method solving for  $\eta_a(\xi)$  is limited less by the step size  $h$  than it is by the accuracy of the values calculated for the error function  $P(u)$ . The most satisfactory representation for  $P(u)$  used in this work comes from Abramowitz (Reference 21, page 299, Equation 7.1.26). This representation is

$$P(u) = 1 - (a_1 t + a_2 t^2 + a_3 t^3 + a_4 t^4 + a_5 t^5) \exp\{-u^2\} \quad (76)$$

where

$$t = 1/(1 + pu) \quad (77)$$

and

$$\begin{array}{ll} p = .3275911 & a_1 = .254829592 \\ a_2 = -.284496736 & a_3 = 1.421413741 \\ a_4 = -1.453152027 & a_5 = 1.061405429 \end{array} \quad (78)$$

Since the machine available for calculations in this work had only a six digit capability, the numerical values in Equation 78 were rounded to

$$\begin{aligned} p &= .327591 & a_1 &= .25483 & a_2 &= -.2845 \\ a_3 &= 1.42141 & a_4 &= -1.45315 & a_5 &= 1.06141 \end{aligned} \quad (79)$$

It is important in this round-off procedure to have the terms  $a_1$  through  $a_5$  to add to exactly 1. For example the rounding of  $a_2$  to -.284497 instead of the value in Equation 79 results in greatly increased error in the  $\eta_a$  values near  $\xi = 0$ . The use of Equation 76 for  $P(u)$  along with the numerical values in Equation 79 in the Runge-Kutta-Taylor solution procedure generates accurately the values of  $\eta_a(\xi)$  tabulated by Kleynen. With this representation of  $P(u)$ , step size  $h$  less than  $h = .01$  does not increase the accuracy of the solution. Step size  $h = .01$  generates the Kleynen (Reference 10) tables for  $\eta_a(\xi)$  accurate to the fourth place for  $\xi \geq 5$ , and  $h = 1.0$  gives good accuracy above  $\xi = 100$ . A BASIC computer language program using Equations 73 through 79 for solving Equation 27 is shown in Figure 6. A sample print-out from the program for  $h = .01$  is shown in Figure 7.

For the case where  $\dot{\eta}_0$  is greater than zero a first examination seems to indicate that a Runge-Kutta method would be better for solving for  $\eta_a(\xi)$  than the Runge-Kutta-Taylor method of Equation 74. Since the third derivative, Equation 64, of  $\eta_a(\xi)$  is unbounded at  $\xi = 0$ , one might expect problems with the calculation of  $\eta_a$  from Equations 73 and 74 which use values of the second derivative of  $\eta_a$ . Note that

$$\dot{f}(\eta_a) = d^2 \eta_a / d\xi^2 \quad (80)$$

This concern is based on the Taylor Theorem. When a function is generated from its first and second derivatives, the remainder term is related to the third derivative. In addition, when  $\dot{\eta}_0$  is greater than zero, the Runge-Kutta methods do not generate the spurious solution  $\eta_a \equiv 0$  as discussed earlier.

However, in practice, the Runge-Kutta-Taylor method yields much quicker convergence than the simplified Runge-Kutta method which uses the same number of function evaluations per step. This superior convergence is obtained over a wide range of values of  $\dot{n}_0$ . The simplified Runge-Kutta method is described by

$$\begin{aligned} n_0 &= 0 \\ n_{n+1} &= n_n + hK_2\{n_n; h\} \end{aligned} \quad (81)$$

with

$$K_2\{n_a; h\} = (1/2)[f\{n_a\} + f\{n_a + hf\{n_a\}\}] \quad (82)$$

where

$$f = dn_a/d\xi \quad (83)$$

and  $f$  is given by Equation 27. The convergence of the Runge-Kutta-Taylor method compared to the convergence of the simplified Runge-Kutta method is shown in Table 1 for the example  $\dot{n}_0 = .003$  at  $\xi = 5.0$ . Later work will show that these conditions correspond approximately to a cathode with  $I_0 = 30 \text{ mA/cm}^2$ ,  $T = 650^\circ\text{C}$ ,  $I = 1.002I_0$ , and cathode-anode spacing  $D = .05 \text{ mm}$ . Table 1 also compares the convergence of these two methods for the example  $\dot{n}_0 = .5$  at  $\xi_c = 1000$ . Later work will show that these conditions correspond approximately to a cathode with  $I_0 = 5\text{A/cm}^2$ ,  $T = 900^\circ\text{C}$ ,  $I = 1.1 I_0$ , and  $D = 1.0 \text{ mm}$ .

The superior convergence of the mixed Runge-Kutta-Taylor method results from its third order convergence, order of  $h^3$ , compared to the second order convergence, order of  $h^2$ , for the simplified Runge-Kutta method. For small values of  $\dot{n}_0$  the simplified Runge-Kutta method generates the solution  $n_a = \dot{n}_0 \xi$  which has nearly the error of the spurious solution  $n_a = 0$  generated for the case  $\dot{n}_0 = 0$ . On the other hand, the third derivative of  $n_a$  is large over a very small interval of values of  $\xi$  for small  $\dot{n}_0$ . For this reason, the total change in the second derivative is not large near  $\xi = 0$  and the Runge-Kutta-Taylor method accurately calculates  $n_a$ . For large values of  $\dot{n}_0$  the value of  $n_a$  is dominated by the first derivative so that large variations in the second derivative

TABLE 1

COMPARISON OF THE CONVERGENCE OF THE MIXED RUNGE-KUTTA-TAYLOR, R-K-T,  
METHOD WITH THE SIMPLIFIED RUNGE-KUTTA, R-K, METHOD

$$\dot{n}_0 = 1 \times 10^{-3} \quad \xi = 5$$

<u>step size</u>	<u><math>n_a</math> from R-K-T</u>	<u><math>n_a</math> from R-K</u>
.005	3.61135	3.61046
.01	3.61139	3.60858
.05	3.61163	3.58151
.1	3.61216	3.53811
.5	3.63247	3.13272
1.0	3.69794	2.62286
5.0	5.79598	.300455

$$\dot{n}_0 = 0.5 \quad \xi = 1000.$$

<u>step size</u>	<u><math>n_a</math> from R-K-T</u>	<u><math>n_a</math> from R-K</u>
.5	7287.76	7286.99
1	7288.19	7286.38
5	7291.94	7276.32
10	7297.70	7259.18
100	7494.38	6838.45
200	7804.92	6328.12

near  $\xi = 0$  do not cause problems with the accuracy. Consequently, the mixed Runge-Kutta-Taylor method accurately calculates  $n_a$  also for large  $n_0$ . Since the mixed Runge-Kutta-Taylor method converges faster for small  $n_0$  and at least as fast for large  $n_0$  it is used for the calculations reported later in this work. The criterion for the choice of  $h$ , used for  $n_0 > 0$  is the same as the criterion for  $n_0 = 0$  discussed above.

#### 4. THE CURRENT - VOLTAGE RELATIONSHIP FOR $J \leq J_0$

If  $J \leq J_0$ , Equations 27 and 28 give the voltage according to the procedure outlined by Langmuir (References 7 and 8). If the space-charge potential minimum occurs at the anode, the voltage can be calculated from Equation 13. Otherwise, the potential minimum occurs somewhere between the cathode and the anode, and the value of the potential minimum relative to the metal surface is  $V_s$  from Equation 11:

$$V_s = (kT/e) \ln \{J_0/J\} \quad (84)$$

The distance from the potential minimum to the cathode is found from Equation 28 since at the cathode  $n_c = (e/kT)V_s$ :

$$\xi \Big|_{\text{cathode}} = \xi_c \{n_a\} = \xi_c \{\ln\{J_0/J\}\} \quad (85)$$

Recall that  $\xi_c$  and  $n_c$  are measured relative to the potential minimum and  $x = \xi_c x_1$  from Equation 21. The distance from the potential minimum to the anode is then the anode - cathode spacing  $D$  minus the distance from the potential minimum to the cathode given by Equation 85. In normalized terms, then, the locations of the anode is  $\xi_a$  where

$$\xi_a = D\sqrt{J} / x_2 + \xi_c \{\ln\{J_0/J\}\} \quad (86)$$

Here the normalizing constant  $x_2$ , based on Equation 24, given by

$$x_2^2 = \epsilon_0 (kT)^{3/2} / e (2\pi m)^{1/2} = x_1^2 J \quad (87)$$

allows the current density  $J$  to appear explicitly in Equation 86. Then from Equation 27 the potential  $V_a$  of the anode relative to the potential minimum is

$$V_a = (kT/e)n_a \{D\sqrt{J}\} / x_2 + \xi_c \{\ln(J_0/J)\} \quad (88)$$

Figure 8 shows a schematic of the potential distribution between the anode and cathode under space-charge-limited conditions. This diagram shows that the anode to cathode voltage  $V$  is

$$V = V_a - V_s \quad (89)$$

and the applied voltage which is offset by the Fermi levels is

$$V_{app} = V + \phi_a - \phi_c \quad (90)$$

(A similar situation is discussed above in the derivation of Equation 12.) Then from Equations 84, 88, and 89

$$V = (kT/e)[\ln(J/J_0) + n_a \{D\sqrt{J}\} / x_2 + \xi_c \{\ln(J_0/J)\}] \quad (91)$$

where  $n_0 = 0$  in Equations 27 and 28 and  $D$  is the cathode-anode spacing.

Equation 91 is instructive as a summary of the solution procedure outlined by Langmuir. Each term in Equation 91 represents a part of the physical behavior of the emission. The term  $\ln(J/J_0)$  is negative and represents a voltage offset due to the existence of the potential minimum  $V_s$ . The term  $\xi_c \{\ln(J_0/J)\}$  is negative and represents the distance from the potential minimum to the cathode. The term  $D\sqrt{J} / x_2$ , serving as the argument for the function  $n_a$ , is responsible for the basic 3/2 power behavior of the current as a function of voltage.

5. BEHAVIOR OF  $J\{V\}$  FOR SPACE-CHARGE-LIMITED CONDITIONS

Three characteristics of the  $J\{V\}$  curve are of special interest for space-charge-limited conditions. Each of these three characteristics, the transition from retarding-field to space-charge-limited operation, the inflection point, and the transition from space-charge-limited operation to the zero-field condition  $J = J_0$ , can be used in an experimental determination of the zero field current density  $J_0$  which is characteristic of the cathode under test. The derivative of Equation 91

$$\frac{dV/dJ}{dJ} = (kT/eJ) [1 + (D\sqrt{J}/2x_2 - d\xi/dn_c \Big|_{n_c'} ) d n_a/d\xi \Big|_{\xi_a'} ] \quad (92)$$

and the second derivative

$$\begin{aligned} \frac{d^2V/dJ^2}{dJ^2} = & (kT/eJ^2) \left[ -1 - (d n_a/d\xi \Big|_{\xi_a'} ) [ -d\xi/dn_c \Big|_{n_c'} + \sqrt{J} D/2x_2 ] \right. \\ & + (d^2 n_a/d\xi^2 \Big|_{\xi_a'} ) [ -d\xi/dn_c \Big|_{n_c'} + \sqrt{J} D/2x_2 ]^2 \quad (93) \\ & \left. + (d n_a/d\xi \Big|_{\xi_a'} ) [ - (d\xi/dn_c \Big|_{n_c'} )^3 (d^2 n_c/d\xi^2 \Big|_{n_c'} ) + D\sqrt{J}/4x_2 ] \right] \end{aligned}$$

show more explicitly the behavior of the current-voltage curve for space-charge-limited conditions. Here  $n_c'$  and  $\xi_a'$  are defined as

$$n_c' = \ln\{J_0/J\} \quad (94)$$

and

$$\xi_a' = \sqrt{J} D/x_2 + \xi_c \{ \ln\{J_0/J\} \} \quad (95)$$

The derivatives  $dJ/dV$  and  $d^2J/dV^2$  are obtained from Equations 92 and 93 through the use of Equations 56 and 57. Equation 57 is also used to express the derivative  $d^2\xi/dn_c^2$  in Equation 93.

Figure 9 shows  $J(V)/J_0$ ,  $(dJ/dV)/J_0$  and  $(d^2J/dV^2)/J_0^2$  for an example cathode having  $J_0 = 10 \text{ mA/cm}^2$ ,  $T = 700^\circ\text{C}$ , and  $D = 0.2 \text{ mm}$ . The curves are normalized by the factor  $J_0$  for ease of plotting. The curves in Figure 9 are shown dashed in the retarding field range and solid in the space-charge range. The retarding-field range is described by Equation 15.

At the transition from the retarding-field range to the space-charge range, Figure 9 indicates that  $J(V)$  is a smooth curve and that  $dJ/dV$  is continuous. The second derivative  $d^2J/dV^2$ , however, is discontinuous at this transition point. The second derivative is much larger on the retarding-field side than it is on the space-charge side. (In the generation of Figure 9, Equations 92 and 93 will generate very curious, though spurious, values when applied in the retarding-field range.)

Toward increased voltage in the space-charge range, notice that  $d^2J/dV^2$  passes through zero, indicating an inflection point in the  $J(V)$  curve. Crowell discusses the existence of this inflection point through plots of the results of many numerical calculations. However he does not relate the behavior of the current-voltage curve back to the equation for  $J(V)$ . Crowell also does not point out that for practical, high-current-density cathodes this inflection point occurs virtually at  $J = J_0$ . Note that the example in Figure 9 is for a cathode with very low current density,  $10 \text{ mA/cm}^2$ , and a very close diode spacing of  $0.2 \text{ mm}$ . A detailed discussion of this inflection point follows below in Subsection b.

Perhaps more important than the existence of the inflection point is the fact that  $J(V)$  tends to  $J_0$  with zero slope. Work discussed below in Subsection a will show that this behavior of  $J(V)$  near  $J_0$  is characteristic of high-current-density cathodes as well as the low-current-density cathode of Figure 9. The work below and the discussions in Section IV on the behavior of  $J(V)$  in the accelerating-field range predict discontinuities in  $dJ/dV$  and  $d^2J/dV^2$  at  $J = J_0$ . This behavior should show up as rapid variations in these derivatives for cases where experimental conditions (such as edge effects or emission patches) obscure details of the  $J(V)$  curve. These rapid variations in the derivative should serve as a better indicator of the value of  $J_0$  than the inflection point measurement discussed by Crowell (Reference 12).

a. Transition to  $J = J_0$ 

At the point where  $J$  is just equal to  $J_0$  from the space-charge range, the space-charge minimum occurs right at the cathode. In this case  $n'_c$  from Equation 94, which represents the voltage offset due to the potential minimum, is zero. Then in Equation 92 since  $dn_c/d\xi$  is zero at this point, the term  $d\xi/dn_c$  is unbounded. Then  $dV/dJ$  is unbounded which implies that

$$dJ/dV = 0 \text{ at } J = J_0 \quad (96)$$

This is true for any value of  $J_0$ . This behavior appears clearly in an example treated by van der Ziel (Reference 9). (See van der Ziel's Figure 1 with  $I_s = 0.01 \text{ A/cm}^2$ .)

For many practical problems this behavior of the space-charge equation only applies over values of  $J$  extremely close to  $J_0$  and is not readily visible in the current-voltage plots. For example, the zero slope of  $J$  as a function of  $V$  at  $J = J_0$  is not visible in Figure 24 which treats a high-current-density cathode. However, later work in Section IV shows that  $dJ/dV$  is greater than zero at  $J = J_0$  from the accelerating-field range. This discontinuity in the first derivative and the accompanying discontinuity in the second derivative should show up in plots of experimentally taken derivatives even when the transition at  $J = J_0$  is masked in the  $J(V)$  plot itself.

## b. The Inflection Point

The inflection-point current is defined as an approximate measure of  $J_0$  in the 1950 I.R.E. Standards on Electron Tubes (Reference 16). This standard is based on the observation that  $J(V)$  has an increasing slope for small  $J$  and a decreasing slope for large  $J$ . The inflection point is then the transition point from increasing to decreasing slope of  $J(V)$ , the point where  $d^2J/dV^2$  is zero. Crowell (Reference 12) was the first to point out that Langmuir space-charge theory predicts an inflection point for some  $J$  less than  $J_0$ . Crowell used a numerical study for many values of  $J_0$  to support the use of the inflection point as an approximate

measure of  $J_0$ . This section goes beyond the work of Crowell by showing on a theoretical basis how Langmuir space-charge theory always produces an inflection point at some  $J$  less than  $J_0$ .

Equation 93 along with Equations 92 and 57 give a fairly complicated expression for  $d^2J/dV^2$ . However, in the limit as  $J$  approaches  $J_0$ , the term  $d\varepsilon/dn_c$  is unbounded. Use of this fact allows a simple expression for  $d^2J/dV^2$  at  $J = J_0$

$$\left. \frac{d^2J}{dV^2} \right|_{J = J_0} = -(J/2)(e/kT)^2 \left. \left( \frac{dn_a}{d\varepsilon} \right) \right|_{\varepsilon_a}^{-2} \quad (97)$$

At  $J = J_0$ ,  $\varepsilon_c$  is zero so from Equation 95

$$\varepsilon_a' = \sqrt{J} D/x_2 \quad (98)$$

Then Equation 97 shows that the second derivative of  $J(V)$  is always negative and finite at  $J_0$ . Although Figure 9 indicates that  $d^2J/dV^2$  has a large negative value for that example, Equation 97 shows that the second derivative is finite.

For small  $J$ , in the retarding-field range, Equation 13 shows that  $J(V)$  and its derivatives are

$$J = J_0 \exp \{e (V_{app} + \phi_c - \phi_a)/kT\} \quad (99)$$

$$dJ/dV = (eJ_0/kT) \exp \{e (V_{app} + \phi_c - \phi_a)/kT\} \quad (100)$$

and

$$d^2J/dV^2 = (e/kT)^2 J_0 \exp \{e (V_{app} + \phi_c - \phi_a)/kT\} \quad (101)$$

Equation 101 shows that the second derivative is always positive for small  $J$ . Comparison of Equations 97 and 101 shows that  $d^2J/dV^2$  changes sign for some value of  $J$  between  $J = 0$  and  $J = J_0$ . In other words, there is an inflection point of  $J(V)$  at this value of  $J$ .

This inflection point has the usual properties except for the case of very small values of  $\sqrt{J} D/x_2$  discussed in Subsection c. In this case a discontinuity in the second derivative coincides with the inflection point. The second derivative then passes discontinuously from positive values to negative values.

c. Transition from Retarding-Field to Space-Charge-Limited Conditions

This section explores the detailed behavior of Langmuir space-charge theory at the transition from the retarding-field range into the space-charge-limited range. Van der Ziel (Reference 9) mentions this transition point and gives it the name "exponential point". However van der Ziel does not discuss the behavior of the derivatives of  $J(V)$  at the exponential point, probably since he did not have Equation 91 or an equivalent. The examination below of  $J(V)$  and its derivatives show that the  $J(V)$  curve is smooth at the transition from the retarding field region into the space charge region ("exponential point"). In addition, the derivative  $dJ/dV$  is continuous but not smooth, and the second derivative is discontinuous at the exponential point.

For the condition that the space-charge just begins to reduce the current from the value it would have in the retarding-field range, the space charge minimum occurs right at the anode. In this case the distance from the potential minimum to the anode is zero so the value of  $\xi$  at the anode, designated  $\xi'_a$  above, is zero. From the definition of  $\xi'_a$  in Equation 95, it follows that

$$\xi'_c \{ \ln(J_0/J_e) \} = -\sqrt{J_e} D/x_2 \equiv \xi'_c \quad (102)$$

where  $J_e$  is the current density at the exponential point. Then since  $n_a$ , evaluated at  $\xi = 0$ , is zero, Equation 91 reduces to

$$V_e = (kT/e) \ln \{ J_e / J_0 \} \quad (103)$$

where  $V_e$  is the voltage at the exponential point. Since  $n_0$ , which is  $dn/d\xi$  evaluated at  $\xi = 0$ , is zero, Equation 92 reduces to

$$\left. \frac{dV/dJ}{J = J_e} \right| = kT/e J_e \quad (104)$$

and Equation 93 reduces to

$$\left. \frac{d^2V/dJ^2}{J = J_e} \right| = (kT/e J_e^2) [ -1 + 1/2 (-d\xi/dn_c \Big|_{n'_c} + \sqrt{J_e} D/2x_2)^2 ] \quad (105)$$

In Equation 105 use has been made of Equation 23 to evaluate  $d^2n_a/d\xi^2$  at  $\xi'_a = 0$ .

If Equations 103 through 105 are written in terms of  $J(V)$  instead of  $V(J)$  they become

$$J_e = J_0 \exp \{eV_e/kT\} \quad (106)$$

$$\frac{dJ}{dV} \Big|_{J=J_e} = \frac{eJ_e}{kT} \quad (107)$$

and

$$\frac{d^2J}{dV^2} \Big|_{J=J_e} = \frac{(e/kT)^2}{J_e} [1 - 1/2 \left( -\frac{d\zeta}{d\eta_c} \right)_{\eta_c=0} + \sqrt{J_0/2x_2}]^2 \quad (108)$$

Comparison of Equations 99 and 100 with Equations 106 and 107 shows that  $J(V)$  and  $dJ/dV$  are both continuous at the exponential point and consequently  $J(V)$  is smooth. Note that  $V$  and  $V_{app} + \zeta_c - \zeta_a$  are the same from Equation 90. Comparison of Equations 101 and 108 shows that  $d^2J/dV^2$  is always greater on the retarding field side of the exponential point than it is on the space-charge side. From Equation 28 the term  $d\zeta/d\eta_c$  in Equation 108 is always negative. (This is also seen in Figure 4.) Then the term in brackets in Equation 108 is always less than the value calculated from Equation 101. Then the second derivative is discontinuous so that the first derivative is not smooth at the exponential point. Figure 10 shows a detailed sketch of  $dJ/dV$  at the exponential point for the example of Figure 9.

For many cathodes where  $J_0$  is relatively large,  $\zeta_c \{ \ln(J_0/J_e) \}$  is very nearly its minimum value of -2.5539 before it is equal in magnitude to  $D\sqrt{J_0/x_2}$ . In this case  $J_e$  at the exponential point is much less than  $J_0$  and, from Equation 102,  $J_e$  is given by

$$J_e = (2.5539 x_2/D)^2 \quad (109)$$

In this case of large  $J_0$  then,  $J_e$  at the exponential point becomes nearly independent of the zero field current  $J_0$ . In this case  $d\zeta/d\eta_c$  at  $\eta_c = 0$  is very small, so the second derivative is approximately

$$\frac{d^2J}{dV^2} \Big|_{J=J_e} = \frac{(e/kT)^2}{J_e} [1 - (1/2)(2.5/2)^2] \quad (110)$$

which is approximately a factor of 5 jump in the second derivative at the exponential point. For the example of Figure 9 the second derivative jumps by a factor of 5.7. Note in Figure 9 that the second derivative is off scale to the retarding field side of the transition point.

For cathodes with very small  $J_0$  the term  $\sqrt{J} D/x_2$  in Equation 102 will be very small leading to a very small  $\xi'_c$ . In this case  $-d\xi/d\xi_c$  would be quite large in Equation 105 rendering  $d^2J/dV^2$  negative. If  $d^2J/dV^2$  is negative to the space-charge-limited side of the exponential point, there is no additional inflection point in the  $J\{V\}$  curve and the slope of  $J\{V\}$  always decreases in the space-charge-limited range. Since  $d^2J/dV^2$  is positive in the retarding field range, this discontinuity to negative  $d^2J/dV^2$  can be quite pronounced for low-current-density cathodes.

#### d. Experimental Use of the Exponential Point

The discontinuity in the second derivative at the exponential point should lead to a sharp peak in the second derivative of experimental  $J\{V\}$  curves. The current  $J_e$  and the applied voltage  $V_{app}$  can then be measured at this peak in the second derivative. Then, if  $J_0$  is not too large, the theory developed in Subsection c and expanded below calculates the zero field current  $J_0$  and the work function difference  $\phi_a - \phi_c$ . A suggested limit on  $J_0$  for accurate calculations is that  $J_e$  be greater than approximately  $J_0/50$ . This condition on  $J_0$  is satisfied for large  $\phi$  cathodes or by sufficiently low temperature  $T$ .

Based on one measurement of current  $J_e$  and voltage  $V_e$ , the zero-field current  $J_0$  of the cathode and the difference in cathode and anode work function can be calculated without reference to the Richardson Equation 8. Equation 8 can then be used to calculate the cathode work function from the zero-field current density. From Equation 90 the measured voltage  $V_{app}$  is related to the voltage  $V_e$  by

$$V_{app} = V_e - (\phi_c - \phi_a) \quad (111)$$

From Equation 102 the current  $J_e$  is related to  $J_0$  by

$$J_0 = J_e \exp\{\eta_c \{\sqrt{J_e} D/x_2\}\} \quad (112)$$

and Equation 103 relates  $V_e$  to  $J_e$  and  $J_0$ . Then Equations 103 and 112 can be used to generate plots of  $J_0$  and  $V_e$  as functions of  $J_e$ . For a measured value of  $J_e$  and with measured values of  $T$  and  $D$ , the zero field current density can be calculated from Equation 112. Then Equation 103 can be used to calculate  $V_e$ . From the calculated value of  $V_e$  and the measured value of  $V_{app}$ , Equation 111 then produces the difference between the cathode and anode work functions ( $\phi_c - \phi_a$ ).

The problem with the use of Equation 112 is that it requires  $\eta_C\{\cdot\}$  in the cathode space. A method for calculating this function could be derived in a straightforward manner. However, since the inverse function  $\xi\{\eta_C\}$  can be calculated from Equations 29 through 31, it seems easier at this point to restate the problem, so that this inverse function can be used. The use of this inverse function is possible through the construction of an auxiliary function  $f\{J\}$  where based on Equation 102

$$f\{J\} = \xi_C\{\ln\{J_0/J\}\} + D\sqrt{J}/x_2 \quad (113)$$

Then finding the solution  $J_e$  to Equation 112 for a given  $J_0$  is equivalent to finding the solution  $J_e$  to Equation 113 such that

$$f\{J_e\} = 0 \quad (114)$$

This allows a value of  $J_e$  to be generated for each  $J_0$  over a range of values of  $J_0$ . This can, of course, still be plotted as  $J_0\{J_e\}$  for use in interpreting experimental data.

A plot generated from the BASIC program discussed below is shown in Figure 11 for two examples. In one example the temperature is 700°C and the spacing is 0.2 mm while in the other example the temperature is 900°C and the spacing is 1.0 mm. Actually, the values of temperature and spacing are not unique to each curve in Figure 11. Rather, the family of curves suggested in Figure 11 depends on the parameter  $\tau$  where

$$\tau = D/x_2 = (D/T^{3/4})(e\sqrt{2\pi m}/\epsilon_0 k^{3/2})^{1/2} \quad (115)$$

as seen in Equation 113. Figure 11 also indicates the asymptotic values where  $J_e$  ceases to increase for increasing values of  $J_0$ . The asymptotic value is, of course, dependent on cathode temperature and diode spacing and is given by Equation 109.

Equation 114 can be solved for  $J_e$  by an iterative technique known as Newton's method (Reference 20, p 277). Based on an initial guess  $J_1$  at the solution, this method generates a sequence of approximations by the recurrence relation

$$J_{n+1} = J_n - f(J_n)/f'(J_n) \quad n = 1, 2, 3, \dots \dots \quad (116)$$

The iteration is terminated when  $J_{n+1}$  is sufficiently close to  $J_n$  and  $J_{n+1}$  is taken as the value of  $J_e$ . Since  $J_e$  is always less than  $(2.554 x_2/D)^2$  from Equation 109, this is a convenient starting value for  $J_1$ . However, for small values of  $J_0$  this formula gives a value of  $J_e$  which is greater than  $J_0$ . In this case a smaller starting value for  $J_1$  is necessary, for example  $J_1 = 0.5 J_0$ . In Equation 116 the notation  $f'(J_n)$  represents  $df/dJ$  evaluated at  $J_n$ , that is

$$f'(J_n) = (-1/J)(d\varepsilon/dn_C) + D/2 x_2 \sqrt{J_n} \quad (117)$$

where  $d\varepsilon/dn_C$  is calculated from Equation 28 with  $n_C$  evaluated at

$$n_C = \ln(J_0/J_n) \quad (118)$$

A BASIC program which solves Equation 114 and generates  $J_e$  and  $V_e$  for a range of values of  $J_0$  is shown in Figure 12.

Another way of representing the behavior of  $J(V)$  at the exponential point is shown in Figure 13. This figure shows both  $J_0$  and  $J_e$  plotted as functions of  $V_e$ . The calculations were made by the BASIC program of Figure 12. Figure 13 is especially convenient for interpreting measured data since it gives both  $J_0$  and  $V_e$  based on the measured value of  $J_e$ . From  $V_e$  and the value of  $V_{app}$  at the transition point, Equation 111 then gives the difference in work function ( $\phi_C - \phi_A$ ). Figure 13 shows the asymptotic value of  $J_e$  for the example  $T = 700^\circ\text{C}$  and  $D = 0.2 \text{ mm}$ . Figure 13 also shows the asymptotic line for  $J_0(V_e)$  which passes through the asymptotic value of  $J_e$  at  $V_e = 0$  with a slope of  $kT/e$ . The existence of an asymptotic line for constant  $J_e$  is seen from Equation 103. For experimental interpretation families of curves of  $J_0$  or  $J_e$  as functions of  $eV/kT$  can be generated just as the sample curve

was generated for Figure 13. With the  $V$  axis normalized to  $eV/kT$ , the family of curves is generated with the single parameter  $\tau = D/x_2$  just as in the generation of the family of curves like those in Figure 11.

Although the representation is not as intuitive as the families of curves suggested in Figures 11 and 13. All of this information can be represented in a single plot of  $J_e\{V_e\}$  and a single plot of  $J_0\{V_e\}$  through proper normalization of the terms. The proper normalization is  $\tau^2 J_e$  and  $\tau^2 J_0$  as functions of  $eV_e/kT$ . Graphs of these two normalized functions are shown in Figure 14.

The derivation for these normalized functions follows from the combination of Equations 102 and 103 to give

$$J_e = (x_2/D)^2 \xi_c^2 \{eV_e/kT\} \quad (119)$$

The combination of Equations 106 and 119 then gives

$$J_0 = (x_2/D)^2 \xi_c^2 \{eV_e/kT\} \exp \{-eV_e/kT\} \quad (120)$$

The normalized functions are then from Equation 115.

$$\tau^2 J_e = \xi_c^2 \{eV_e/kT\} \quad (121)$$

and

$$\tau^2 J_0 = \xi_c^2 \{eV_e/kT\} \exp \{-eV_e/kT\} \quad (122)$$

The function  $\xi_c$  is conveniently calculated from Equations 29 through 31. Figure 14 shows the asymptotic value of 6.5224 for  $\tau^2 J_e$  and the asymptotic slope of 4 for  $\tau^2 J_e$  as a function of  $eV_e/kT$  near  $V_e = 0$ . The limiting value of  $\tau^2 J_e$  is just the square of the limiting value of  $\xi_c$  from Equation 31, and the limiting slope is apparent from the square of Equation 29.

Equation 112 gives  $J_0$  and consequently the cathode work function (from Equation 8) based on the measurement of current, cathode temperature, and diode spacing. It does not require a knowledge of the anode work function or the value of the applied voltage. Equation 112 in principle allows the determination of  $J_0$  for any value of  $J_e$ . However, for large  $J_0$

the value of  $\sqrt{J} / x_2$  has nearly the limiting value of -2.5539. In this case  $n_c$  is such a steeply rising function that the method is not useful. In practice the problem with high values of  $J_0$  can be overcome by lowering the temperature, since  $J_0$  is an exponential function of the temperature.

## 6. COMPARISON OF $J\{V\}$ WITH CHILD'S LAW

For many practical cathode tests the temperature is around  $1300^\circ\text{K}$ , the cathode-anode spacing is of the order of 1 mm and the current density  $J_0$  is of the order of  $1 \text{ A/cm}^2$  requiring 100V or more to obtain  $J_0$  from the cathode. Then in Equation 91 the term  $kT/e$  is of the order of .1 volt, and the voltage offset due to the potential minimum,  $(kT/e)\ln\{J/J_0\}$ , is about 0.2 volts for  $J = J_0/10$  and decreases as  $J$  approaches  $J_0$ . This term, then, has very little effect on an applied voltage in the 100 volt range. An examination of other terms in Equation 91 shows that  $D\sqrt{J} / x_2$  is in the range of a few hundred. Since  $\xi_c$  has a maximum magnitude of 2.5 and decrease for  $J$  approaching  $J_0$ , this term has only a small effect on the argument of  $n_a$  in Equation 91. Then Equation 91 is accurately approximated by

$$V_{\text{app}} \doteq (kT/e) n_a \{D\sqrt{J} / x_2\} \quad (123)$$

The function  $n_a\{\xi\}$  for large  $\xi$  can be approximated using Equation 27. For large  $\xi$ ,  $n_a$  is also large as seen for example in Figure 4. For large  $n_a$  Equation 76 shows that the function  $P\{u\}$  is accurately approximated by

$$P\{u\} \doteq 1 - \exp\{-u^2\} \quad (124)$$

Then for large  $\xi$ , Equation 27 is accurately approximated by

$$dn_a/d\xi \doteq (2/\pi)^{1/4} n_a^{1/4} \quad (125)$$

Figure 15 gives a graphical comparison of the approximate expression from Equation 125 compared to the exact value of the derivative calculated from Equation 27. This graph shows that the magnitude of the error in using Equation 125 decreases slowly as  $\xi$  increases. However the error expressed as a percentage of the value of  $d\eta_a/d\xi$  becomes small very rapidly for  $\xi$  greater than 50. In generating Figure 15, Equations 32 through 34 were used to calculate  $\eta_a\{\xi\}$ . Then Equation 27 and 125 were used to calculate the derivative and the approximate derivative as functions of  $\xi$ . Integration of Equation 125 shows that

$$\eta_a\{\xi\} = (3/4)(3/\pi)^{1/3} \xi^{4/3} \quad (126)$$

Here the integration constant is zero since  $\eta_a\{0\}$  is zero. Equation 126 also follows from Equation 34, though less intuitively. The number 1.2552 in Equation 34 is just  $[(3/4)(3/\pi)^{1/3}]^{3/4}$  rounded to 5 digits. The combination of Equations 123 and 126 gives

$$V_{app} = [(9/4)(D^2/\epsilon_0)(m/2e)]^{1/2} J^{2/3} \quad (127)$$

or, which is equivalent

$$J = (4/9)\epsilon_0 (2e/m)^{1/2} V^{3/2} / D^2 \quad (128)$$

Equation 128 is known as Child's law (Reference 7). Review of the above procedure then shows that the term  $2\sqrt{\eta_a/\pi}$  in Equation 27 is responsible for the basic three halves behavior of  $J\{V\}$ .

### SECTION III

#### SCHOTTKY THEORY

The space-charge-theory developed to this point in Section II suggests that there will be a zero-field current density  $J_0$  for some voltage  $V_0$  and that there will be no increase in  $J$  above  $J_0$  for  $V > V_0$ . However, Schottky (Reference 4) suggests that a linear applied accelerating field across a diode will interact with the intrinsic field near the cathode surface to lower the cathode work function. Consequently, the current density will increase above  $J_0$  for accelerating fields at the cathode surface. A review of Schottky's derivation is found in Hutchison (Reference 6, pp 305 to 309). Although this section neglects space-charge effects, as did Schottky, space-charge effects will be brought into this theory and accounted for in Section IV.

#### 1. DERIVATION OF THE SCHOTTKY EQUATION

As discussed by Ramo, Whinnery, and Van Duzier (Reference 22), the force exerted on an electron of charge- $e$  located at position  $x$  away from a conducting plane is the same as the force exerted on the electron by a charge  $+e$  located at position  $-x$ . Then the electric field experienced by the electron is

$$F = e/4\pi\epsilon_0 (2x)^2 \quad (129)$$

The work done on an electron in bringing it from a great distance away from the conducting plane to position  $x$  is then

$$W = -\int_{\infty}^x [(+e)(-e)/16\pi\epsilon_0 (x')^2] dx' = -e(e/16\pi\epsilon_0 x) \quad (130)$$

If this work is defined in terms of a motive potential  $\phi_m$  so that

$$W = (-e) \phi_m \quad (131)$$

then

$$\phi_m = e/16\pi\epsilon_0 x \quad (132)$$

This potential is shown in Figure 16 where the Fermi level is displaced above the vacuum level by an amount  $\phi$ , the work function. Due to the way which  $\phi_m$  is defined, the reference zero potential is the vacuum level with no applied voltage. In principle, Equation 132 predicts that the motive potential is unbounded at the cathode surface so that the work function would have to be infinite. However, the idea of an image charge due to a perfectly conducting surface breaks down at distances of the order of interatomic spacings. As discussed by Nottingham, (Reference 13), this changes the shape of the motive potential very near the surface and leads to a finite work function. Beyond a few angstroms from the surface, the fact that the motive potential is accurately described by Equation 132 has been proven for many types of cathodes by the agreement of experimental data with the Schottky equation derived below (Reference 5, p 109).

If a potential  $V$  is applied to a plane anode at a distance  $D$  from a plane cathode, the applied potential depresses the vacuum potential  $V_x$  linearly with distance from the cathode surface according to

$$V_x = Fx \quad (133)$$

where

$$F = V/D \quad (134)$$

is a constant electric field. The total field  $V(x)$ , which is the sum of the fields from Equations 132 and 133, is expressed

$$V(x) = e/16\pi\epsilon_0 x + Fx \quad (135)$$

and is plotted in Figure 17. The value of  $x$  for which  $V$  is minimum is found from the zero of the derivative to be

$$x_{\min} = \sqrt{e/F} / \sqrt{16\pi\epsilon_0} \quad (136)$$

The value of  $V$  at  $x_{\min}$  is

$$V_{\min} = \sqrt{eF} / \sqrt{4\pi\epsilon_0} \quad (137)$$

As seen in Figure 17, this  $V_{min}$  represents a decrease in the work function from the value with no applied external voltage. The reduced work function  $\phi_r$  is then

$$\phi_r = \phi - \sqrt{eF} / \sqrt{4\pi\epsilon_0} \quad (138)$$

Using this modified work function in the Richardson equation, Equation 8, gives

$$J = AT^2 \exp \{ -(\phi - \sqrt{eF/4\pi\epsilon_0})e/kT \} \quad (139)$$

or

$$J = J_0 \exp \{ (e/kT)\sqrt{eF/4\pi\epsilon_0} \} \quad (140)$$

where  $F = V/D$ . Calculating this effect for 5000 volts applied across 1 millimeter gives  $x_{min} = 84 \text{ \AA}$  and  $V_{min} = .085 \text{ volts}$  or  $J = 2.3 J_0$  at  $900^\circ\text{C}$ . Calculations for 1000 volts across 1 millimeter give  $x_{min} = 190 \text{ \AA}$ ,  $V_{min} = .038 \text{ volts}$  and  $J = 1.4 J_0$  at  $900^\circ\text{C}$ .

## 2. EDGE EFFECTS AND SCHOTTKY THEORY

One goal of cathode testing is to determine basic physical properties of a cathode from specific electrical measurements. This allows cathode performance to be predicted independently of the test vehicle. For this purpose Langmuir space charge theory (References 7 and 8) and Schottky theory (Reference 4) are available to interpret electrical test data from the cathode. However, these theories are well developed only for certain simple geometries such as parallel planes and concentric cylinders and spheres. In practice the test vehicle only approximates one of these ideal geometries. When the theory is used to interpret the measured data, errors are introduced. The calculated "basic properties" of the cathode are then dependent to a certain extent on the geometry of the test vehicle.

A close-spaced diode which is often used for testing cathode emission is shown in Figure 18. Langmuir and Schottky theories for infinite planes are used to interpret the measured data. The most obvious error comes from electric field variations across the emitting surface due to electric field enhancement by the edge of the sleeve. Additional error comes from

the finite extent of the emitting region which generally is smaller than the total cathode surface (see Figure 18). The presence of a boundary to the emitting layer is contrary to the conditions assumed in the derivation of Langmuir space charge theory for parallel planes. The space charge is dissipated more easily at the boundary resulting in greater current density than is predicted for the parallel plane case. This problem is discussed by Pierce (Reference 23) who shows that uniform emission can be obtained if a focus electrode is added at cathode potential which makes a 67.5 degree angle with the normal to the cathode surface (see also Reference 22). With or without the focus electrode the current varies with the three halves power of voltage under space charge limited conditions, as discussed by Langmuir (Reference 8, p 251) and Spangenberg (Reference 24). Without the focus electrode, the saturation is not abrupt due to the nonuniform current density. Also, the slope of the three halves power curve is not simply related to the square of the cathode-anode spacing.

Focus electrode geometries other than the 67.5 degree sleeve can improve the uniformity of the space charge limited emission current. Computer programs for traveling wave tube gun design (Reference 25) are available which can evaluate more complex geometries. Although these designs lead to a more accurate representation of the emission by Langmuir space-charge theory for parallel planes, they will not improve the representation by Schottky theory under temperature limited conditions.

Schottky theory for parallel planes becomes more applicable when an electrode at cathode potential (guard ring) extends the plane of the emitting surface. The guard ring gives a more uniform electric field once the applied voltage is high enough to decrease the space charge effects. Traveling wave tube gun design programs can also calculate the electric field for the test diode in the absence of space charge. Comparing the Schottky theory for the true field distribution with the Schottky theory for parallel planes shows the errors in the parallel plane assumption.

If the errors in the parallel plane assumption are not large, a simpler analytical approach gives an accurate approximation to the true field distribution. This approach begins with the calculation of the electric field about a plane edge above an infinite plane as shown in Figure 19. The Schwartz transformation relates the distance from the cathode edge to the electric potential and flux through a procedure outlined by Ramo, Whinnery and Van Duzier (Reference 22).

The Schwartz transformation allows one to find a mapping from the complex  $z'$  plane into the complex  $z$  plane which preserves both the properties of the static electric field and the boundary conditions. If the  $z'$  plane is chosen as shown in Figure 20(a), the solution to the static electric field problem can be found in a straightforward manner. Let the boundary condition be  $V$  equals  $V_0$  to the left of  $x = 0$  and  $V = 0$  to the right of  $x = 0$ . Then electric potential  $v$  and flux function  $u$  are given by

$$u + iv = (V_0/\pi) \ln\{z'\} \quad (141)$$

where

$$u = \text{flux function} = - \int E_x dy + \int E_y dx \quad (142)$$

$$i = \sqrt{-1}$$

$F$  = electric field intensity

A quick check of Equation 141 shows that

$$v = (V_0/\pi) \arctan\{y'/x'\} \quad (143)$$

satisfies both Laplace's equation and the boundary condition specified above as required for the electric potential. The inverse of Equation 141

$$z' = \exp\{\pi w/V_0\} \quad (144)$$

where

$$w = u + iv \quad (145)$$

will be required below in the derivation.

For this particular problem the  $z$  plane would be that of Figure 19 and the required transformation is (Reference 22, p 189)

$$dz/dz' = K (z' - x'_1)^{(\alpha_1/\pi-1)} (z' - x'_2)^{(\alpha_2/\pi-1)} \quad (146)$$

The angles  $\alpha_1$  and  $\alpha_2$  and the positions  $x'_1$  and  $x'_2$  are shown in Figure 20(a) and (b). Including the appropriate values for  $x'_1$ ,  $x'_2$ ,  $\alpha_1$  and  $\alpha_2$  in Equation 146 gives

$$dz/dz' = (K/z') \sqrt{z' - 1} \quad (147)$$

Integration of Equation 147 gives

$$z = 2K[\sqrt{z' - 1} - \arctan \{\sqrt{z' - 1}\}] + C \quad (148)$$

where  $C$  is the integration constant. The constant  $C$  can be evaluated by the requirement that the point  $z' = 1$  transform into the point  $z = ih$ . This requirement imposed on Equation 148 gives

$$C = ih \quad (149)$$

where  $h$  is the diode spacing. The constant  $K$  is evaluated from Equation 147 through an integration from point B to point C shown in Figure 20 in both the  $z$  and  $z'$  planes. It must be that

$$\int_B^C dz = \int_B^C (dz/dz') dz' \quad (150)$$

If the integration is about a small semicircle in the  $z'$  plane at  $B - C$ , then  $dz/dz'$  becomes arbitrarily close to  $iK/z'$  and  $dz'$  can be expressed as  $iz'd\theta'$ . Then Equation 150 can be expressed

$$\int_{\infty+ih}^{\infty+io} dz = \int_{\pi}^0 (ik/z') iz'd\theta' \quad (151)$$

Evaluation of Equation 151 then gives

$$K = ih/\pi \quad (152)$$

Finally, a combination of Equations 152, 149, 148, and 144 gives

$$x + iy = (2ih/\pi) [\pi/2 - \arctan\{\sqrt{\exp\{\pi w/V_0\} - 1}\} + \sqrt{\exp\{\pi w/V_0\} - 1}] \quad (153)$$

Since the arctangent is related to the logarithm by (Reference 19, p 80)

$$\arctan x = (-i/2) \ln \{(1 + ix)/(1 - ix)\} \quad (154)$$

the real part of Equation 153 can be expressed along the cathode surface as

$$(x/h) = (1/\pi) \ln \{(1 + \sqrt{1 - \exp\{\pi u/V_0\}})/(1 - \sqrt{1 - \exp\{\pi u/V_0\}})\} - (2/\pi) \sqrt{1 - \exp\{\pi u/V_0\}} \quad (155)$$

since  $w = u + i\phi$  along the cathode surface. Note that  $u$  ranges from 0 to  $-\infty$  along the cathode surface. From Equation 142 the perpendicular component of the electric field  $F_y$  is just  $du/dx$ . Taking this derivative in Equation 155 gives

$$(h/V_0) F_y = d(u/V_0)/d(x/h) = -1/\sqrt{1 - \exp\{\pi u/V_0\}} \quad (156)$$

The behavior of Equation 155 can be checked for  $u$  having large negative values. In this case Equation 155 can be approximated as

$$x/h \approx (1/\pi) \ln \{4 \exp\{-\pi u/V_0\}\} - 2/\pi \quad (157)$$

which says that

$$u \approx -(V_0/h)x \quad (158)$$

for large  $u$  and  $x$ . This is expected since  $u$  is just the line integral of the electric field.

The expression of Equation 155 is in an inconvenient form for further use since distance is given as a function of voltage. Attempts to get an analytical inverse have been unsuccessful. However, a numerical inverse is straightforward by means of the Newton iteration (Reference 20) also used in Subsection 5(d) of Section II. The Newton iteration is implemented for this problem by the function  $f(u)$  for a specified  $x$  such that

$$f(u) = (1/\pi) \ln\{(1 + \sqrt{1 - \exp\{\pi u/V_0\}})/(1 - \sqrt{1 - \exp\{\pi u/V_0\}})\} - 2/\pi \sqrt{1 - \exp\{\pi u/V_0\}} - x/h \quad (159)$$

Then the desired  $u(x)$  is found by solving for

$$f(u) = 0 \quad (160)$$

by constructing the sequence

$$u_1 = V_0 x/h + .2 \text{ if } x/h > .2 \quad (161)$$

or

$$u_1 = V_0 x/h \quad \text{if } x/h < .2$$

and

$$u_{n+1} = u_n - f(u_n) / f'(u_n) \quad n = 1, 2, 3, \dots \quad (162)$$

The choice of starting value  $u_1$  comes from an inspection of Equation 157. The function  $f(u_n) = df/du$  comes by direct calculation on Equation 159 or by inspection of Equation 156 and is expressed by

$$f'(u_n) = -\sqrt{1 - \exp\{\pi u_n/V_0\}} \quad (163)$$

The series is truncated when  $hf(u)/x$  is sufficiently close to zero and this  $u_n$  is taken as  $u(x)$ . Then  $F_y(x)$  is calculated from Equation 156.

If space charge is neglected and the surface electric field is known, the emission current density can be calculated from the Schottky Equation 140. A convenient procedure is to divide the cathode surface

into  $M$  rings of equal area. Then the mean radius which divides the  $N$ th ring into equal areas is

$$r(N) = (d/2)\sqrt{N/M} - .5/M \quad (164)$$

The distance from the cathode edge to this mean radius is

$$x(N) = S + (d/2) (1 - \sqrt{N/M} - .5/M) \quad (165)$$

where

$S$  = sleeve width

$d$  = diameter of the emitting area

A detailed sketch of this diode geometry is shown in Figure 18. The electric field  $F_y$  at a distance  $x(N)$  from the cathode edge is calculated by means of the Newton iteration with Equations 155 and 156. This is, of course, an approximation since the cylindrical nature of the cathode is ignored in the field solution. The current density at each  $x(N)$  is then calculated from Equation 140 and the average is taken over the  $M$  rings. The process is repeated for different values of applied voltage generating an I-V curve. The Newton iteration and Equations 155 and 156 have to be used only once to solve the field problem since the electric field is found in terms of the applied voltage.

The solution for the current density and electric field for a particular example are shown in Figure 21. The parameters chosen are cathode diameter  $d = 3$  mm, sleeve thickness  $S = 0.175$  mm, cathode-anode spacing  $h = 1.5$  mm, cathode temperature  $T = 900^\circ\text{C}$ , and cathode-anode voltage  $V_0 = 1800$  V. The voltage enhancement is 39% at the edge of the emission layer while the current enhancement is only about 8%. This is surprising at first glance, since the current varies as an exponential of the square root of the voltage. The coefficient in the exponent is small, however, so that the dominant function is the square root rather than the exponential for these experimental conditions.

The average current as a function of voltage in terms of Schottky coordinates is shown in Figure 22. The effect of the edge is to increase slightly the average current density at a given applied voltage. Although the effect appears small in Figure 22, the increase in slope of the  $\ln\{J/J_0\}$  versus  $V$  curve gives an apparent decrease in temperature from 900°C to 834°C. The temperature is calculated from the Schottky plot by means of Equation 140 in the form

$$T = \sqrt{e/4\pi\epsilon_0} (e/k) \sqrt{F_y} / \ln\{J/J_s\} \quad (166)$$

In this case the Schottky curve including edge effects is very nearly a straight line passing through  $J = J_0$  at  $V = 0$ . The curve including edge effects is straight since the argument of the exponential in Equation 140 is small for this example. This gives support to the common practice of using the Schottky line intercept to find the zero field current even when the slope of the Schottky line doesn't agree with the measured temperature.

## SECTION IV

## EXTENDING SPACE-CHARGE THEORY INTO THE ACCELERATING FIELD RANGE

Figure 1 shows schematically the assumption made in the derivation of Equation 12. For this derivation, the potential due to the surface forces which the electrons must overcome occurs as a step function right at the cathode surface and has a value of  $\phi$  electron volts below the Fermi level. Actually, the potential is not a true step function but acts over a short distance outside the surface due to the image force on the electron. Becker (Reference 5) points out that neglecting the finite extent of the image force has little effect on the space-charge distribution as long as there is a space-charge minimum  $V_s$  volts below  $\phi$ . However, if there is no space charge minimum, the space charge potential interacts with the image force to lower the value of  $\phi$ .

## 1. BACKGROUND

This interaction of the image force with the space charge occurs in much the same manner as discussed in the derivation of the Schottky effect in Subsection 1 of Section III. The derivation of the Schottky effect is based on the superposition of the image potential of the electron and a linear applied potential. The following discussion shows how the initial slope of the space-charge potential serves as the linear applied potential in the Schottky derivation.

Due to its own image, an electron experiences a surface potential field

$$V_{\text{image}} = e/4\pi\epsilon_0 (4x) \quad (167)$$

where  $x$  is the distance from the cathode surface, and  $V_{\text{image}}$  is measured relative to the potential a long distance from the cathode (vacuum level). In addition an electron experiences a space-charge potential field given by Equation 27 in normalized form. Figure 23(a) shows the image potential as a function of distance from the cathode surface while Figure 23(b) shows the space-charge potential as a function of distance from an example cathode. The example cathode of curve ① has a current density  $J_0$  of  $5 \text{ A/cm}^2$  at  $900^\circ\text{C}$  for  $dV/dx = 0$  at the cathode surface. To illustrate

the behavior of the space charge potential for accelerating field conditions, Figure 23(b) also shows the potential-distance curve according to Equation 27 for a cathode with an accelerating field  $dV/dx = 6.44 \times 10^{-4}$  volts/meter at the cathode surface. Although this value of field strength (corresponding to the arbitrarily chosen  $5.5 \text{ A/cm}^2$ ) is chosen at this point for demonstration purposes only, the following discussion shows how this increased field strength gives an increased current density of  $5.5 \text{ A/cm}^2$  at  $900^\circ\text{C}$  for the same example cathode. Note that the x scale in Figure 23(a) is expanded by a factor of 100 over the x scale in Figure 23(b).

Figure 23 shows that over the range where the image potential is effective (from the cathode surface out to about  $5 \times 10^{-8}$  meters) the space-charge potential can be approximated very accurately as an extension of the initial slope of the space charge curve

$$V_{\substack{\text{space} \\ \text{charge}}} \{x\} = \left. dV/dx \right|_{\substack{\text{cathode} \\ \text{surface}}} (x) = F_x x \quad (168)$$

Based on this assumption, namely, that the space-charge potential is linear near the cathode surface, the derivation for the Schottky effect applies if this  $F_x$  instead of  $V/D$  is used. The result is a potential minimum at a distance  $x_{\min}$  as in Equation 136

$$x_{\min} = (e/F_x)^{1/2}/(16\pi\epsilon_0)^{1/2} \quad (169)$$

from the cathode surface, and the magnitude of the potential minimum is reduced from the work function  $\phi$  by an amount  $\Delta\phi$  where from Equation 137

$$\Delta\phi = (eF_x)^{1/2}/(4\pi\epsilon_0)^{1/2} \quad (170)$$

For these conditions replacement of  $\phi$  with  $\phi - \Delta\phi$  in Equation 8 gives

$$J = AT^2 \exp \{ -e(\phi - (eF_x/4\pi\epsilon_0)^{1/2})/kT \} \quad (171)$$

Equation 171 with  $F_x = 0$  gives the zero-field current density

$$J_0 = AT^2 \exp \{-e\phi/kT\} \quad (172)$$

which is the Richardson-Dushman equation. With this expression for  $J_0$ , Equation 171 becomes

$$J = J_0 \exp \{e(F_x/4\pi\epsilon_0)^{1/2}/kT\} \quad (173)$$

## 2. GENERATION OF $J(V)$ IN THE ACCELERATING FIELD RANGE

The previous discussion now provides a framework for calculating the voltage needed to give a specified current. Let  $V_{app}$  be the voltage of the anode relative to the cathode. Then, referring to Figure 8,

$$V_{app} = V(x) \Big|_{\text{anode}} - V_s + \phi_a - \phi_c \quad (174)$$

where  $x = D - x_c$  at the anode,  $D$  is the cathode-anode spacing,  $x_c$  is the distance from the cathode to the potential minimum, and  $\phi_a$  and  $\phi_c$  are the work functions of the anode and cathode respectively. For simplicity, the remainder of this section takes  $\phi_a = \phi_c$  and refers to the applied voltage as  $V$ . If  $J = J_0$ , Equations 27 and 28 give the voltage according to the procedure outlined by Langmuir with  $\dot{n}_0 = 0$ . Equation 91 summarizes this procedure.

If  $J > J_0$ , Equations 27 and 20 give the voltage

$$V = (kT/e) n_a (D\sqrt{J}/x_2) \quad (175)$$

where  $n_a$  is calculated by a mixed Runge-Kutta-Taylor method using

$$\dot{n}_0 = (e/kT)(x_2/\sqrt{J}) F_x \quad (176)$$

In Equation 27. The expression of  $\dot{n}_0$  in Equation 176 is just an expression of the electric field in normalized units using Equations 87, 21, and 20. From Equations 173 and 176

$$\dot{n}_0 = (4\pi\epsilon_0^{3/2}/e)(kT/e)^{7/4}(e/2\pi m)^{1/4} \ln^2(J/J_0)/\sqrt{J} \quad (177)$$

or

$$\dot{n}_0 = 6.4976 \times 10^{-2} T^{(7/4)} \ln^2(J/J_0) / \sqrt{J} \quad (178)$$

with  $T$  in degrees Kelvin and  $J$  in amperes per square meter.

Figure 24 shows an example current-voltage plot for  $J$  ranging from small values up through  $J > J_0$ . For this example  $J_0$  is  $5 \text{ A/cm}^2$ ,  $T$  is  $900^\circ\text{C}$  and the cathode-anode spacing  $D$  is 1 mm. Figure 24 also shows the Child's law line, Equation 128, and the Schottky line, Equation 140 for comparison with this extended theory. For this example the extended theory matches Child's law closely up to  $J = 1.15 J_0$  but the approach to the Schottky line is only very gradual.

### 3. BEHAVIOR OF $J(V)$ NEAR $J$ EQUAL TO AND GREATER THAN $J_0$

At the point where the space-charge range meets the accelerating-field range, the space-charge minimum occurs right at the cathode. The derivative of Equation 175 with respect to  $J$  shows the behavior of the current-voltage curve from the accelerating-field side at the transition from the space-charge range to the accelerating-field range. Since  $n_0$  is also a function of  $J$ , the derivative is

$$\frac{dV/dJ}{ } = (kT/e) \left[ \left. \frac{D/2x_2 \sqrt{J}}{ } \right. \frac{d n_a/d\xi}{ } \right]_{\xi_a'} + \left. \left( \frac{d n_0/dJ}{ } \right) \frac{d n_a/d n_0}{ } \right]_{\xi_a'} \quad (179)$$

where

$$\xi_a' = \sqrt{J} D/x_2 \quad (180)$$

Inspection of Equation 177 shows that  $d n_0/dJ = 0$  at  $J = J_0$ . In addition an expression of  $n_a$  as an integral evaluated at  $\xi_a'$  along with the definition of the derivative shows that  $d n_a/d n_0$  is zero for  $n_0 = 0$  (i.e., at  $J = J_0$ ). This expression for  $d n_a/d n_0$  is

$$\frac{d n_a/d n_0}{ } = \frac{d}{d n_0} \int_0^{\xi_a'} [\dot{n}_0^2 + (1 - P(\sqrt{n})) \exp\{n\} - (1 - 2\sqrt{n}/\pi)]^{1/2} d\xi \quad (181)$$

The derivative evaluated at  $n_0 = 0$  is then

$$\begin{aligned} \left. \frac{d n_a/d n_0}{ } \right|_{n_0=0} &= \lim_{n_0 \rightarrow 0} \int_0^{\xi_a'} [\dot{n}_0^2 + (1 - P(\sqrt{n})) \exp\{n\} - (1 - 2\sqrt{n}/\pi)]^{1/2} d\xi \\ &- \int_0^{\xi_a'} [(1 - P(\sqrt{n})) \exp\{n\} - (1 - 2\sqrt{n}/\pi)]^{1/2} d\xi / \dot{n}_0 \end{aligned} \quad (182)$$

For the left hand integral in Equation 182 choose same  $\xi = \Delta$  so that  $n(\xi)$  satisfies

$$\dot{n}_0^2 = (1/2)[(1 - P(\sqrt{n})) \exp\{n\} - (1 - 2\sqrt{n}/\pi)] \quad (183)$$

Then a portion of the left hand integral can be bounded by

$$\int_0^\Delta [\dot{n}_0^2 + (1 - P(\sqrt{n})) \exp\{n\} - (1 - 2\sqrt{n}/\pi)]^{1/2} d\xi < \int_0^\Delta [\dot{n}_0^2]^{1/2} d\xi = \dot{n}_0 \Delta \quad (184)$$

Observe that the expression  $\sqrt{1+x}$  is bounded by  $1 + x/2$  for positive  $x$  since

$$\sqrt{1+x} < \sqrt{1+x+(x^2/4)} = 1+x/2 \quad (185)$$

Use of this expression in the remaining portion of the left hand integral in Equation 182 gives

$$\begin{aligned} \int_{\Delta}^{\dot{n}_0} [\dot{n}_0^2 + (1 - P(\sqrt{n})) \exp\{n\} - (1 - 2\sqrt{n}/\pi)]^{1/2} d\xi &< \int_0^{\dot{n}_0} [(1 - P(\sqrt{n})) \exp\{n\} - (1 - 2\sqrt{n}/\pi)]^{1/2} d\xi \\ &+ 1/2 \int_0^{\dot{n}_0} (\dot{n}_0^2 / [(1 - P(\sqrt{n})) \exp\{n\} - (1 - 2\sqrt{n}/\pi)])^{1/2} d\xi \end{aligned} \quad (186)$$

where the integrals on the right hand side have been extended to  $\xi = 0$ . This preserves the inequality since the integrals are positive. Then from Equations 182, 184, and 186 the derivative is bounded by

$$\left. \frac{dn_a}{d\dot{n}_0} \right|_{\dot{n}_0=0} \leq \lim_{\dot{n}_0 \rightarrow 0} \frac{1}{\dot{n}_0} [\dot{n}_0 \Delta + \frac{\dot{n}_0^2}{2} \int_0^{\dot{n}_0} [(1 - P(\sqrt{n})) \exp\{n\} - (1 - 2\sqrt{n}/\pi)]^{-1/2} d\xi] \quad (187)$$

A comparison of Figure 4 and Equation 183 shows that  $\Delta$  must go to zero as  $\dot{n}_0$  goes to zero. Then, since the dependence of  $n_a$  on  $\dot{n}_0$  has to be greater than or equal to zero, Equation 187 shows that

$$\left. \frac{dn_a}{d\dot{n}_0} \right|_{\dot{n}_0=0} = 0 \quad (188)$$

A combination of observations on Equations 177, 179, and 188 shows that the derivative of voltage with current at the zero field current  $J_0$  is

$$\left. \frac{dV/dJ}{J=J_0} = (kT/e)(D/2x_2\sqrt{J})dn_a/d\xi_a \right|_{\xi_a = \sqrt{J_0} D/x_2} \quad (189)$$

which has a finite, non-zero, value. Since the slope at  $J = J_0$  is zero from the space-charge side and it has a finite, non-zero value from the accelerating field side, this theory predicts a discontinuity in the slope of  $J$  as a function of  $V$  at  $J = J_0$ .

Figure 25 shows an example where this discontinuity in the slope is apparent. The dashed lines intersecting at  $J = J_0$  in Figure 25 show the limiting slopes as  $J$  approaches  $J_0$  from the space-charge range and from the accelerating-field range. Van der Ziel (Reference 9) treated this example in the space-charge range, and his Figure 1 shows  $J$  approaching  $J_0$  with a zero slope as does this Figure 25. Equation 189 gives the limiting slope as  $J$  approaches  $J_0$  from the accelerating-field range. Figure 25 shows that the limiting slope from the accelerating field range is almost the same as the slope of the Child's law line at  $J = J_0$ , although Child's law does not approximate  $J$  as a function of  $V$  for this example. The following discussion shows that the agreement between the limiting slope and the Child's law slope is not a coincidence.

In many practical examples such as the one treated in Figure 24, the discontinuity in the slope of  $J\{V\}$  causes only a small perturbation in the curve. In this case the extended theory provides a nearly smooth transition from the space-charge range into the accelerating field range and then produces a gradual approach to the Schottky line. In this case the term  $dr_c/dn_c$  in Equation 92 is small except for a very small region near  $n'_c = 0$ . Then Equation 92 reduces to Equation 189 and remains accurate for  $J$  somewhat greater than  $J_0$ . For many experimental conditions including those of Figure 24, Equation 27 which gives  $dn_a/d\xi_a$ , is

accurately represented by only one term - the one involving  $2\sqrt{n_a/\pi}$ . Consequently, Equation 189 reduces to

$$dV/dJ = (kT/e)(D/2x_2\sqrt{J}) 2 (n_a/\pi)^{1/4} \quad (190)$$

Replacement of  $x_2$  and  $n_a$  in Equation 190 with their equivalent expressions from Equations 20 and 87 removes the normalizing factors and gives

$$dV/dJ = (m/2e)^{1/4} \epsilon_0^{-1/2} V^{1/4} / J^{1/2} \quad (191)$$

Rearrangement and integration of Equation 191 gives

$$J = 4/9 \epsilon_0 \sqrt{2e/m} V^{3/2} / D^2 \quad (192)$$

which is the same as Equation 128, Child's law. This exercise shows that Child's law is a good approximation for the current as a function of voltage not only in the space-charge range, but also a good approximation for a certain interval into the accelerating-field range. Figure 24 shows, for that example, that  $J$  follows Child's law closely up to about  $J = 1.15 J_0$ .

#### 4. FIELDS AND CHARGE IN THE INTERELECTRODE SPACE

With the theory developed in Subsection 1 of Section II and Subsection 1 of Section IV, it is now possible to plot the voltage  $V$ , the electric field  $F$  and the number-density of electrons  $N$  as a function of distance from the cathode for various conditions of cathode loading  $J/J_0$ . At a specified temperature  $T$  and current density  $J_0$ , a family of these plots can be made with  $J/J_0$  as a parameter. These curves show the changing conditions in the interelectrode space as the current drawn from the cathode changes, and they help to develop a firmer concept of the fields and charge in the interelectrode space.

For space-charge-limited conditions, Equations 28 gives the distance as a function of voltage to the cathode side of the potential minimum. After the addition of the normalizing constants from Equations 20, 21, and 87 this relationship can be expressed as

$$x = (x_2/\sqrt{J}) \epsilon_C \{eV/kT\} \quad (193)$$

From Equations 84 and 85,  $V$  ranges from 0 to  $V_s$  in Equation 193 causing  $x$  to vary from 0 to  $x_m$  with

$$x_m = (x_2/\sqrt{J}) \xi_c \{ \ln(J_0/J) \} \quad (194)$$

and

$$V_s = (kT/e) \ln(J_0/J) \quad (195)$$

The terms  $x$  and  $V$  are measured relative to the potential minimum; although it is more desirable to have  $x'$  and  $V'$  measured relative to the cathode surface where

$$x' = x - x_m \quad (196)$$

and

$$V' = V - V_s \quad (197)$$

Note that  $x$  is negative and  $V$  is positive while  $x'$  is positive and  $V'$  is negative in the cathode space. Then Equation 193 can be expressed as

$$x' = (x_2/\sqrt{J}) \xi_c \{ e(V' + V_s)/kT \} - x_m \quad (198)$$

The electric field  $F$  is then  $-dV/dx$  where from Equation 28

$$\begin{aligned} dV/dx = & -(kT/e)(\sqrt{J}/x_2) \{ [1 + P\{\sqrt{n_c}\}] \exp\{n_c\} \\ & - [1 + 2(n_c/\pi)^{1/2}] \}^{1/2} \end{aligned} \quad (199)$$

with

$$n_c = eV/kT \quad (200)$$

The number density of electrons from Equation 19 is

$$N = (\epsilon_0/e) d^2V/dx^2 \quad (201)$$

and from Equation 23 this is

$$N = (\epsilon_0 kT/2e^2) (J/x_2^2) \exp\{n_c\} [1 + P\{\sqrt{n_c}\}] \quad (202)$$

To the anode side of the potential minimum Equation 27 gives the voltage as a function of distance. After addition of the normalizing constants this relationship is expressed as

$$V = (kT/e)n_a \{x\sqrt{J}/x_2\} \quad (203)$$

or

$$V' = (kT/e)n_a \{(x' + x_m)\sqrt{J}/x_2\} - V_s \quad (204)$$

The electric field is then  $-dV/dx$  where

$$dV/dx = (kT/e)(\sqrt{J}/x_2) \{[1 - P(\sqrt{n_a})] \exp\{n_a\} - [1 - 2\sqrt{n_a}/\pi]\}^{1/2} \quad (205)$$

The number density of electrons from Equations 23 and 201 is then

$$N = (\epsilon_0 kT/2e^2)(J/x_2^2) \exp\{n_a\} [1 - P(\sqrt{n_a})] \quad (206)$$

For accelerating field conditions Equation 27 gives the voltage as a function of distance with the added condition on  $n_0$  from Equation 177. The expression for the voltage is then

$$V = (kT/e)n_a \{x\sqrt{J}/x_2\} \quad (207)$$

with

$$n_0 = (4\pi/e)\epsilon_0^{3/2} (kT/e)^{7/4} (e/2\pi m)^{1/4} \ln^2(J/J_0)/\sqrt{J} \quad (208)$$

Then from Equation 27 the electric field  $F$  is given by  $-dV/dx$  where

$$dV/dx = (kT/e)(\sqrt{J}/x_2) \{n_0^2 + [1 - P(\sqrt{n_a})] \exp\{n_a\} - [1 - 2(n_a/\pi)]^{1/2}\}^{1/2} \quad (209)$$

In addition, from Equations 23 and 201, the number density of electrons is given by

$$N = (\epsilon_0 kT/2e^2)(J/x_2^2) \exp\{n_a\} [1 - P(\sqrt{n_a})] \quad (210)$$

with the added condition on  $n_0$  in Equation 208.

Figures 26 through 28 show the fields and charge in the interelectrode space for an example cathode at 900°C with a current density of 5A/cm<sup>2</sup>. Figure 26 shows the electric potential as a function of distance away from the cathode surface. The curve at  $J/J_0 = .6$  shows clearly the potential minimum. The curve at  $J/J_0 = 1$  shows the zero slope of  $V(x)$  at  $x = 0$ . The curves for  $J/J_0 > 1$  show the linear behavior of  $V(x)$  near  $x = 0$ . The function  $J(V)$  can, in principle, be constructed from Figure 26 by drawing a line of constant  $x$  at the distance  $x = D$  representing the diode spacing. The intersection of this line with the  $J(V)$  lines then gives the voltage associated with each value of  $J$  for the specified diode spacing. This line of constant  $x$  must fall to the right of the potential minimum to generate a valid  $J(V)$  curve, however, since the retarding field range requires a non-zero  $n_0$  in the solution for  $\xi\{n_c\}$ . In contrast to the accelerating field field range, this  $n_0$  for the retarding field range depends on the spacing  $D$  and cannot be incorporated into the series of curves in Figure 26 which are independent of  $D$  (see Reference 9).

Figure 27 shows the derivative  $dV/dx$  which is the negative of the electric field  $F$ . The curve at  $J/J_0 = .6$  shows  $-F$  to be negative near the cathode. The electric field goes to zero at the potential minimum, and then becomes positive in the anode space. The curve for  $J/J_0 = 1$  shows  $F = 0$  at  $x = 0$  as required for the zero field current density. As  $J$  increases above  $J_0$  the curve for  $-F$  rises rapidly near the cathode and then levels off at distances away from the cathode. This tendency becomes more pronounced for large  $J/J_0$  until the electric field is nearly constant in the interelectrode space. This constant electric field is, of course, expected as space-charge effects become small.

Figure 28 shows the number density  $N$  of electrons as a function of distance from the cathode. For small  $J/J_0$  the number density of electrons is large near the cathode due to electrons returning from the potential minimum. However the number density falls off rapidly away from the cathode toward the potential minimum. For  $J/J_0$  closer to 1, the number density of electrons is smaller near the cathode but it does not fall off

so rapidly going away from the cathode. From Equations 195, 200, and 202 the electron number density at the cathode is

$$N(x = 0) = (\epsilon_0 kT/2e^2)(J_0/x_2^2)[1 + P\{\ln(J_0/J)\}] \quad (211)$$

At the zero field current density  $J_0$ , Equation 211 shows that

$$N(x = 0) \bigg|_{J=J_0} = (\epsilon_0 kT/2e^2)(J_0/x_2^2) \quad (212)$$

As  $J/J_0$  becomes very small, Equation 211 shows that the number density of electrons becomes twice that given in Equation 212,

$$N(x = 0) \bigg|_{J=0} = (\epsilon_0 kT/e^2)(J_0/x_2^2) = 2N(x = 0) \bigg|_{J=J_0} \quad (213)$$

since the error function  $P(u)$  tends to 1 for large argument. Equation 213 is reasonable since at  $J = J_0$  none of the electrons are returning while at  $J = 0$  all the electrons are returning to give twice the density at the cathode surface. As  $J$  becomes larger than  $J_0$  the electron density at the cathode is again larger than it is at  $J = J_0$  and it falls away much more rapidly at distances away from the cathode. From Equation 210 the electron density at the cathode surface is

$$N(x = 0) = (\epsilon_0 kT/2e^2)(J/x_2^2) \quad (214)$$

which increases linearly with increasing  $J$ .

Figure 28 suggests that the electron density decreases away from the cathode with a finite slope for  $J$  less than or equal to  $J_0$ . However for  $J > J_0$  the electron density has a decreasing slope with unbounded magnitude at the cathode surface. This can be shown rigorously from the equations involved. From Equations 28 and 202

$$\begin{aligned} dN/dx = & -(\epsilon_0 kT/2e^2)(J^{3/2}/x_2^3)[\exp\{n_c\}(1 + P\{\sqrt{n_c}\})] \\ & + 1/\sqrt{n_c}][(1 + P\{\sqrt{n_c}\})\exp\{n_c\} - (1 + 2\sqrt{n_c}/\pi)]^{1/2} \end{aligned} \quad (215)$$

For large  $n_c$  this tends to the limiting value

$$dN/dx = -(\sqrt{2} \epsilon_0 kT/e^2) (J_0^{3/2}/x_2^3) \quad (216)$$

which gives the slope at the cathode surface for  $J$  much less than  $J_0$ .

Here use is made of Equations 195 and 200 and it is noted that

$1/\sqrt{n_c}$  and  $\sqrt{n_c}/\exp\{n_c\}$  both become small for large  $n_c$ . It is also assumed for this illustration that the anode is sufficiently far away to allow a potential minimum in the cathode space. For  $n_c$  near zero, corresponding to  $J$  near  $J_0$ , Equations 45, 54, and 215 show that  $dN/dx$  has the limiting value

$$dN/dx = -(\epsilon_0 kT/2\sqrt{\pi} e^2) (J_0^{3/2}/x_2^3) \quad (217)$$

This can also be shown directly from Equation 215 by the use of L. Hospital's rule to show that

$$\lim_{n_c \rightarrow 0} (1/2\sqrt{\pi}) \left( \frac{[1 + P\{\sqrt{n_c}\}] \exp\{n_c\} - [1 + 2\sqrt{n_c/\pi}]^2}{n_c} \right)^{1/2} = (1/2\sqrt{\pi}) \quad (218)$$

In all these cases, then, from very small  $J$  up to  $J = J_0$ , the slope of the electron density  $dN/dx$  is finite at the cathode.

For  $J > J_0$  the derivative  $dN/dx$  is found from Equations 64 and 210

$$dN/dx = (\epsilon_0 kT/2e^2) (J^{3/2}/x_2^3) [(1 - P\{\sqrt{n_a}\}) \exp\{n_a\}] \quad (219)$$

$$-1/\sqrt{\pi n_a} [\dot{n}_0^2 + (1 - P\{\sqrt{n_a}\}) \exp\{n_a\}]$$

$$-1 (1 - 2\sqrt{n_a/\pi})^{1/2}$$

The term  $1/\sqrt{n_a}$  increases without bound as  $n_a$  approaches zero showing that the slope of the electron density is unbounded at the cathode.

This is true for any  $\dot{n}_0 > 0$  corresponding to  $J > J_0$ .

5. EFFECTS OF DIODE SPACING ON  $J\{V\}$ 

The zero-field current density  $J_0$  is often estimated from experimental data through a determination of the "space-charge breakaway point." This is the point where the  $J\{V\}$  curve departs by a specified amount from Child's law. One method of specifying this "breakaway point" uses the projections of the slopes of the  $J\{V\}$  curve from the space-charge region and from the accelerating-field region plotted on two-thirds power paper. The intersection of the two lines representing these projected slopes is taken as an estimate of  $J_0$ . The dashed lines in Figure 29 give an example of this method. Affleck (Reference 17) presents experimental data showing that the diode spacing affects the value of the "breakaway point" determined in this manner. The following discussion uses the extended theory developed in this report to show how the "breakaway-point" technique leads to erroneous values of  $J_0$  which are dependent on the diode spacing.

The extended theory of Subsection 2 of Section IV is used to calculate the  $J\{V\}$  curve for a cathode similar to the one tested by Affleck. Figure 29 shows the current density as a function of applied voltage for two values of diode spacing, 0.3 mm and 0.9 mm. For the example the temperature is 900°C and the zero-field current density is  $5 \text{ A/cm}^2$ . The dashed lines in Figure 29 show that the "space-charge breakaway point" gives values of " $J_0$ " higher than the true value of  $J_0$  in each case. The projected slopes intersect at " $J_0$ " =  $7.6 \text{ A/cm}^2$  for the 0.3 mm spacing and at " $J_0$ " =  $6.3 \text{ A/cm}^2$  for the 0.9 mm spacing. This property of the "breakaway point" giving higher values of " $J_0$ " for the close-spaced diodes than for those with wider spacings agrees with Affleck's conclusions based on data from a diode with variable electrode spacing.

The above example shows that the "breakaway point" gives only a very crude estimate of the value for  $J_0$ . In the 0.3 mm case the estimate is 50% too high, while in the 0.9 mm case it is 25% too high. One reason for the erroneously high values of  $J_0$  is that  $J\{V\}$  follows the Child's law

line to higher values of  $J$  above  $J_0$  in the close-spaced diode than for the one with a wider spacing. A second reason is that the comparison for the cases with different diode spacing is made over the same range of diode voltage. Since the electric field is higher in the close-spaced diode the current density rises to a considerably higher values in this case. This causes the line projecting the slope of  $J\{V\}$  from the accelerating-field range to lie in the region of higher values of  $J$  for the close-spaced diode. In conclusion, the use of intercepting slopes on two-thirds power paper to determine the "space-charge breakaway point" leads to erroneous values of  $J_0$  which are dependent on the diode spacing.

## SECTION V

## CONCLUSIONS

A method for treating space-charge effects in the accelerating-field range is given. The method results in the current as a function of voltage for close-spaced, parallel-plane diodes. The space-charge theory developed by Langmuir is applied to the accelerating-field range along with the image-potential theory suggested by Schottky. The key to combining these two theories is to note that the space-charge potential is essentially a linear function of distance over the range of action of the image potential. The combined theory produces a current-voltage curve which begins at the zero-field current and voltage predicted by space-charge theory and then gradually approaches the Schottky line. For those conditions where Child's law approximates the current-voltage curve in the space-charge range, Child's law also approximates the current-voltage curve generated by the combined theory for an interval of current values extending above the zero-field current.

The solution procedure outlined by Langmuir is summarized in a single equation. The derivative of this equation shows more explicitly the behavior of the current-voltage curve at the transition points from the exponential range to the space-charge range and from the space-charge range to the accelerating-field range. The current and the derivative of the current are both continuous functions of voltage at the transition from the exponential range into the space-charge range. At the transition from the space-charge range into the accelerating-field range the current is a continuous function of voltage, but the derivative of the current is discontinuous. This discontinuity arises because Langmuir space-charge theory always gives a zero slope for the current-voltage curve at the zero field current. However, the combined theory gives a finite, non-zero slope for the current-voltage curve at this transition point.

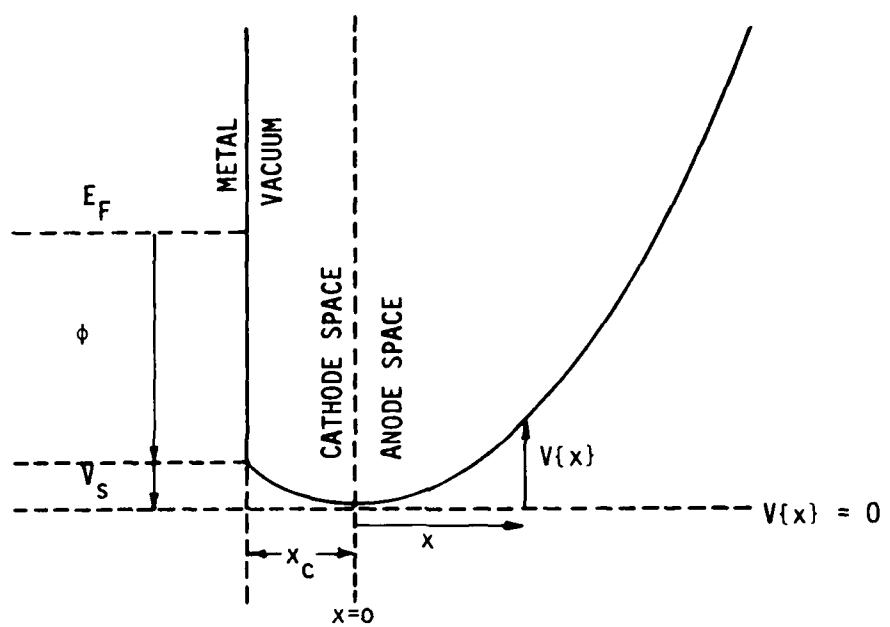


Figure 1. Schematic of the Space-Charge Region Outside an Emitting Surface.

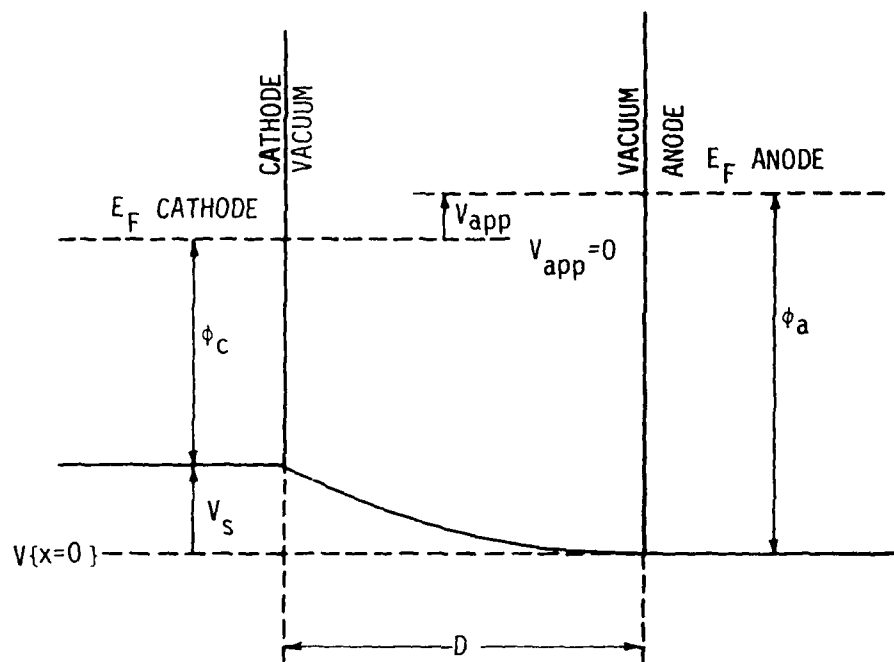


Figure 2. Schematic of the Potential Distribution Between the Anode and Cathode under Retarding Field Conditions.

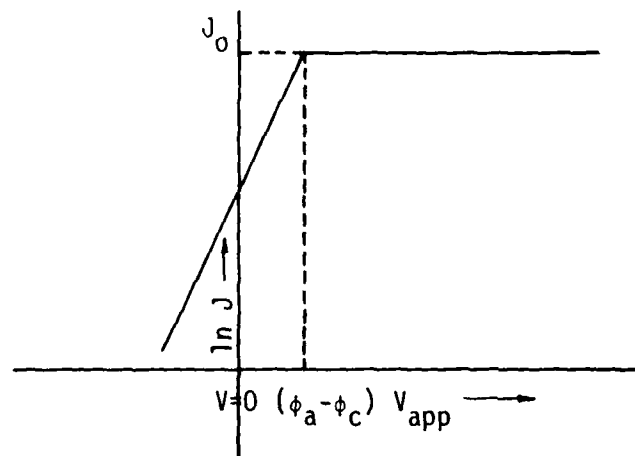


Figure 3. Schematic of the J-V Curve Under Retarding Field Conditions.

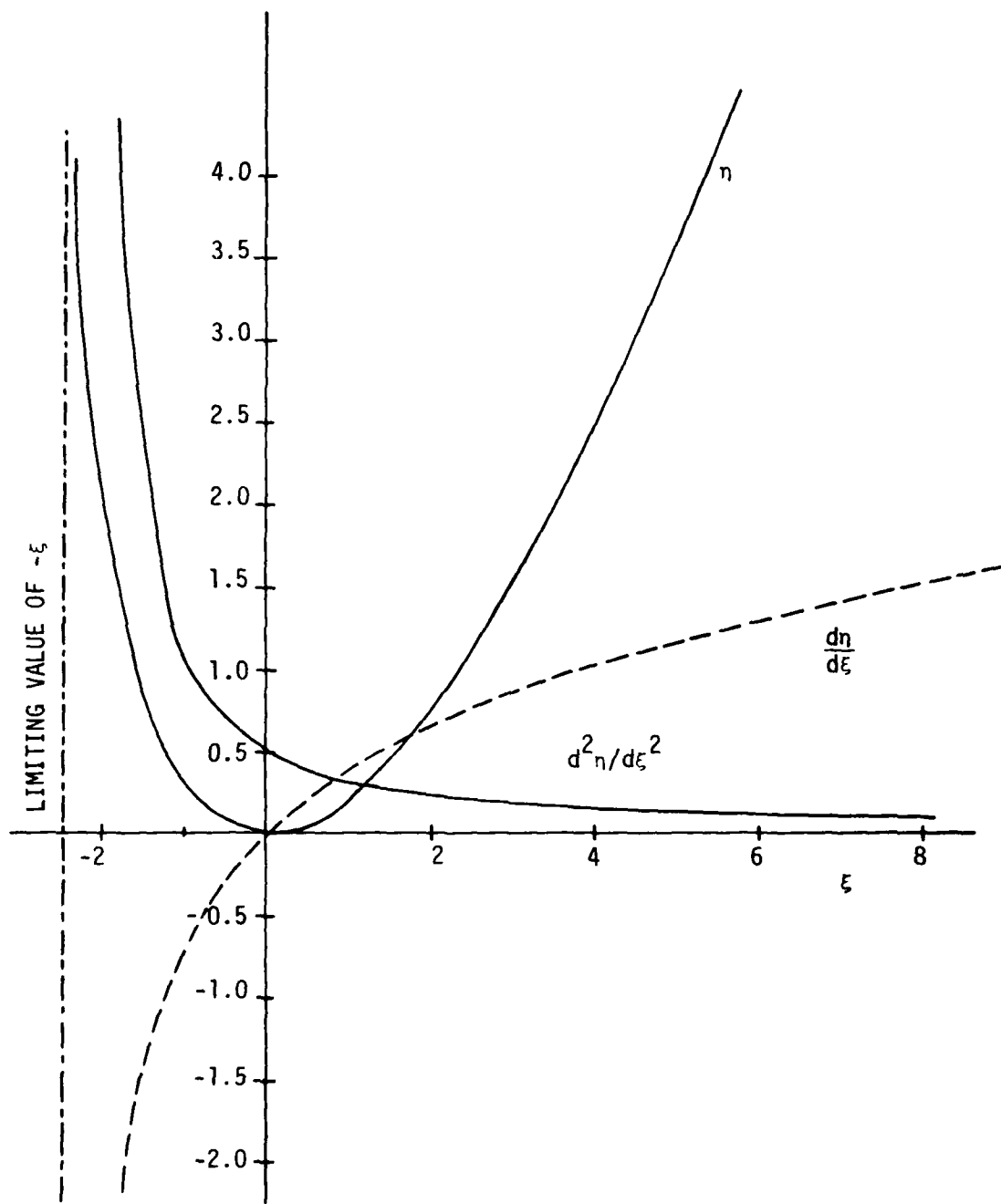


Figure 4. The Function  $n(\xi)$  and its First and Second Derivatives. Notice that  $\xi$  has a Minimum Value of -2.55389.

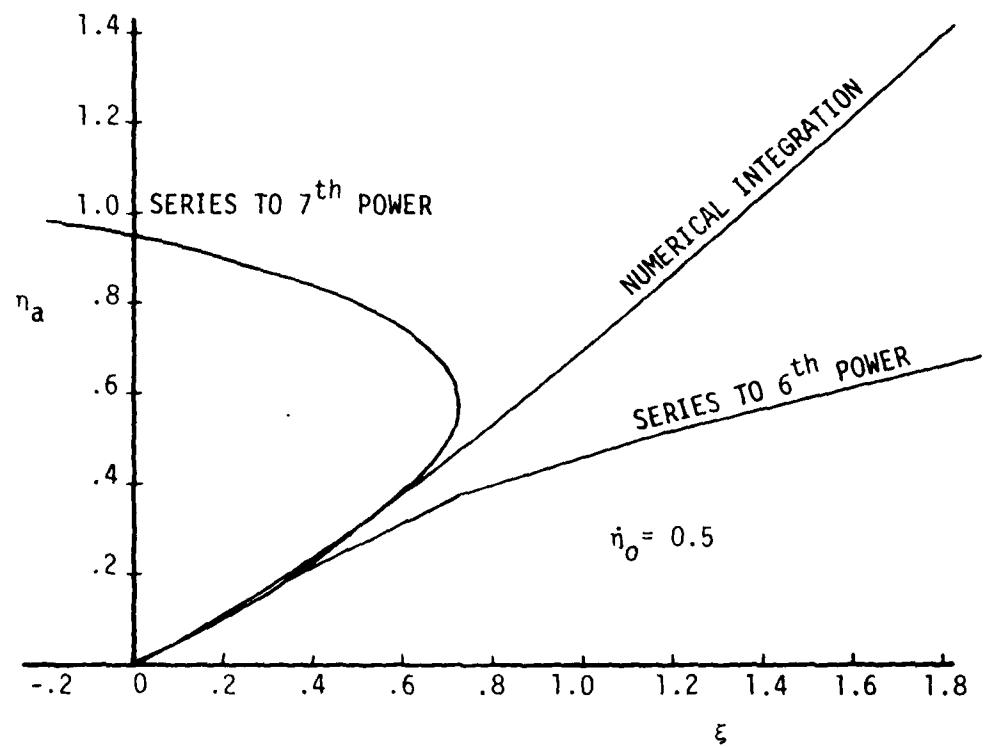


Figure 5. Series Solution to Langmuir's Differential Equation for the  $n_a$ ,  $\xi$  Function for  $n_0 = 0.5$ .

```

6  REM Data is dEta/dXi at X=0, delta X, print steps,Xmax
15  READ D0,H,L,B
20  DISPLAY "DELTA Xi=",H,"dY/dX(at X=0)=",D0
22  DISPLAY
30  LET X=Y=Q=0
40  LET E=1/L
90  DISPLAY "Value of Xi","Value of Eta"
100  GOSUB 320
120  GOTO 160
130  LET U=Y
131  GOSUB 1000
132  LET F1=P5-(1-2*U1/1.77245)+D0*D0
136  IF F1<0 LET F1=0
137  LET F1=SQR(F1)
138  LET U=Y+H/3*F1
139  GOSUB 1000
140  LET Y=Y+H*(F1+H/4*P5)
150  LET X=X+H
160  IF (X+H-B)+1E-07 >= 0 THEN 190
170  LET R=X+H
180  GOTO 200
190  LET R=B
200  LET A=INT(E*R)/E
210  IF (A+L-R)-1E-07 >= 0 THEN 230
220  LET A=A+L
230  IF (X-A)+1E-07 >= 0 THEN 260
240  LET Q=A
250  GOSUB 320
260  IF R=B THEN 280
270  GOTO 130
280  IF ABS(R-A)<.5*.000001 THEN 311
290  LET Q=R
300  GOSUB 320
311  STOP
320  LET U=Y
321  GOSUB 1000
322  LET F1=P5-(1-2*U1/1.77245)+D0*D0
323  LET F1=SQR(F1)
324  LET U=Y+(Q-X)/3*F1
325  LET X1=X
326  LET X=Q
327  GOSUB 1000
328  LET Y1=Y+(Q-X1)*(F1+(Q-X1)/4*P5)
329  LET X=X1
370  DISPLAY Q,Y1
380  RETURN
390  DATA 0,.01,.01,.2
980  REM THIS SUBROUTINE CALCULATES (1-ERF(SQR(Y)))*EXP(Y)
1000  LET U1=SQR(U)
1010  LET T=1/(1+.327591*U1)
1020  LET P5=T*(1.42141+T*(-1.45315+T*1.06141))
1030  LET P5=T*(.25483+T*(-.2845+P5))
1040  RETURN
1040  RETURN

```

Figure 6. BASIC Language Program Using Mixed Runge-Kutta-Taylor Method to Solve for  $\eta_a(\xi)$ .

DELTA X1 = .01	dY/dX (at X=0) = 0
Value of Xi	Value of Eta
0	0
.01	.000025
.02	9.97337E-05
.03	2.23642E-04
.04	3.96808E-04
.05	6.19072E-04
.06	8.89864E-04
.07	1.20892E-03
.08	1.57608E-03
.09	1.99116E-03
.1	2.45376E-03
.11	2.96366E-03
.12	3.52062E-03
.13	4.12445E-03
.14	4.77483E-03
.15	5.47154E-03
.16	6.21435E-03
.17	.007003
.18	7.83726E-03
.19	8.71690E-03
.2	9.64169E-03

Figure 7. Sample Output from the Program of Figure 5.

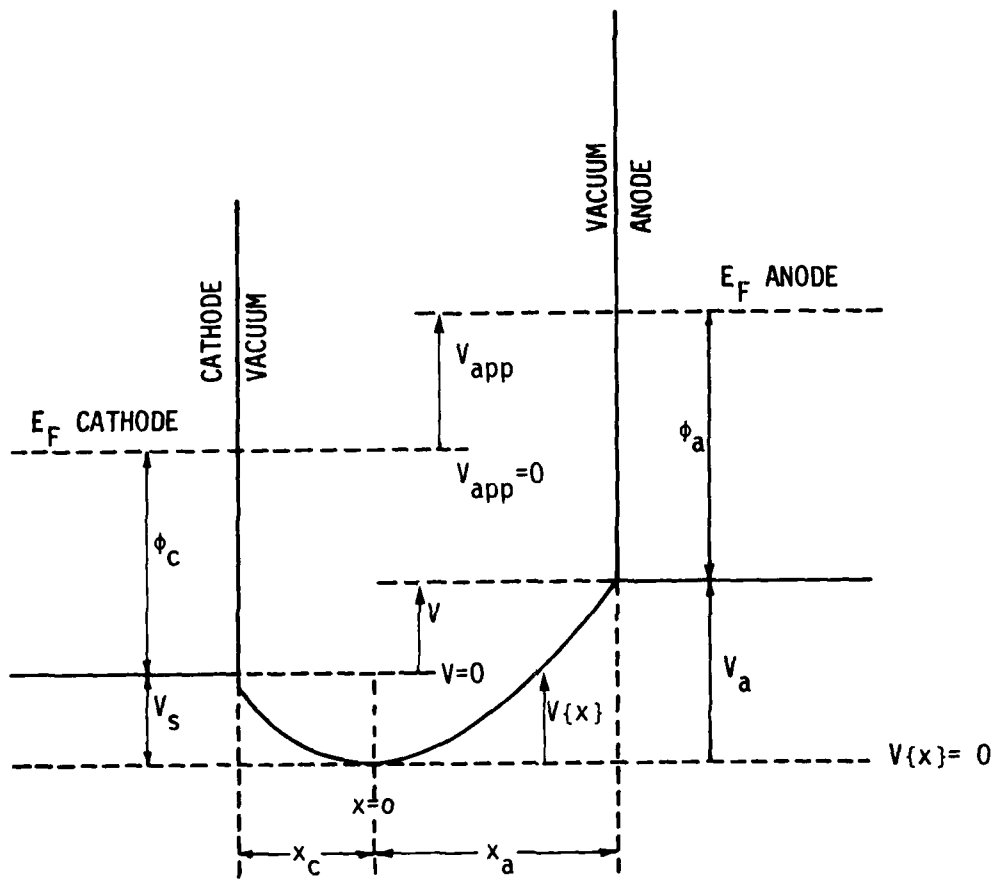


Figure 8. Schematic of the Potential Distribution Between the Anode and Cathode under Space-Charge Limited Conditions.

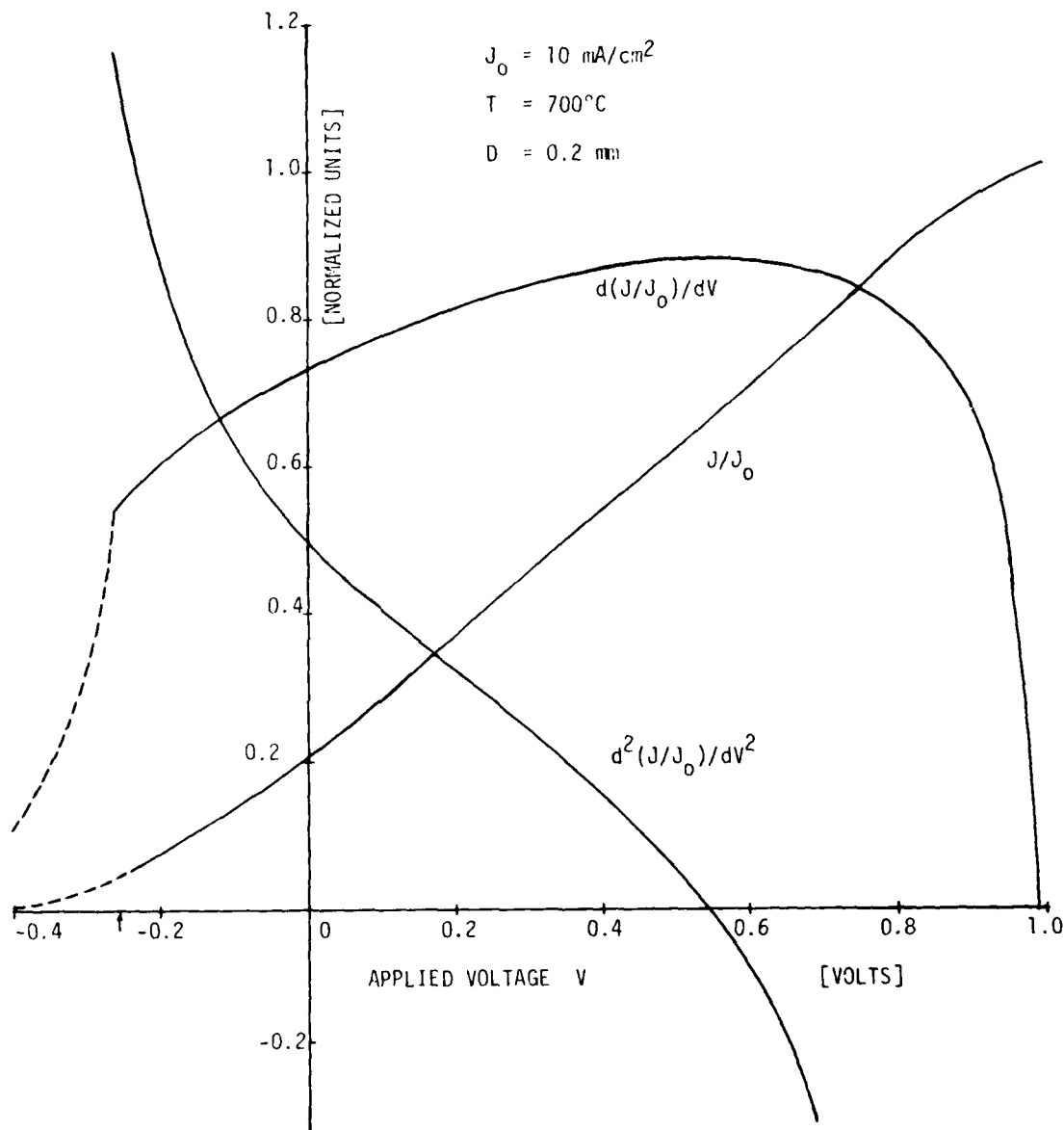


Figure 9. The Current Density and its First and Second Derivatives as a Function of the Applied Voltage for an Example Cathode. For this example  $\tau$  is assumed equal to  $\tau_c$ . The dashed lines cover the retarding field range while the continuous curves cover the space charge range. The value of the voltage at  $J = J_0$  is 0.9954 only by coincidence in this particular example.

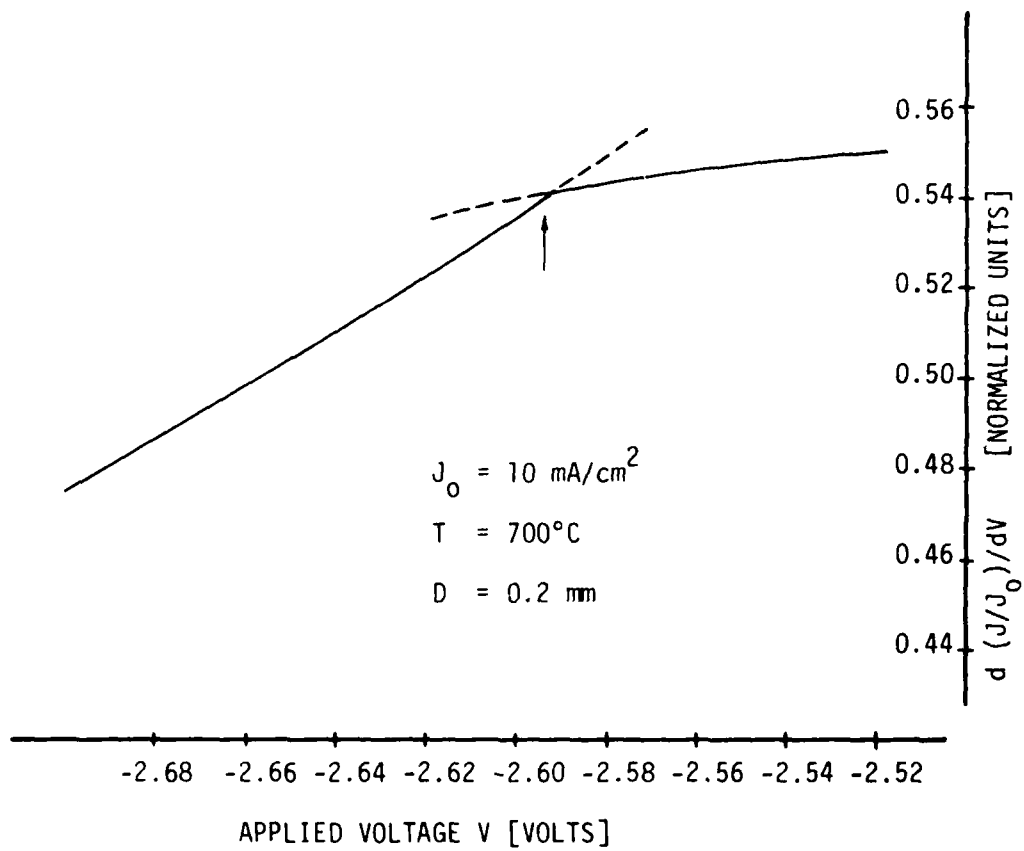


Figure 10. Detail of the First Derivative of  $J(V)$  for the example in Figure 8. The arrow marks the transition from retarding field to space-charge-limited operation. The dashed lines show the projection of the curve at constant slope from either range of operation.

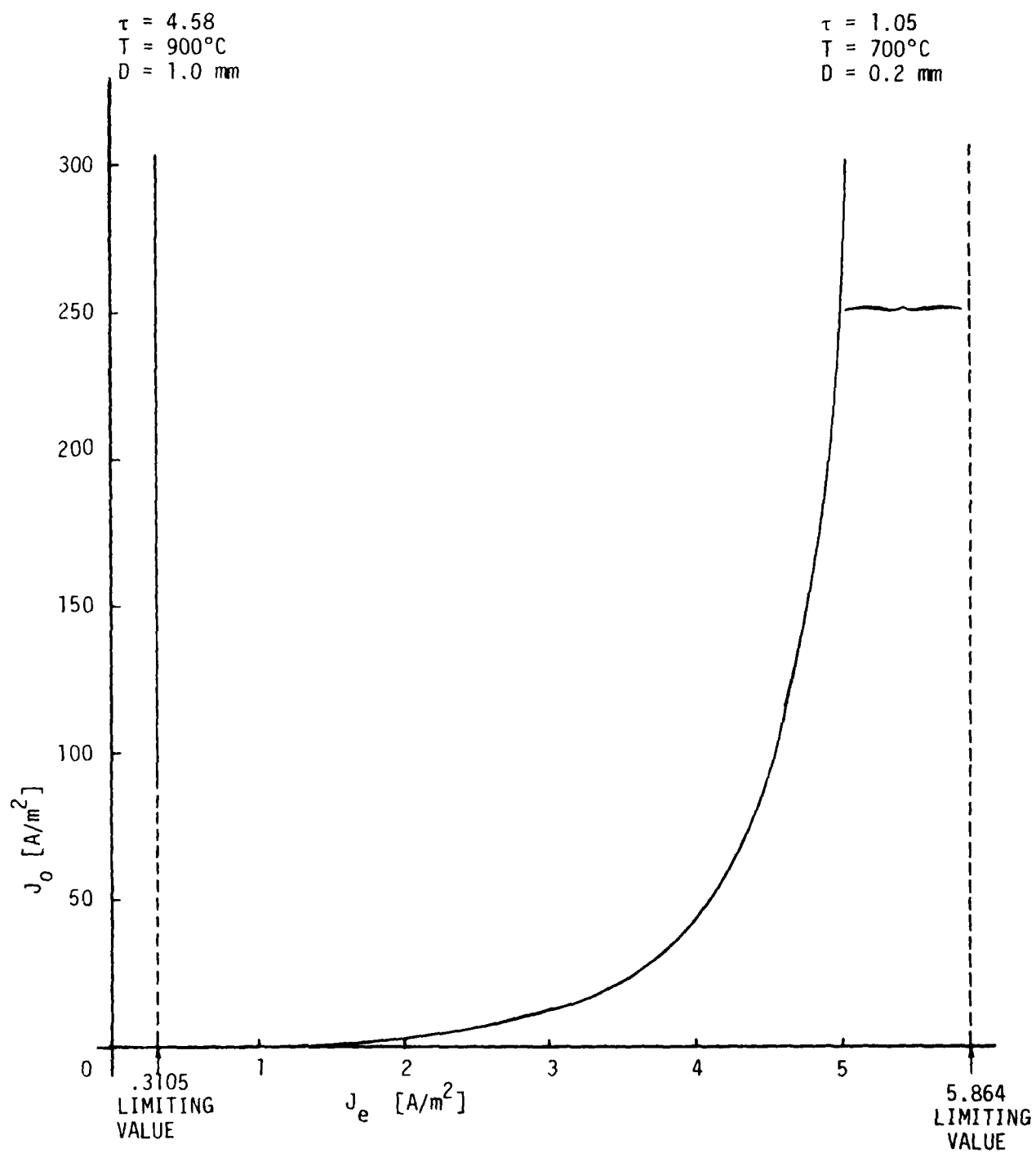


Figure 11. The zero field current  $J_0$  as a Function of  $J_e$  the Current at the Transition from Retarding Field to Space-Charge-Limited Operation for  $D = 1 \text{ mm}$ ,  $T = 900^\circ\text{C}$  and for  $D = 0.2 \text{ mm}$ ,  $T = 700^\circ\text{C}$ .

```

2 DISPLAY "Program of 3 Nov 80"
4 DISPLAY "Prints JK as a function of Jo"
5 DISPLAY
10 LET T=1073
20 LET D=.0001
30 DISPLAY "TEMP=(K)",T,"DIST=(M)",D
45 LET A2=(T+.75)*1.0886E-06
49 LET N=.1
50 DISPLAY "D/X2=",D/A2
51 DISPLAY
52 DISPLAY "Jo","JK","V<","XIC"
53 FOR O=1 TO 4 STEP 1
54 LET N=N*10
55 FOR I5=N TO 10*N STEP N
56 LET I=6.5*(A2/D)*(A2/D)
57 IF I >= I5 LET I=.5*I5
58 LET E1=-LOG(I/I5)
59 IF E1<0 LET E1=0
60 LET V1=E1*T+.62E-05
61 LET E=E1
62 GOSUB 1400
63 LET H=Z+D/A2*SQR(I)
64 LET T1=1/(1+.327591*SQR(E1))
65 LET P5=1.42141+(-1.45315+1.86141*T1)*T1
66 LET P5=(-.25483+(-.284497+P5*T1)*T1)*T1
67 LET F2=2*EXP(E1)-P5-1-SQR(E1)*1.12838
68 IF F2 <= 0 LET F2=1E-12
69 LET F2=1/SQR(F2)
70 LET H1=F2/I+D/2/A2/SQR(I)
71 LET I1=I-H/H1
72 IF ABS((I-I1)/I)<.0001 GOTO 332
73 LET I=I1
74 GOTO 70
75 DISPLAY I5,I,V1,Z
76 NEXT I5
77 NEXT O
78 STOP
79 REM THIS SUBROUTINE CALCULATES ZC AS A FUNCTION OF ETAC
80 IF E >= .2 THEN 1450
81 LET R=SQR(E)
82 LET Z=-2*R+.376126*E+2.51956E-02*E*R+6.9163E-04*E*R
83 LET Z=Z-.9409E-04*E*E*R
84 RETURN
85 IF E >= .3 THEN 1490
86 LET Z=-(-6.15614*E-65.6912*E*E-59.4893*E^3+4.10335*E^4)
87 LET Z=Z/(-.262909-14.6202*E-49.5951*E^2-16.0639*E^3+E^4)
88 RETURN
89 LET Z=-2.55389+1.41421*EXP(-E/2)-.0123*EXP(-E)
90 LET Z=Z+1/3/1.41421*(SQR(E/3.14159)+1)*EXP(-3*E/2)
91 RETURN
92 STOP

```

Figure 12. BASIC Program to Solve Equation 113 and Generate  $J_e$  and  $V_e$  as Functions of  $J_0$ .

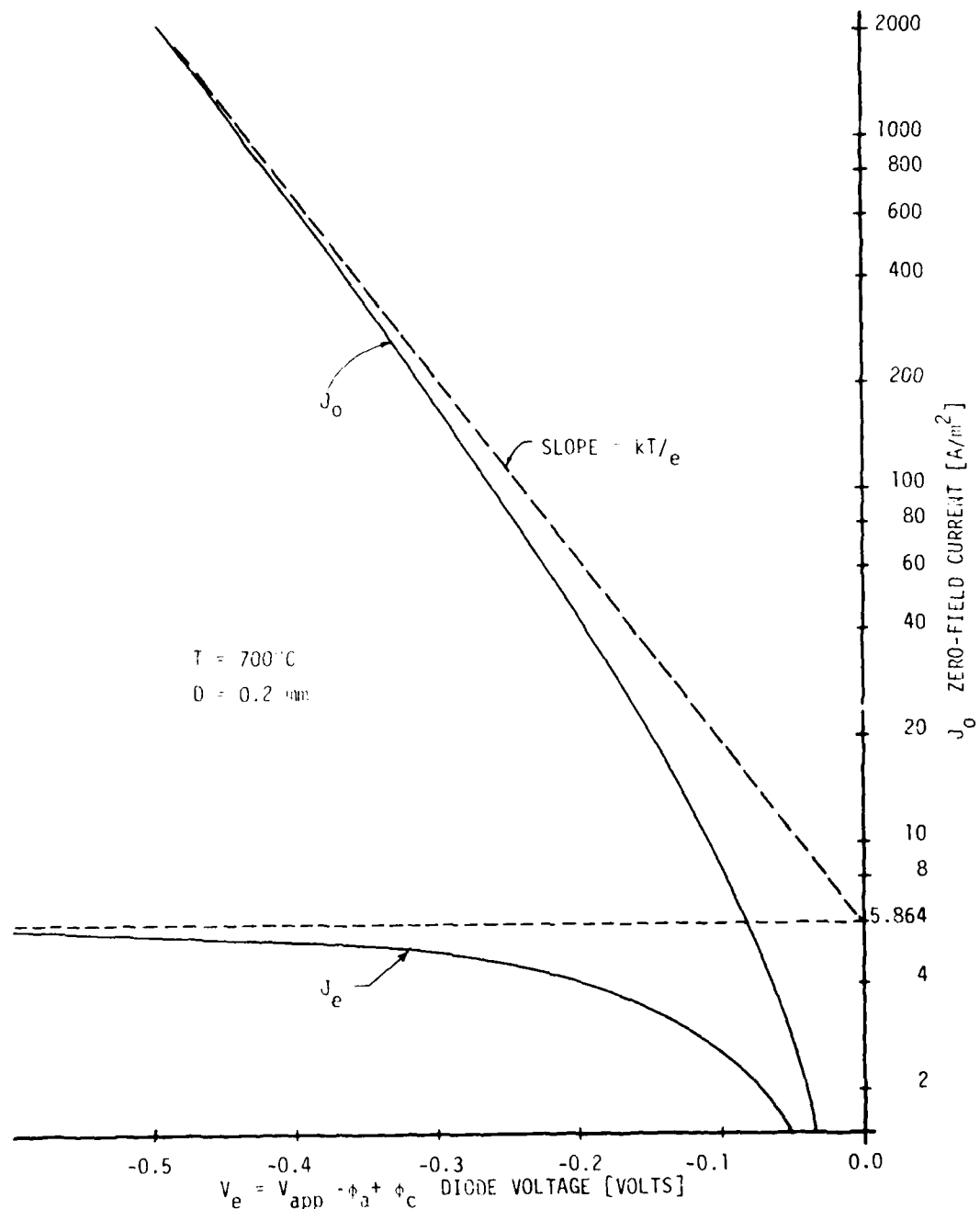


Figure 13. The Zero-Field Current  $J_0$  and the Transition Current  $J_e$  Plotted as Functions of the Transition Voltage  $V_e$  for  $D = 0.2\text{mm}$ ,  $T = 700^\circ C$ .

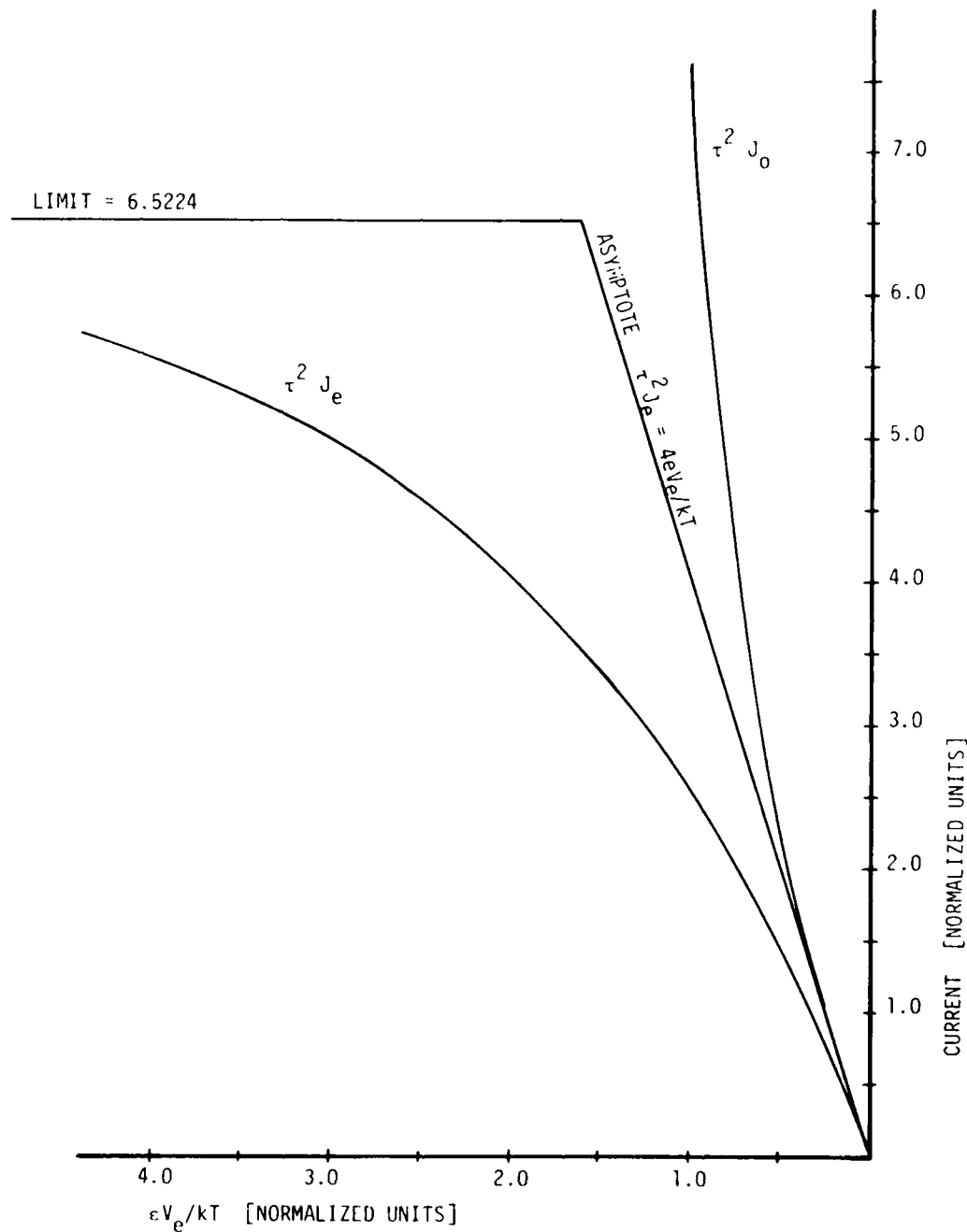


Figure 14. Graphs of  $J_e$  and  $J_0$  as Functions of  $V_e$ . These Universal Curves Relate the Measured Current at the Exponential Point to the Zero Field Current of the Cathode.

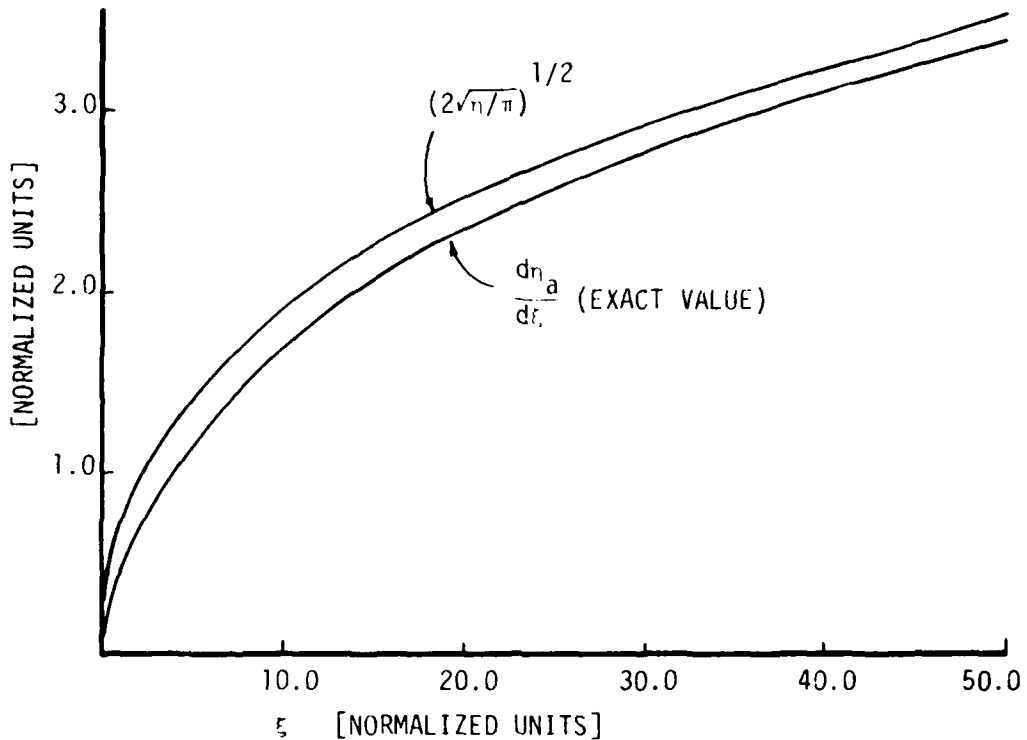


Figure 15. Comparison of the Derivative  $d\eta/d\xi$  from Langmuir's Theory with the Approximate Form of the Derivative which Leads to Child's Law.

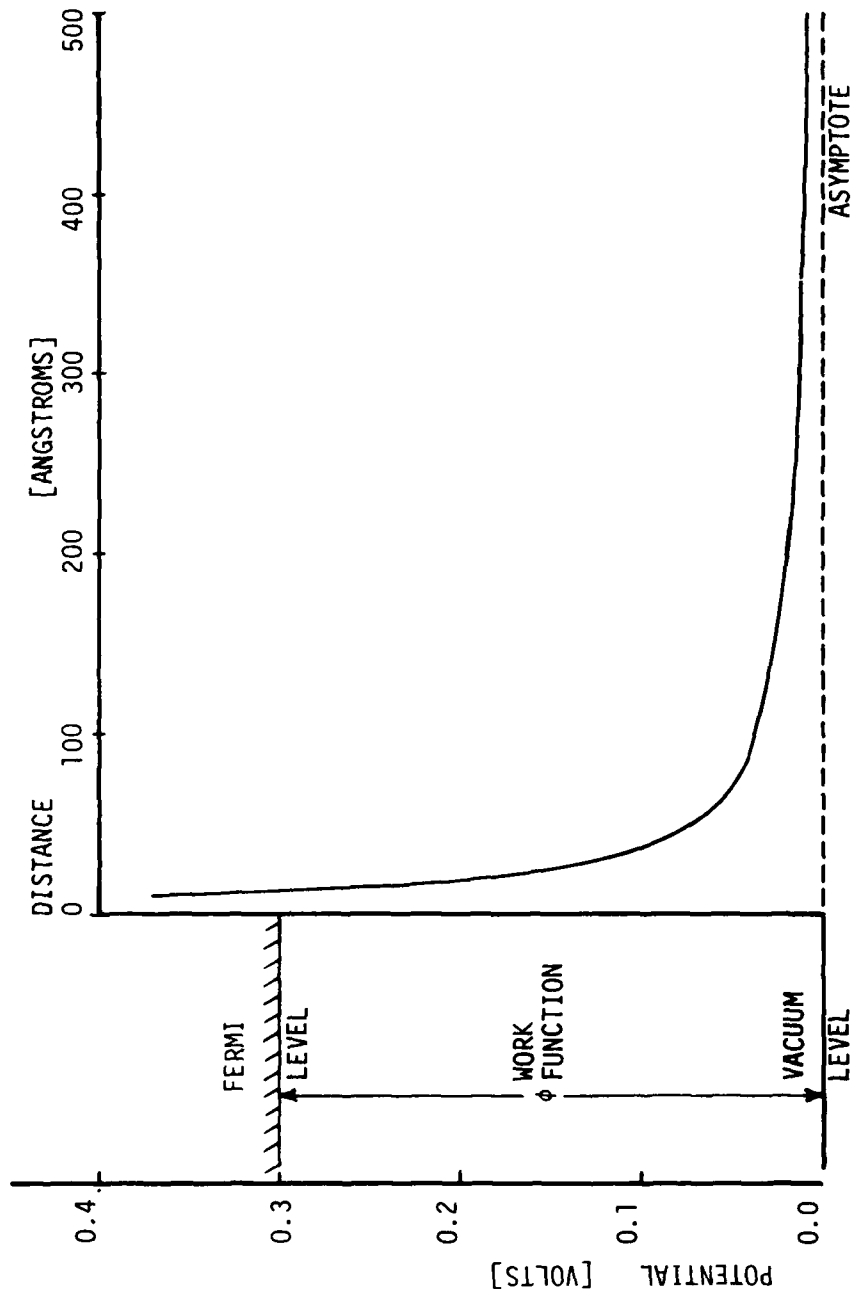


Figure 16. Potential as a Function of Distance from a Metal Surface.  
Assigned  $\phi = 0.3$  V is arbitrary.

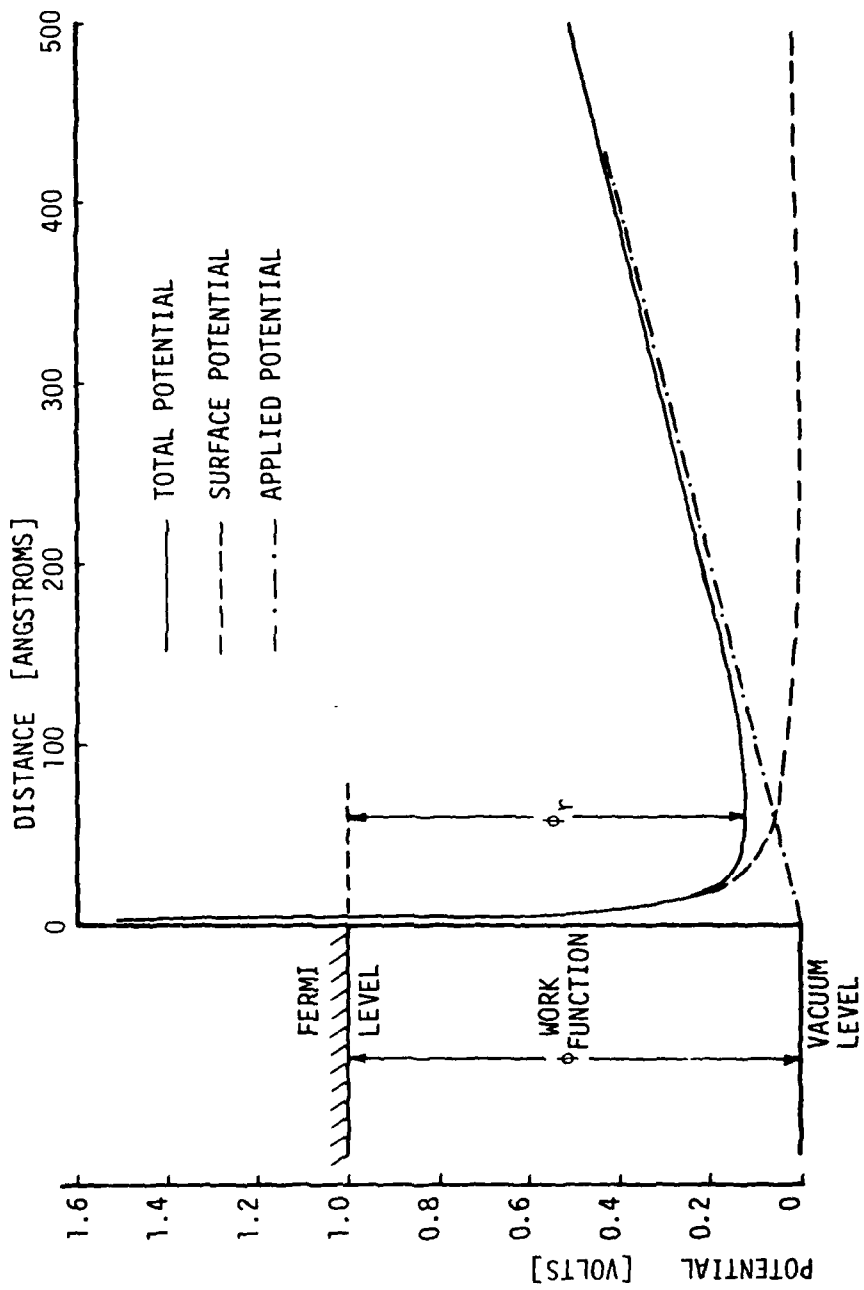


Figure 17. The Electric Potential as a Function of Distance from a Metal Surface Shown as the Sum of a Surface Field and an Applied External Field. Zero potential is referred to vacuum level. Assigned  $\phi = 1.0V$  is arbitrary. The applied external field is  $10^7$  volts/meter.

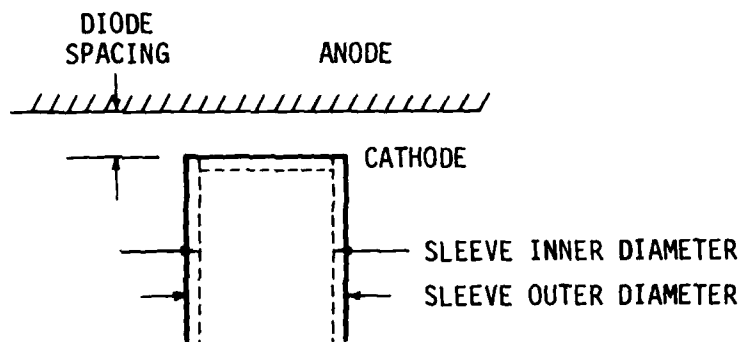


Figure 18. Schematic of a Close-Spaced Diode Tester Showing the Cross Section of a Cylindrical Cathode and Anode. The diameter of the emitting layer is the same as the sleeve inner diameter.

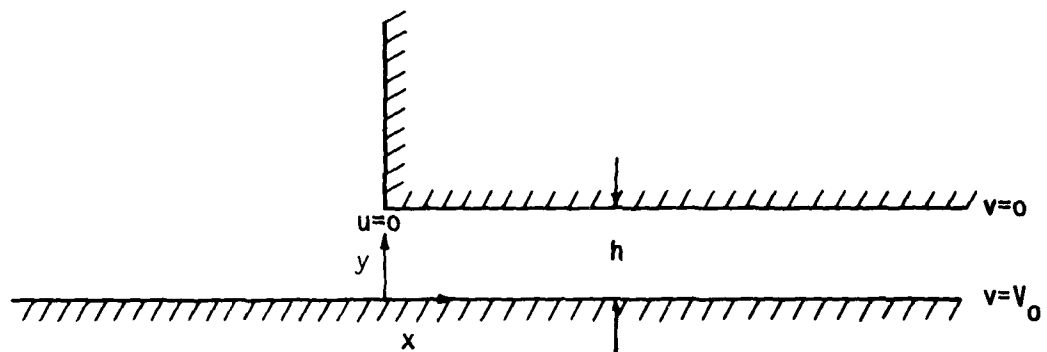
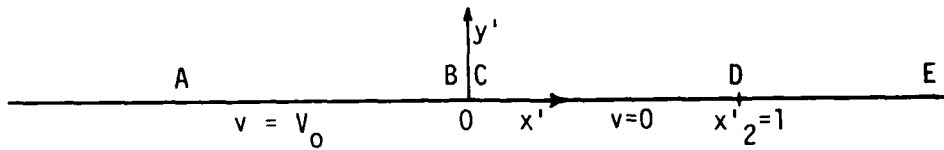
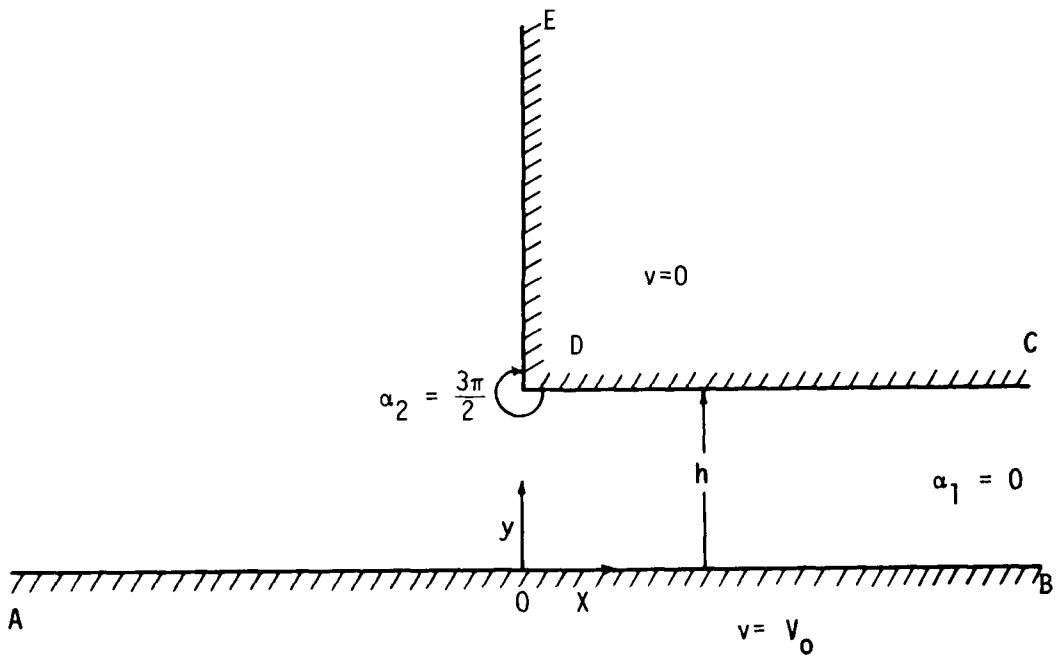


Figure 19. A Plane Edge Above a Conducting Plane. The flux function  $u$  is set to zero at  $x = 0, y = h$ .



(a) THE Z' PLANE



(b) THE Z PLANE

Figure 20. Schematic Showing Details of the Mapping from the  $Z'$  Plane to the  $Z$  Plane. This is used to solve the boundary value problem for the electric field of a plane edge above an infinite plane.

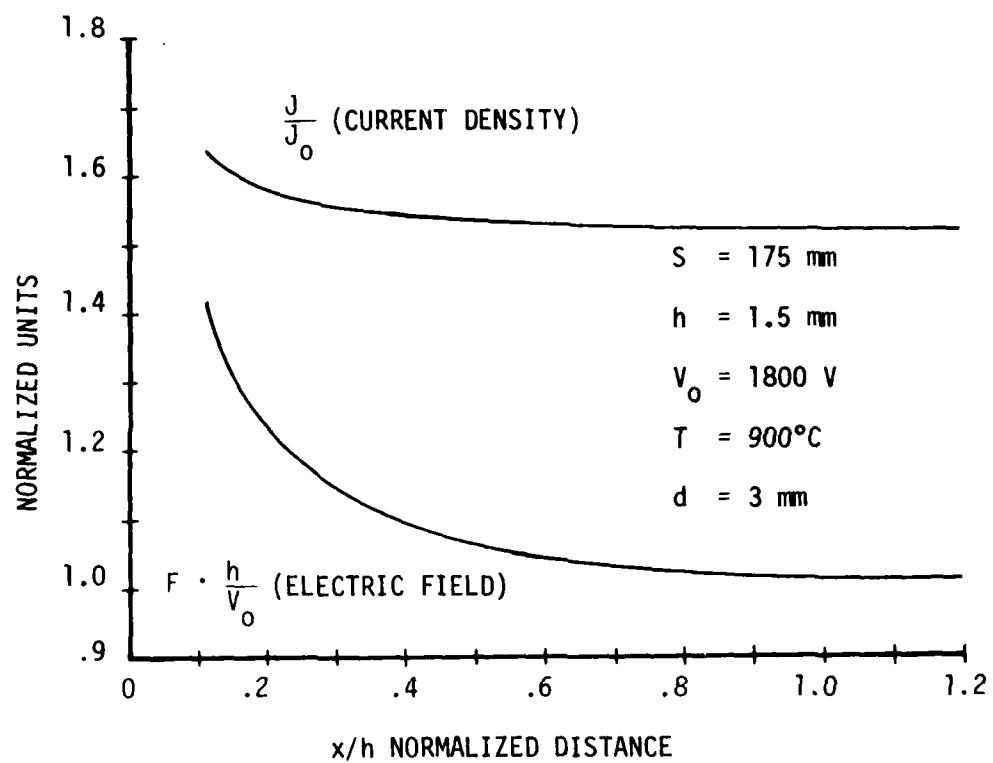


Figure 21. Current Density and Electric Field at the Cathode Surface as a Function of Distance from the Cathode Edge - All in Normalized Units. Here  $S$  = sleeve thickness,  $h$  = cathode to anode spacing,  $V_0$  = applied voltage,  $T$  = temperature of the cathode,  $d$  = diameter of the emitting area,  $X$  = distance from cathode edge, and  $J_0$  = zero-field current density.

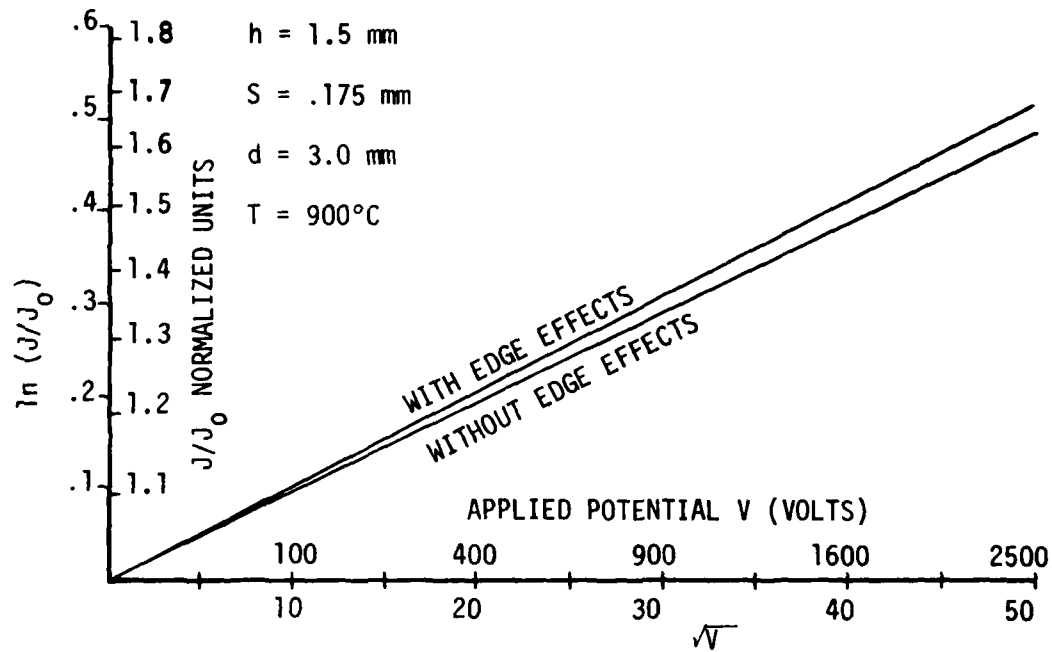


Figure 22. Theoretical Schottky Plots. The curve "with edge effects" takes into account the enhanced field at the cathode edge. The curve "without edge effects" refers to infinite parallel planes.

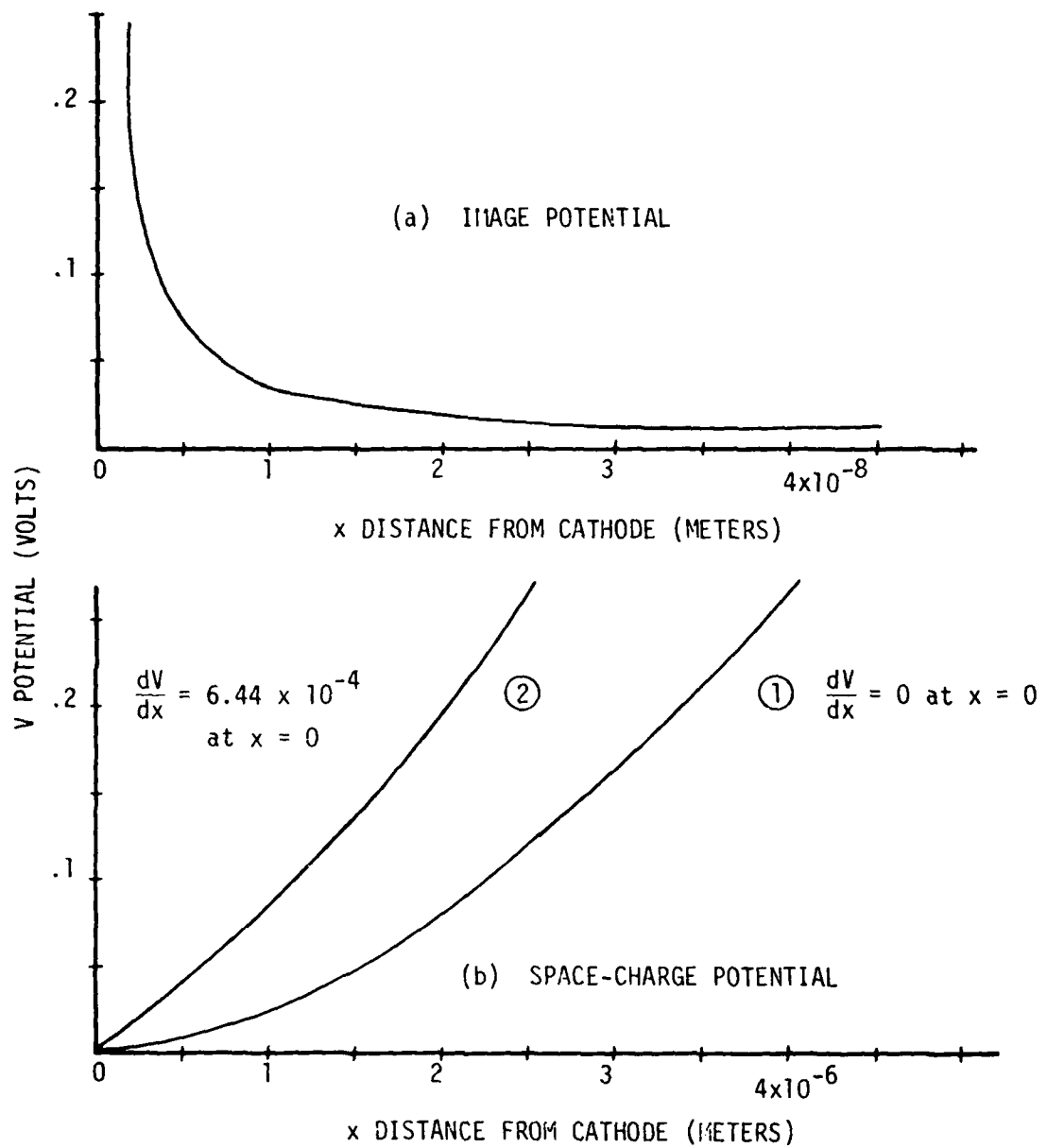


Figure 23. Electric Potential as a Function of Distance from the Cathode Surface for (a) The Image Field and for (b) The Space-Charge Field of an Example Cathode.

① For the example  $J_0 = 5 \text{ A/cm}^2$  and  $T = 900^\circ\text{C}$ . ② For the case where  $dV/dx = 6.44 \times 10^{-4}$  volts/meter, the current density  $J = 5.5 \text{ A/cm}^2$ . Note that the x-scale in (a) is expanded by a factor of 100 over (b). Curves ① and ② are linear near  $x = 0$ .

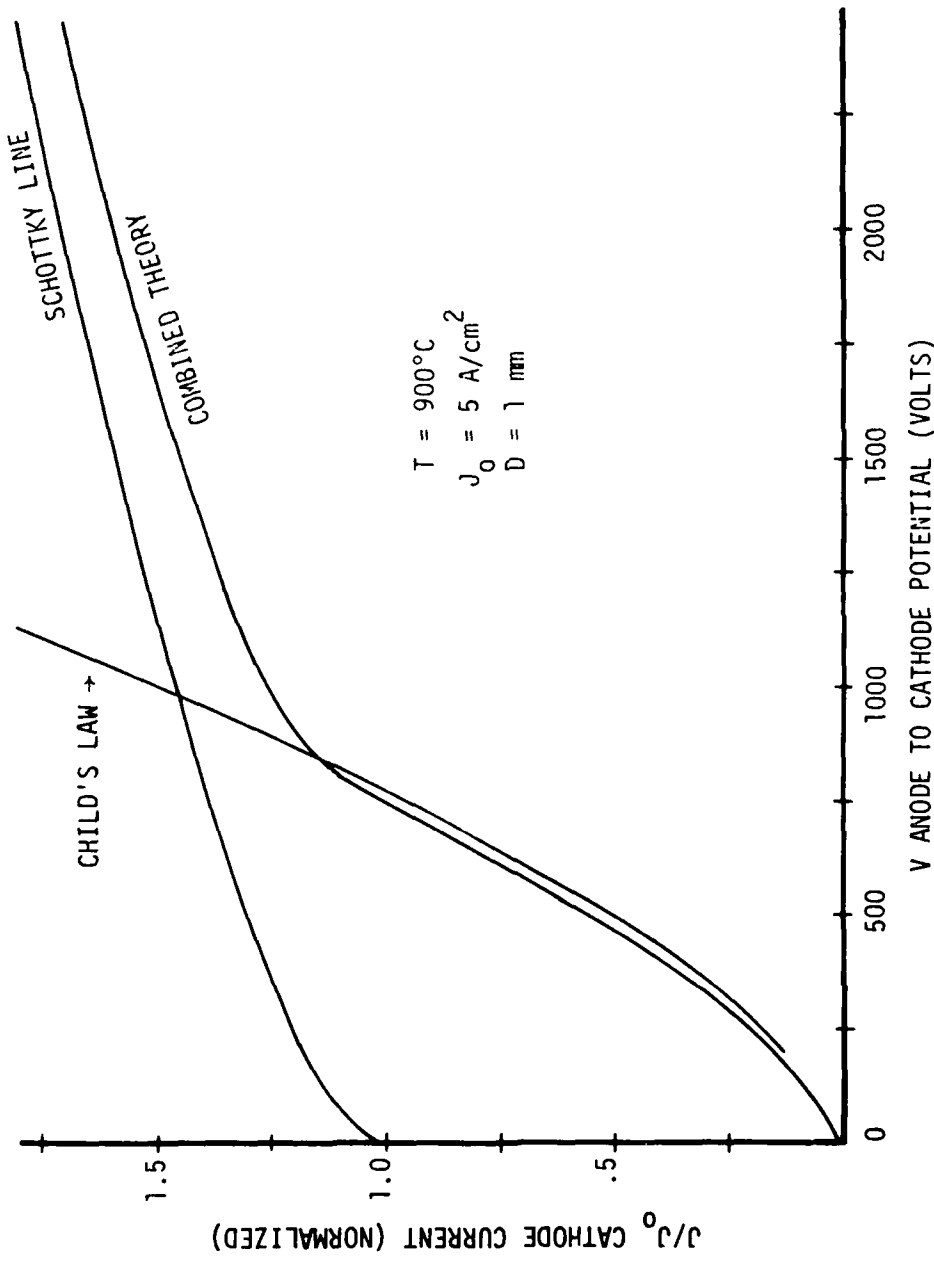


Figure 24. Current-Voltage Plot for  $J$  Ranging from Small Values up Through  $J > J_0$ . The Child's law line and the Schottky line are shown for comparison with the combined theory developed in this paper.

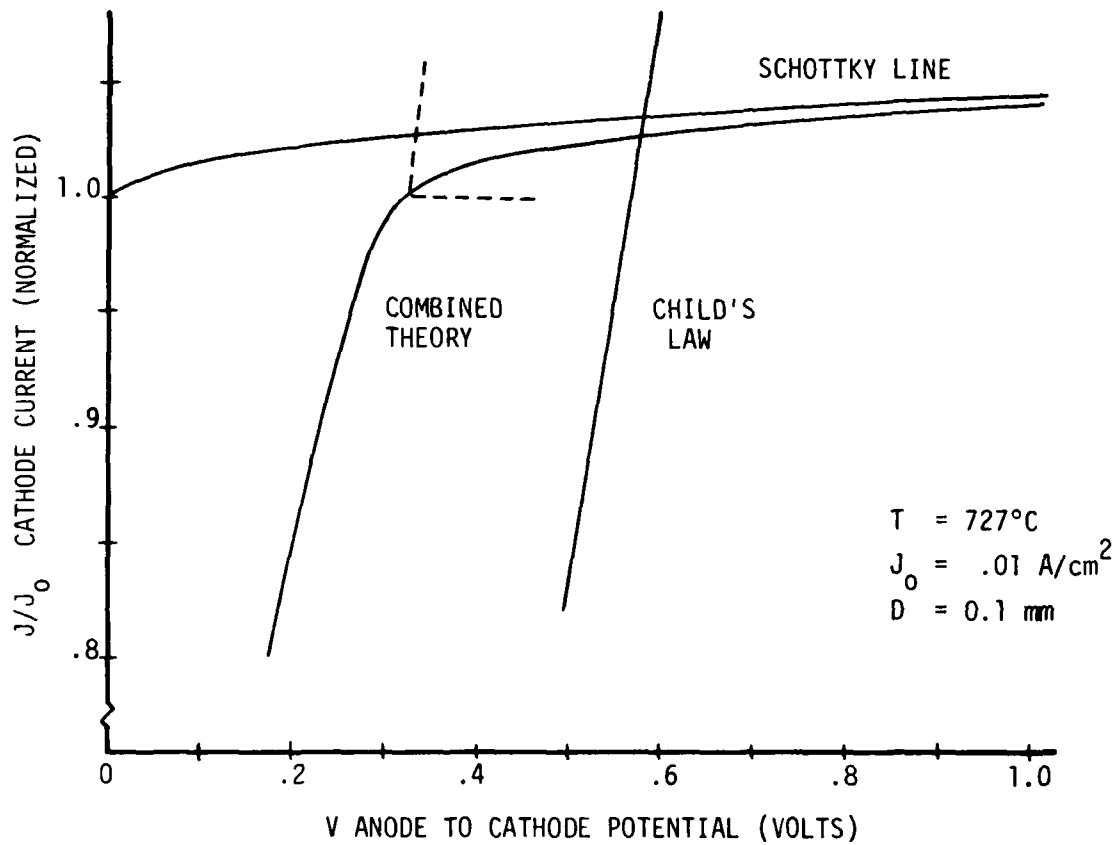


Figure 25. Current-Voltage Plot Showing a Break in the Slope of  $J$  as a Function of  $V$  at  $J = J_0$ . The dashed lines show the limiting values of the slope at  $J = J_0$ . The Child's law line and the Schottky line are shown for comparison with the combined theory developed in this paper.

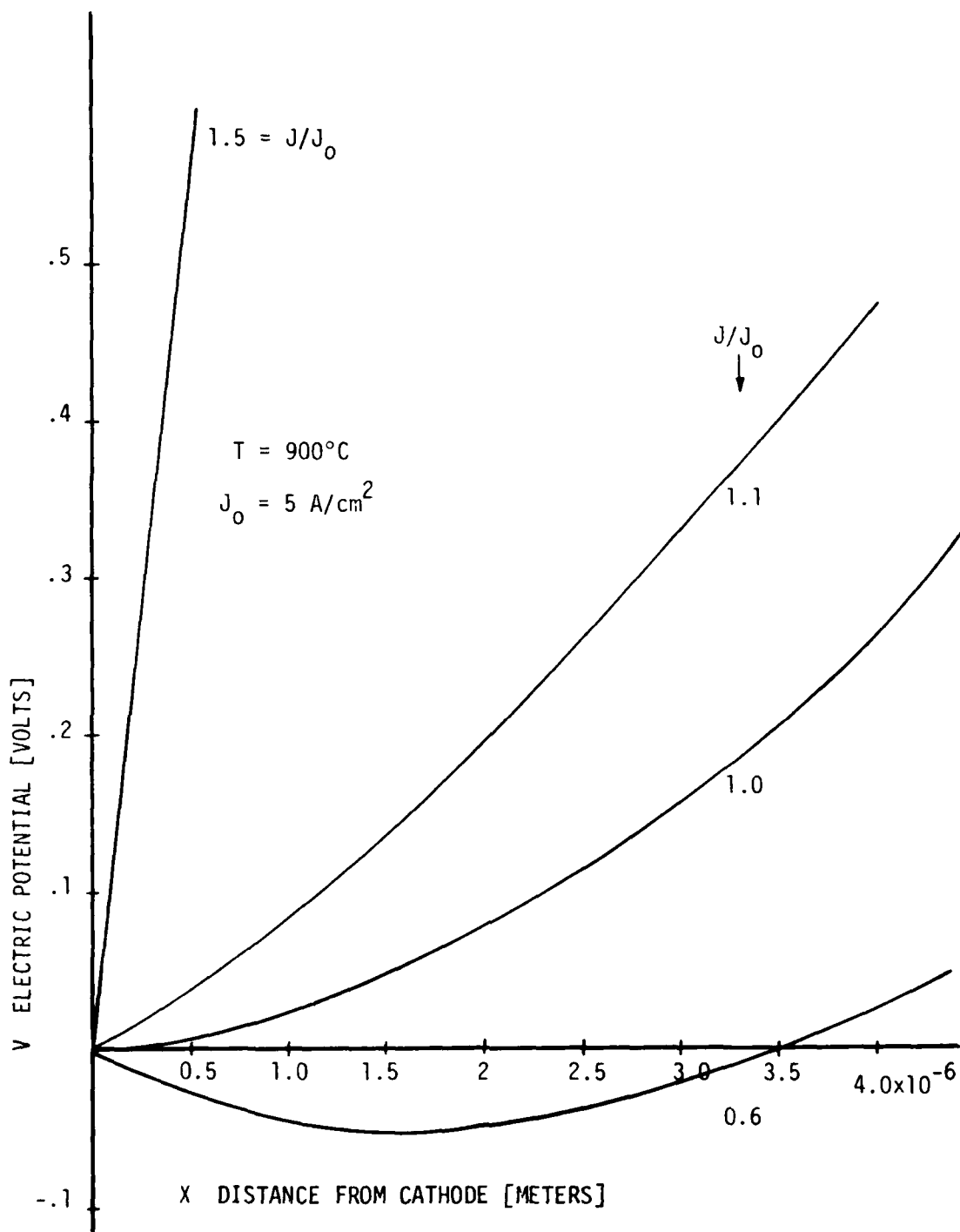


Figure 26. The Electric Potential as a Function of Distance from the Cathode Surface for Various Values of Cathode Loading  $J/J_0$ .

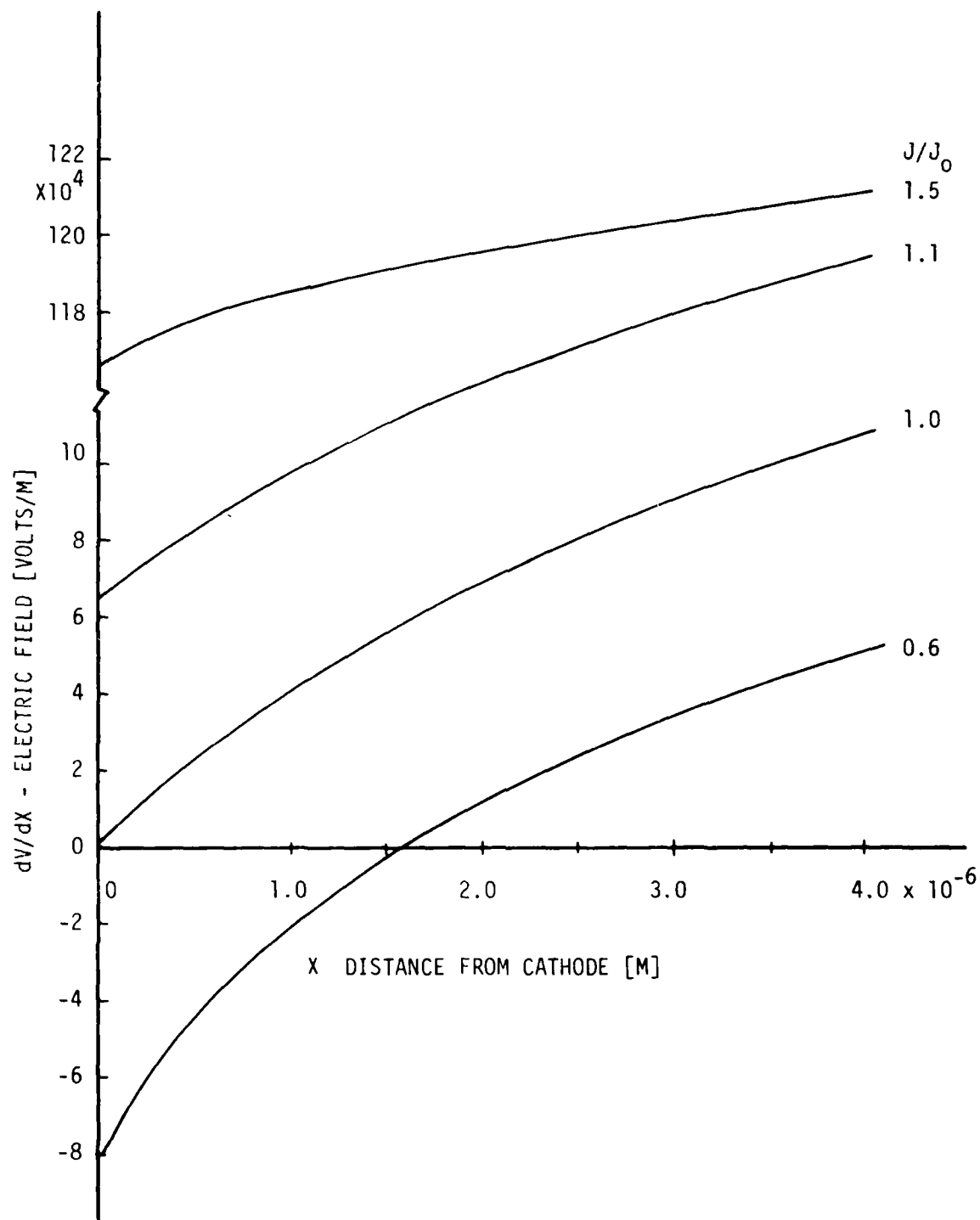


Figure 27. The Negative of the Electric Field.

$-F = dV/dX$  as a function of distance from the cathode surface for various values of cathode loading  $J/J_0$ .

AD-A102 861 AIR FORCE WRIGHT AERONAUTICAL LABS WRIGHT-PATTERSON AFB OH F/G 20/3  
THERMIONIC EMISSION AND SPACE-CHARGE THEORY. (U)  
MAY 81 J B SCOTT  
UNCLASSIFIED AFWAL-TR-81-1019

NL

2 in 2  
AD  
MAY 12 1981

END  
DATE  
FILED  
O B!  
DTIC

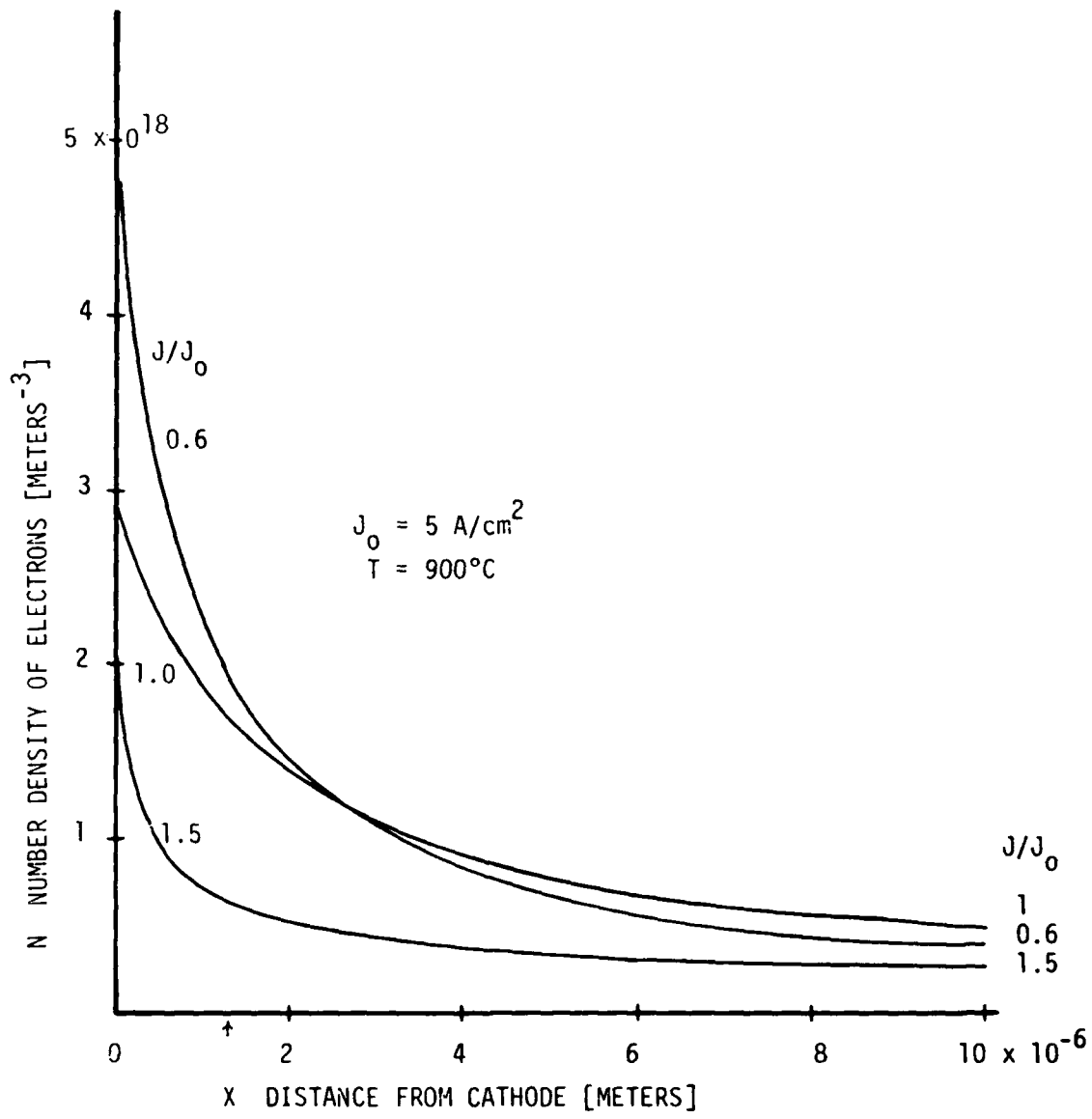


Figure 28. The Number Density of Electrons as a Function of Distance from the Cathode Surface for Various Values of Cathode Loading  $J/J_0$ .

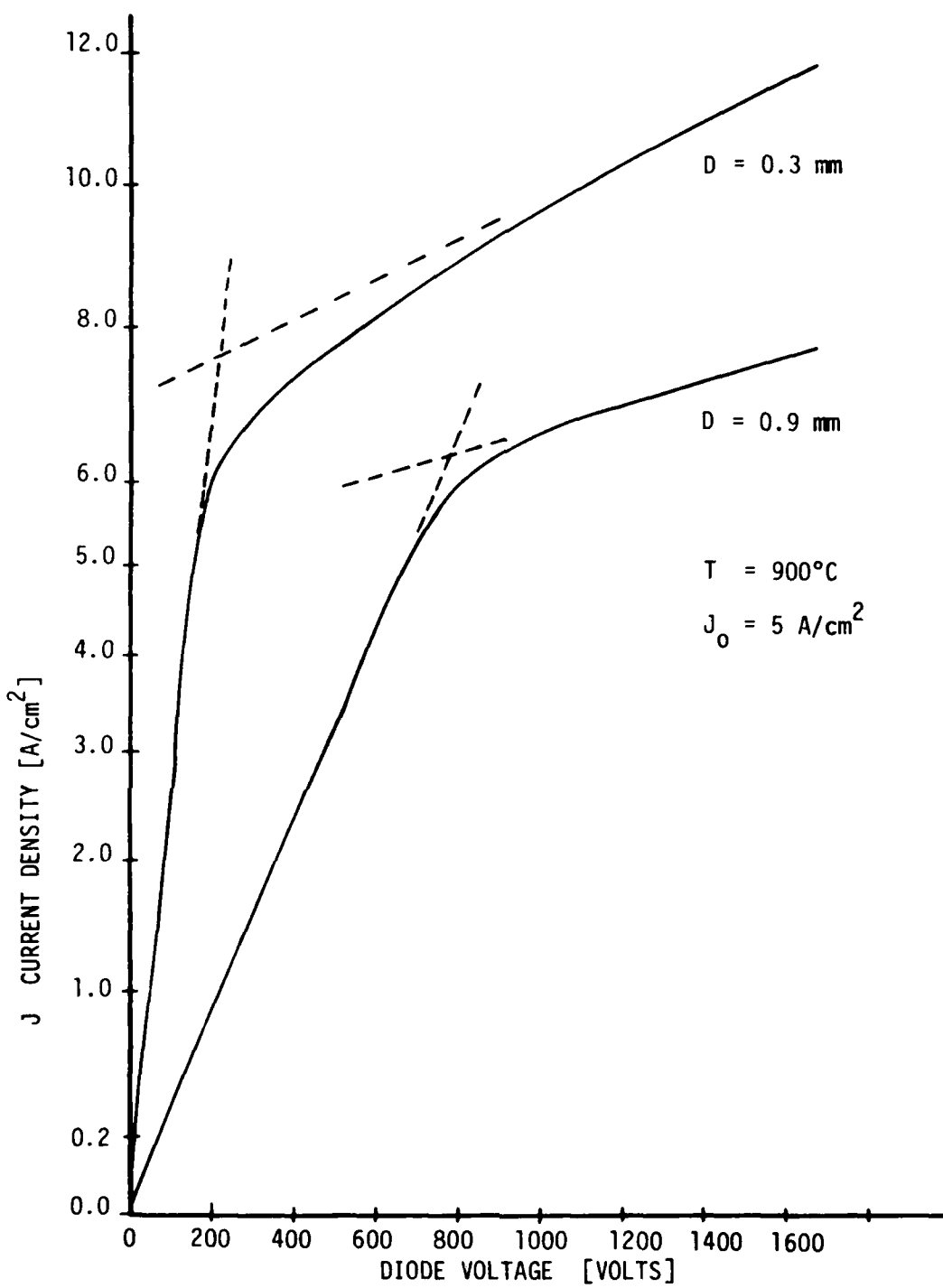


Figure 29. Current Density as a Function of Applied Voltage for Two Values of Diode Spacing, 0.3mm and 0.9mm, for a Cathode Temperature of  $900^\circ\text{C}$  and  $J_0$  of  $5 \text{ A/cm}^2$ . The dashed lines show a common method of estimating  $J_0$  from a projection of the slopes of the curve from the space-charge region and from the accelerating-field region. Note that the closer spaced diode gives a higher estimate of  $J_0$  by this method.

## REFERENCES

1. C. Davisson, "The Relation Between Thermionic Emission and Contact Difference of Potential," Physical Review, Vol. 23, p 299, 1924.
2. H. Shelton, "Thermionic Emission from a Planar Tantalum Crystal," Physical Review, Vol. 107, pp 1553-1557, 1957.
3. G. Medicus, "Thermionic Constants Determined from Retarding-Field Data," Journal of Applied Physics, Vol. 50, pp 3666-3673, 1979.
4. W. Schottky, "Über den Einfluss von Strukturwirkungen, Besonders der Thomsonschen Bildkraft, auf die Elecktronemission der Metalle," Physik Zeitschr, Vol. 15, pp 872-878, 1914.
5. J. A. Becker, "Thermionic Electron Emission and Adsorption," Reviews of Modern Physics, Vol. 7, pp 95-128, April 1935.
6. T. S. Hutchison, The Physics of Engineering Solids, New York: John Wiley, pp 298-309, 1968.
7. I. Langmuir, "The Effect of Space Charge and Initial Velocities on the Potential Distribution and Thermionic Current Between Parallel Plane Electrodes," Physical Review, Vol. 21, p 419, April 1923.
8. I. Langmuir and K. T. Compton, "Electrical Discharges in Gases Part II. Fundamental Phenomena in Electrical Discharges," Reviews of Modern Physics, Vol. 3, pp 191-257, April 1931.
9. A. van der Ziel, "Extension and Application of Langmuir's Calculations on a Plane Diode with Maxwellian Velocity Distribution of the Electrons," Philips Research Reports, Vol. 1, pp 97-118, 1946.
10. P. H. J. A. Kleynen, "Extension of Langmuir's  $(n, \xi)$  Tables for a Plane Diode with a Maxwellian Distribution of the Electrons," Philips Research Reports, Vol. 1, pp 81-96, 1946.
11. W. R. Ferris, "Some Characteristics of Diodes with Oxide-Coated Cathodes," R. C. A. Review, Vol. 10, pp 134-149, 1949.
12. C. R. Crowell, "Effects of the Cathode Work Function on the Space-Charge-Limited Characteristics of Plane Diodes," Journal of Applied Physics, Vol. 27, p 93, 1956.
13. W. B. Nottingham, Thermionic Emission, Technical Report 321, Research Laboratory of Electronics, Massachusetts Institute of Technology, Cambridge, Massachusetts, 1956.
14. E. S. Rittner, "On the Theory of the Close-Spaced Impregnated Cathode Thermionic Converter," Journal of Applied Physics, Vol. 31, pp 1065-1071, June 1970.

REFERENCES (CONCLUDED)

15. C. R. Crowell, "Theoretical Basis for Measuring the Saturation Emission of Highly Emitting Cathodes under Space-Charge-Limited Conditions," Journal of Applied Physics, Vol. 26, No. 11, pp 1353-1356, November 1955.
16. J. G. Brainerd, "Standards on Electron Tubes," Proceeding of the Institute of Radio Engineers, Vol. 38, pp 426-438, 1950.
17. J. H. Affleck and W. T. Boyd, Investigation of Various Activator Refractory Substrate Combinations, Technical Report No. RADC-TR-66-656, National Technical Information Service, No. AD649885, Springfield, Virginia, 1967.
18. R. E. Johnson and F. F. Kiokemeister, Calculus with Analytic Geometry, Boston; Allyn and Bacon, 1964.
19. B. O. Pierce, A Short Table of Integrals, New York; Ginn and Company, 1910.
20. P. Henrici, Elements of Numerical Analysis, New York; John Wiley, 1964.
21. M. Abramowitz and I. A. Stegun, Handbook of Mathematical Functions with Formulas and Mathematical Tables, New York; Dover, 1965.
22. S. Ramo, J. R. Winnery, and J. R. Van Duser, Fields and Waves in Communications Electronics, New York; John Wiley, 1965, pp 177-193.
23. J. R. Pierce, Theory and Design of Electron Beams, New York; Van Nostrand, 1954, pp 174-178.
24. K. R. Spangenberg, Vacuum Tubes, New York; McGraw Hill, 1948, pp 181-182.
25. W. B. Herrmannsfeldt, Electron Trajectory Program, Springfield, Virginia; National Technical Information Service, 1973.